UNIVERSITY OF SOUTHAMPTON
FACULTY OF ENGINEERING AND THE ENVIRONMENT
School of Civil Engineering and the Environment

Effects of Principal Stress Rotation and Drainage on the Resilient Stiffness of Railway Foundations

by
Anna Mamou

A thesis submitted in fulfillment of the degree of Doctor of Philosophy in the Faculty of Engineering and the Environment
at the University of Southampton

May, 2013

For Christos, Panagis, Elena, Paulina
Giorgos, Kalliopi, Margarita, Nikos, Christina

UNIVERSITY OF SOUTHAMPTON

ABSTRACT

FACULTY OF ENGINEERING AND THE ENVIRONMENT
School of Civil Engineering and the Environment

Doctor of Philosophy

EFFECTS OF PRINCIPAL STRESS ROTATION AND DRAINAGE ON THE RESILIENT STIFFNESS OF RAILWAY FOUNDATIONS

By Anna Mamou

Railway foundations play an integral role in controlling the stability of the overlying track structure and the maintenance of the overall track geometry. Premature failures of railway track foundation are likely to result in frequent maintenance, which may entail significant costs since railway track foundations are less easily accessible than the other layers of railway track. Premature failures of track foundations may arise if the service loads exceed the design specifications, but may also develop as a result of the shortcomings of the design codes to simulate in situ stress paths, which involve cyclic stress changes in the horizontal as well as vertical direction, which result in principal stress rotation (PSR). Laboratory investigations have suggested that cyclic changes in the horizontal as well as vertical direction may result in a higher rate of plastic strain accumulation than cycling the vertical stress only. The effect of PSR on the soil stiffness is less certain however. Furthermore little consideration has been given to how the gradation of different soils may affect in situ drainage conditions and therefore influence the rate of railway track deterioration during PSR. A knowledge gap exists as to how cyclic changes in the directions of principal stresses may affect the pore pressure and stiffness of soils under different drainage conditions.

In order to improve our understanding of the effects of PSR on the long term performance of railway track foundations, a series of laboratory tests were conducted which investigated the effects of cyclic changes in the direction of principal stresses on the pore pressure, stiffness and susceptibility to failure of saturated railway track foundation soils under different drainage conditions. The investigated sand-clay mixes were selected so as to replicate the gradation of an in situ railway track foundation. It was found that even small additions of clay to the volume of a sand significantly affected the response of the mixes during cyclic changes in principal stress direction. Moderate additions of clay in the pore space of a sand reduced the susceptibility to principal stress rotation by reducing the tendency for excess pore pressure generation and by increasing the cyclic shear stress the mixes were able to sustain before rapid plastic strain accumulation occurred. Increases in principal stress rotation below the cyclic shear threshold increased the resilient stiffness of the sand-clay mixes, however once this threshold was exceeded rapid stiffness degradation occurred. Below the cyclic shear threshold, the response of the mixes was stable over a high number of loading cycles and no abrupt fatigue failures were observed. The sand-clay mixes were sensitive to even small changes in the magnitude of PSR near the cyclic shear threshold. Small increases in PSR could trigger the sudden collapse of a previously stable sand-clay mix. Under conditions where the rate of pore pressure dissipation was regulated by the permeability and the volumetric compressibility of the soil, the sand clay mixes with moderate additions of fines were stable over a range of cyclic increases in PSR which correspond to the maximum expected changes in magnitude within the depth of a ballasted railway track foundation.

Contents

List of Figures

List of Tables

List of Symbols and Abbreviations

Symbols

b	Magnitude of σ_2 relative to σ_1 and σ_3
D_R	Relative density of soil
e	Global void ratio
e_G	Intergranular void ratio
e_{Ge}	Equivalent granular void ratio
$e_{max,}$ e_{min}	Maximum and minimum global void ratio
e_{sk}	Skeleton void ratio
E_r	Resilient Young's modulus
$E_{m,}$	Young's modulus of a rubber membrane
F	Axial load
G_{smix}	Specific gravity of soil mixture
G_{ssand}	Specific gravity of sand
G_{ssilt}	Specific gravity of silt
G_{sclay}	Specific gravity of clay
H	Initial height
ΔH	Axial displacement
M_{sand}	Mass of sand
M_{silt}	Mass of silt
M_{clay}	Mass of clay
N	Number of load applications
p’	Mean effective stress

p_o	Outer cell pressure
p_i	Inner cell pressure
q	Deviator stress
r_i	Inner radius
r_o	Outer radius
rio	Initial inner radius
Δr_i	Inner radial displacement
Δr_o	Outer radial displacement
R	Principal stress ratio
T	Torque
$t_{m,}$	Membrane's average thickness
Vi	Inner volume
ΔVi	Change in inner volume
V_{voids}	Volume of voids
V_{water}	Volume of water
V_{air}	Volume of air
V_{sand}	Volume of sand
V_{fines}	Volume of fines
v_c	Rayleigh wave velocity
v_s	Shear wave velocity

α	Orientation of the major principal stress to the vertical
$\gamma_{\theta z}$	Shear strain
ε_z	Axial strain
ε_θ	Circumferential strain
ε_{zc}	Axial strain during consolidation
$\varepsilon_{\theta c}$	Circumferential strain during consolidation
ε_{res}	Resilient axial strain

ε_r	Radial strain
θ	Angular circumferential displacement
ρ_{dry}	Dry density of soil
ρ_{water}	Density of water
σ_z	Vertical stress
σ_r	Radial stress
σ_θ	Circumferential stress
σ_1	Major principal stress
σ_2	Intermediate principal stress
σ_3	Minor principal stress
$\tau_{z\theta}$	Horizontal shear stress
τ_{zr}	Radial shear stress
ν	Poisson's ratio

Abbreviations

AREA	American Railway Engineering Association
ASTM	American Society for Testing and Materials
B	Skempton's pore water pressure coefficient
BS	British Standard
CO_2	Carbon dioxide
DAF	Dynamic Amplification Factor
EWS	English, Welsh and Scottish Railways
FEM	Finite Element Modelling
GDS	Global Digital Systems
HCA	Hollow Cylinder Apparatus
HPC	Hymod Prima Clay
LBSFB	Leighton Buzzard Sand Fraction B

LBSFC	Leighton Buzzard Sand Fraction C
LBSFD	Leighton Buzzard Sand Fraction D
Ltd	Limited
LVDT	Linear Variable Differential Transformer
OCR	Over Consolidation Ratio
PSR	Principal Stress Rotation
UK	United Kingdom
3D	3 Dimensional

Declaration of Authorship

I, Anna Mamou declare that this thesis, 'Effects of Principal Stress Rotation and Drainage on the Resilient Stiffness of Railway Foundations', and the work presented in it are my own and has been generated by me as the result of my own original research. I confirm that:

- This work was done wholly or mainly while in candidature for a research degree at this University;
- Where any part of this thesis has previously been submitted for a degree or any other qualification at this University or any other institution, this has been clearly stated;
- Where I have consulted the published work of others, this is always clearly attributed;
- Where I have quoted from the work of others, the source is always given. With the exception of such quotations, this thesis is entirely my own work;
- I have acknowledged all main sources of help;
- Where the thesis is based on work done by myself jointly with others, I have made clear exactly what was done by others and what I have contributed myself;
- None of this work has been published before submission.

Signed:……

Date:……

Acknowledgements

The author would like to thank the following people and organisations who have made this research possible:

First of all I would like to express my gratitude to my supervisors Prof. William Powrie and Dr. Jeffrey Priest for giving me the opportunity to work with them on this exciting research project and for all their wisdom, patience guidance and support throughout these years.

I would also like to extend a very big thank you to Harvey Skinner, Karl Scammell from the Civil Engineering laboratory and Karl Snelling, Nick Warren and Chris Jones from GDS Instruments Ltd who helped solving countless technical problems. It would not have been possible to complete the experimental work without them.

The Engineering and Physical Sciences Research Council (EPSRC) for the financial support of this research.

Sinthu, Aingaa, Louise, Manolis, Amit, Femi, Taufan, Geoff and so many more for all the laughs we shared in the laboratory, which made all the difficult moments so much easier.

My family and above all my parents and my husband for all their unquestionable love and for being my strongest supporters.

Stamatia, Petros, Nena, who were always at the other end of the line for me and last but not least Mpampis whom we lost so early, but who will always live in our hearts.

Chapter 1

INTRODUCTION

1.1 Background

The construction, operation and maintenance of a robust railway network are fundamental to a country's economy. The focus of this research was the foundation layer of the railway track (Figure 1.1). The foundation of a railway track plays a critical role in controlling the stability of the overlying track structure and maintaining the overall track geometry. Repeated traffic loading may cause excessive deformations of a poorly designed foundation which will be translated upwards, irrespective of the quality of the overlying layers. In contrast to the ballast which can be easily accessed and maintained, foundation related failures are less easily rectified and are therefore a key driver of the overall maintenance costs.

Historically, most railway track foundations were constructed using empirical design methods based on results of simple static tests on the soil ignoring the effects of repeated

wheel loads. This may have contributed to the premature failures of railway tracks and the associated high maintenance costs. Improved design guidelines, based on cyclic triaxial tests in which the wheel load is modelled as a cyclic axial stress, still do not adequately represent the true stress regime imposed by trains on a soil element in the railway track foundation. As trains approach, recede, accelerate or brake the soil experiences changes in vertical and horizontal shear stresses, thereby leading to a rotation of principal stresses.

Cyclic changes in the directions of the principal stresses have been shown to affect the development of plastic strains (Chan & Brown, 1994), with the effects of principal stress rotation (PSR) on the rate of plastic strain accumulation being more pronounced for some soils and less significant for others (Gräbe, 2002, Gräbe & Clayton, 2009). The influence of PSR on the soil stiffness is less certain however. Understanding the effects of PSR on the stiffness of soils however is critical as the stiffness may control the magnitudes of deflections. The data presented by Gräbe (2002) suggest that although PSR significantly accelerated the development of permanent strains in granular materials, the effects of PSR on the rate of resilient stiffness degradation was not as important.

Further uncertainties regarding the significance of PSR on the behaviour of railway foundations are associated with the scarcity of comprehensive numerical analysis detailing representative stress paths for laboratory testing. Depending on the depth within the railway track foundation, the magnitude of horizontal shear stress can vary significantly. To date no comprehensive laboratory tests have been reported where the significance of cyclic changes in the magnitude of horizontal stress on the stability of different soils was investigated. Furthermore little consideration has been given to how the gradation of different soils may affect in situ drainage conditions and therefore influence the rate of railway track deterioration during PSR. A knowledge gap exists as to how cyclic changes in the magnitude of PSR may affect the pore pressure and stiffness of soils under different drainage conditions.

1.2 Aims and Objectives

The aim of this research was to understand the influence of cyclic changes in principal stress direction on the pore pressure, stiffness and susceptibility to failure of railway track foundation soils under different drainage conditions. The investigated materials, four sand-clay mixes with varying clay contents, were selected so as to replicate the grading of the South African Coal Line foundation for which there is a well documented baseline comprising both laboratory and field data (Priest et al., 2010; Otter, 2011).

The objective of this research was met by subjecting each sand-clay mix to gradual increases in the magnitude of cyclic shear stresses until failure was observed. This allowed a range of PSR changes typically expected within railway track foundations to be investigated. Cyclic changes in the magnitude of PSR were investigated under both undrained and free to drain conditions. Undrained changes in PSR were intended to enable investigation of the susceptibility to cyclic increases in PSR under conditions where drainage may become reduced or restricted. Free to drain tests were designed to simulate field conditions, where the degree of any excess pore pressure accumulation is controlled by the permeability and the volumetric compressibility of the soil comprising the railway track foundation and the operational drainage path length.

1.3 Thesis Outline

The thesis consists of the following chapters

Chapter 2 presents a comprehensive literature review, detailing the importance of principal stress rotation on railway foundation material and justifying why further research in this area is required.

Chapter 3 introduces the experimental apparatus and outlines the materials, specimen preparation and testing methods used in this research.

Chapter 4 presents and discusses the experimental results in comparison with previous relevant published work.

Chapter 5 discusses the conclusions and their implications for practice, and suggests areas for future research.

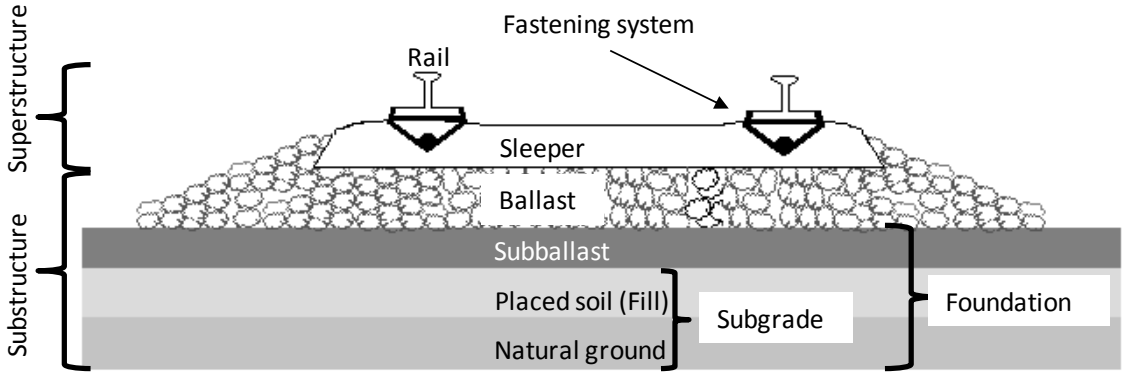

Figure 1.1: Track structure components of a ballasted railway track. Redrawn from Selig & Waters (1994).

Chapter 2

BACKGROUND

The main aim of this chapter is to set the background of the stress paths relevant to railway track foundations, with an emphasis on the effects of principal stress rotation. The discussion includes a review of relevant reported experimental investigations, highlighting the knowledge gaps in our current understanding of how principal stress rotation may affect different soils. Finally the analysis concludes with a review of the possible factors, that may influence the response to principal stress rotation.

2.1 Performance of railway track foundations

Throughout their design life, railway track foundations are subjected to a high number of load repetitions. Each repeated loading cycle contributes an increment to the total accumulation of permanent strain, which may gradually give rise to progressive shear failure and excessive plastic deformations of railway track foundations (Miller et al.,

2000; Liu & Xiao, 2010). Progressive shear failure usually starts to develop at the top of the foundation where the overstressed soil is gradually squeezed sideways and upwards into the sub-ballast or ballast (Li & Selig, 1995). The settlement of the foundation is matched by a corresponding heave of soil at the side of the track, which inhibits drainage and therefore accelerates rail track deterioration further (Figure 2.1). In contrast to progressive shear failure, failure by excessive plastic deformation usually affects a substantial depth of the track foundation. Excessive plastic deformation results in the formation of ballast pockets and may be accompanied by soil heave at the track side (Figure 2.1). Other types of foundation failures include attrition and massive shear failure. Attrition of the foundation by the overlying ballast in the presence of water results in the formation of a slurry at the ballast/subballast interface. Massive shear failures can occur when the shearing capacity, which resists the weight of the superstructure and external train loads is exceeded, resulting in deep seated rotational type slippages (Selig & Waters, 1994; Li & Selig, 1995).

2.2 Design parameters of track foundations

2.2.1 Simulating the train passage through a static vertical stress

In the past, railway track foundations were predominantly designed using simplified analytical and empirical design approaches. For example the American Railway Engineering Association design philosophy was based on the construction of a sufficiently thick granular layer, so as to reduce the stresses transferred to the foundations to acceptable levels, thereby avoiding premature deteriorations of the railway track geometry (AREA, 1996). The granular layer thickness was determined as a function of the magnitude of vertical stress and of the foundation bearing pressure which was selected irrespective of soil type. Raymond (1985) extended the design approach recommended by the AREA using the Casagrande soil classification (Casagrande, 1948) to relate allowable bearing pressures to the soil type. Although this was an improvement

there were still serious shortcomings since the effects of the train passage on the stability of the railway track foundation was estimated on the basis of static loading, ignoring the effects of repeated loading cycles. This gave rise to failures of railway track foundations and associated unacceptably high maintenance costs.

2.2.2 Simulating the train passage through cyclic vertical stress changes

In reality the loading conditions of railway track foundations are cyclic by nature. Each repeated loading cycle contributes an increment to the total accumulation of permanent strain, which may gradually result in the deterioration of the overall rail track geometry (Lekarp et al., 2000). Improved design guidelines were therefore based on the results of laboratory tests in which the wheel load was simulated as a cyclic vertical stress (Heath et al., 1972; Raymond et al., 1979; Li & Selig, 1998; Miller et al., 2000; Shahu et al., 2000; Suiker et al., 2005). It was found that when the vertical design stress was kept below a cyclic threshold stress, the additional plastic strain accumulating at the end of each cycle reduced with increasing number of cycles. In terms of recoverable deformations this implies that for values of the repeated vertical stress less than a threshold stress the resilient strains become approximately constant and the material behaves essentially elastically (Larew & Leonards, 1962). The resilient and permanent components of a cycle of loading are illustrated in Figure 2.2. The cyclic stress threshold was found to be lower than the static deviator stress causing failure in a monotonic test, illustrating why railway track foundations failed even though the design loads were lower than the ultimate bearing pressure.

2.2.2.1 The resilient Young's modulus

The rate of plastic strain accumulation is a necessary but not sufficient criterion in assessing the performance of a railway track foundation. The magnitude of deformation is ultimately controlled by the soil stiffness which may either decrease or increase under the

effects of cyclic loading until the soil has reached a resilient state (O'Reilly et al., 1991). The stiffness of the soil corresponding to the resilient response is defined as the resilient Young's modulus and was first introduced at the University of California, Berkeley (Brown, 1996). The resilient Young's modulus is defined as the magnitude of the deviator stress change divided by the resilient axial strain during a load cycle

$$E_r = \frac{(q_{max} - q_{min})}{\varepsilon_{res}} \tag{2.1}$$

with q_{max} and q_{min} the maximum and minimum values of the repeated deviator stress and ε_{res} the recoverable axial strain per cycle. The objective of a successful railway track foundation design is therefore to achieve a resilient response, so as to avoid the progressive deterioration of the railway track geometry with increasing loading cycles. In response to this, a number of models have been developed which project the rate of plastic strain accumulation and the corresponding recoverable strain and resilient stiffness (Appendix A).

However despite these significant design improvements, premature failures of railway track foundations requiring excessive maintenance are still reported. For example Burrow et al. (2007) reported that the accelerated deterioration of railway track foundations could not be prevented despite a significant increase in the granular layer thickness which was greater than that indicated by all of the design methods considered and similar observations were reported by Read & Li (1995) cited in Miller et al. (2000).

2.2.3 Simulating the train passage through cyclic vertical and horizontal stress changes

It has been hypothesised that premature deteriorations of the railway track geometry may be associated with the inability of the design standards to reflect the true stress regime

experienced by soil elements in railway track foundations. As trains approach, recede, accelerate or brake, a soil element in the foundation layer of a railway track will experience complex cyclic stress changes in the horizontal as well as vertical direction, which result in principal stress rotation (PSR) (Figure 2.3) (Chan & Brown, 1994; Brown, 1996; Gräbe, 2002; Momoya et al., 2007; Powrie et al., 2007; Gräbe & Clayton, 2009).

Laboratory investigations on granular materials have indicated that cyclic changes in the horizontal and vertical directions may result in a higher rate of plastic strain accumulation than cycling the vertical stress only (Figures 2.4-2.5) (Chan, 1990; Chan & Brown, 1994; Momoya et al., 2007). Recent tests on sand-clay mixes representative of the gradation of the South African Coal Line foundation suggested that the effect of PSR on the rate of plastic strain accumulation was more pronounced for the granular mixes and was less significant for the mixes dominated by the fines fraction (Figure 2.6) (Gräbe & Clayton, 2009). Rotating the principal stresses resulted in significant excess pore pressure generation in the granular mix, whereas insignificant pore pressures accumulated in the mixes dominated by the fines fraction (Figures 2.7-2.8). The effect of PSR on the rate of resilient stiffness degradation however was found to be less significant irrespective of the mix gradation (Figure 2.9) (Gräbe, 2002).

The reviewed literature illustrates that the influence of principal stress rotation on the rate of plastic strain accumulation appears to be relatively well researched and understood. The rate of plastic strain accumulation however may not be a complete indicator of the influence of PSR on the performance of railway track foundations. Other parameters which control the susceptibility to failure under cyclic changes in PSR include the pore pressure response and resilient stiffness of the soil. These two parameters have been researched primarily in the context of granular materials or in the context of anisotropic effects on stiffness at very small strain (Symes et al., 1984; Zdravkovic & Jardine, 1997; Gasparre et al., 2007; Georgiannou & Tsomokos, 2008). Further uncertainties regarding the significance of PSR on the performance of railway foundations are associated with the scarcity of comprehensive numerical analysis detailing the range of likely stress changes within a railway track foundation.

2.3 Quantification of stress changes bellow ballasted track foundations

2.3.1 Stress changes based on FEM

Finite element models (FEM) have been developed to calculate the likely stress changes assuming both elastic and elastoplastic constitutive laws for the soil. The main justification for using elastic theory is the assumption that below a cyclic threshold stress the irrecoverable strains will be small relative to the resilient component (Brown, 1996). Proposed linear elastic FEM models include GEOTRACK, KENTRACK and FEARAT (Fateen, 1972; Chang et al., 1980; Huang et al., 1984; Li & Selig, 1998; Shahu et al., 2000; Rose et al., 2010). Elastoplastic FEM were reported by Shahu (1993) cited in Shahu et al. (2000). Most of these studies however have focused on the vertical stress changes with comparatively little reference to the horizontal stress changes which cause principal stress rotation (Figures 2.10-2.11).

Quantification of horizontal and vertical stress changes of ballasted railway track foundations was reported by Gräbe (2002). Figure 2.12 illustrates the results of a linear elastic FEM at a depth of 0.5m below foundation level on the centre line of the railway track under a 60 km/h, 26 tons/axle configuration (Gräbe, 2002). The results suggest that the deviator and shear stress are cycled 90^{o} out of phase. The magnitudes of the deviator and shear stress cycles were approximately 60kPa and 17kPa respectively.

Powrie et al. (2007) extended the numerical analysis by investigating the stress path at various depths within the trackbed utilising 3D linear elastic FEM. The geometry of the track structure was based on the International Union of Railways Code 719R and the UK Channel Tunnel Rail Link. The numerical analysis was performed for a typical 25.5 tons/axle freight car used by English, Welsh and Scottish Railways (EWS) (the maximum normally permitted on the UK rail network), corresponding to a static wheel load of 125kN. At the top of the foundation level along the centre line of the rail-track, the amplitudes of the deviator and shear stress pulses were found to be approximately

$\Delta\sigma$=70kPa and $\Delta\tau_{\theta z}$=±26kPa respectively (Figure 2.13). At a depth of 0.7m below foundation level the amplitude of the deviator and shear stress pulses had fallen to approximately $\Delta\sigma$=13kPa $\Delta\tau_{\theta z}$=±8kPa respectively (Figure 2.13). In both cases the deviator stress was found to be 90^0 degrees out of phase with the shear stress $\tau_{\theta z}$. Powrie et al. (2007) noted that in addition to the aforementioned stress changes due to vertical loads, stress changes due to horizontal forces applied during train acceleration and/or braking have to be accounted for. With a maximum horizontal force of 25% of the wheel load, the increase in the deviator and shear stress at the top of the foundation were 14% and 6% respectively, and at the bottom of the sub-base 4.5% and 9%.

The numerical analysis of Powrie et al. (2007) was based on the assumption of a static wheel load. In reality the stress changes induced during train passage are dynamic in nature. Depending on whether the train is accelerating or braking the actual induced stress changes may be higher or lower than those calculated in a static FEM. Dynamic effects become more pronounced under conditions where the speed of the train approaches the Rayleigh wave velocity v_c [1] for the soil (Krylov, 1995). Recent dynamic finite element analyses on an ideal smooth railway line with no track geometry irregularities, showed that the soil behaves in a quasi-static manner when the train speed is less than $0.1v_c$ (Yang et al., 2009). Dynamic effects begin to have an effect on the stresses imposed on the soil when the train speed is increased above $0.1v_c$. At a train speed of $0.5v_c$, a static analysis may underestimate shear stresses by 30%.

Assuming a Young's modulus of approximately 118MPa for the track foundation, similar to the minimum in the range of values considered by Priest et al. (2010) and Powrie et al. (2007) (Table 2.1), the corresponding Rayleigh wave velocity v_c may be approximately 140 m/s, depending on the Poisson's ratio. For dynamic effects to be important under these conditions, the train speed would have to be in excess of 240 km/h (67m/s). Similar

[1] $v_c = Cv_s$ where C depends on the Poisson's ratio and generally ranges from 0.911-0.955, $v_s=\sqrt{(E/2(1+v))/\rho}$ = shear wave velocity; E = Young's modulus; v = Poisson's ratio and ρ = soil density.

observations were made by Gräbe (2002), who observed that for train speeds up to 140 km/h the ground response was quasi-static, while the impact of dynamic effects on the calculated maximum stress changes was small for speeds beyond 140km/h and up to 240 km/h (Gräbe, 2002). Since most railway lines operate at speeds less than 240 km/h (67m/s) the dynamic effects on the foundation may be considered negligible and therefore the numerical analysis of Powrie et al. (2007) is sufficiently accurate.

2.3.1.1 Comparison of stress changes from different numerical models

The rate of change in the shear stress magnitude with depth within the railway track foundation is in relatively good agreement with the numerical analysis of Gräbe (2002). However, the numerical analysis of Gräbe (2002) suggests a more pronounced magnitude of change in deviator stress. The fact that Gräbe (2002) performed a dynamic numerical analysis compared with the static analysis of Powrie et al. (2007) may have influenced the magnitude of cyclic stress changes, albeit to a small degree since low train speeds were considered 60 km/h (Gräbe, 2002; Yang et al., 2009). The influence on the horizontal and vertical stress changes would be expected to be proportional, however.

2.3.2 Stress changes based on field measurements

Stress changes can be also estimated by either direct in situ measurement, or indirectly by measuring in situ displacements and calculating the corresponding stresses using numerical methods. Direct in situ measurements of stresses however may be less practical, as they are affected by the installation procedures appropriate to the characteristics of the individual site (Richards et al., 2007) and by the relative stress cell to soil stiffness ratio (Clayton & Bica, 1993). In situ displacement measurements have been reported in the literature and although in some cases models were developed and calibrated against in situ measurements, no reference was made to the corresponding

stress changes (Kaynia et al., 2000; Ju et al., 2007; Chebli et al., 2008; Xianzhang et al., 2009).

Vertical stress changes on the Jinan-Qingdao and Tianjin-Pukou railway subgrade in China were recently reported by Liu & Xiao (2010). The stress changes were back-calculated from the measured deflections caused during the passage of 120km/h freight and 200km/h passenger trains. The maximum vertical stress changes at the top of the subgrade were 30kPa and 15kPa under the 120km/h 22.5tons/axle load freight train and the 200km/h 14tons/axle load passenger train respectively (Figure 2.14). As can be seen, the sub-grade was not completely unloaded before the approach of the second axle. Stress changes were also derived at different depths within the subgrade under both freight and passenger train traffic loads (Figure 2.15). The field measurements suggest that the dynamic stress attenuated with increasing depth. At a depth of 0.25m below the subgrade surface, two adjacent axles under the same bogie generated approximately a single stress pulse, and at 0.80m from the subgrade surface, four axles under two adjacent cars generated approximately a single stress pulse. Although Liu & Xiao (2010) undertook a systematic research effort to determine the vertical stress changes based on the measured displacements, no reference to the horizontal stress changes was made.

Changes in vertical as well as horizontal stresses below a ballasted railway track were reported by Indraratna et al. (2010). The stress changes were obtained from direct in situ measurement using pressure cells. The maximum stress at different depths below the base of the sleeper is presented in Figure 2.16. The results suggest that the vertical stresses decreased significantly with depth, in contrast to the horizontal stress changes which remained pronounced. The maximum measured horizontal and vertical stresses due to the passage of a passenger train at the bottom of the ballast on the centreline of the rail were approximately 20kPa and 50kPa respectively. The maximum horizontal and vertical stresses measured at the bottom of the ballast on the centreline of the rail due to the passage of a coal train with a 25tons/axle configuration were as expected greater and measured approximately 25kPa and 75kPa respectively. The reported field measurements

focused mostly on the response of the ballast layer and as a result the measurements were confined to relatively shallow depths below the base of the sleeper.

Vertical as well as horizontal stress changes at various locations below a ballasted railway track were reported by Powrie et al. (2008) and Priest et al. (2010). The stress changes were obtained from FEM using the measured field displacements and back-calculating the corresponding stiffness. Figure 2.17(a) illustrates the measured vertical deflections at different positions below the centreline of the railway track. As can be observed the peak vertical deflections did not occur simultaneously, owing to a slight offset of the boreholes along the direction of travel of the train, relative to the monitored sleeper. The magnitude of the recorded vertical displacement decreased with increasing depth. The attenuation of frequency of vertical loads with increasing depth is illustrated in Figure 2.18. The dominant frequency corresponded to the passage of pairs of bogies at adjacent ends of coupled wagons. The measured horizontal displacements at different depths below the centre line of the railway track are shown in Figure 2.17(b). Unlike the maximum recorded vertical deflections which reduced with increasing depth, the largest horizontal displacement was measured 0.78m below the sleeper base, rather than at the sleeper. In contrast to the vertical sleeper displacements, where the dominant movement was caused by bogie pairs, horizontal displacements were dominated by the passage of individual axles (Figure 2.21) (Priest et al., 2010).

Figure 2.20 illustrates the calculated vertical and horizontal stress changes at a depth of 0.8m below the sleeper bottom (Priest et al., 2010). The ballast thickness along the line varied, with the minimum depth of ballast beneath the sleeper along the centreline of the track being about 0.3m. Thus the measurements shown correspond to an approximate depth of 0.5m bellow the ballast. The amplitude of the vertical and horizontal stress change was approximately 80kPa and 30kPa respectively.

2.3.3 Comparison of stress changes from numerical modelling and field measurements

The horizontal and vertical stress changes obtained from the numerical analysis by Powrie et al. (2007) at the top of the railway track foundation due to the passage of a 25 tons/axle configuration are close to the in situ stress changes measured by Indraratna et al. (2010) at similar locations and axle load configurations. The comparably higher cyclic stress magnitudes back calculated from the numerical analysis of Priest et al. (2010) at similar locations and for the same axle load configuration as Powrie et al. (2007) are to be expected since a much higher Young's Modulus was used for the track layers. For example in the numerical analysis by Priest et al. (2010) the natural ground comprised a hard, dense weathered mudrock and the back-calculated Young's Modulus based on in situ displacement measurements corresponded to 27000MPa compared with a Young's Modulus of 30MPa assumed for the natural ground in the analysis by Powrie et al. (2007). Dynamic effects considered in the numerical analysis of Priest et al. (2010) are thought to have played a less important role due to the low train speeds (47.5 km/h) (Gräbe, 2002; Yang et al., 2009).

2.4 Factors affecting the response of ballasted track foundations during principal stress rotation

2.4.1 Degree of saturation-moisture content changes

Throughout the design life of a railway track foundation, the moisture content of the soil is likely to vary as a result of climate change fluctuations between extreme dry and wet periods. Extreme dry periods may lower the water table such that parts of the railway track foundation void structure are filled with air and others with water, resulting in an overall unsaturated structure.

Suction in soils has been shown to increase the soil strength and stiffness to an extend dependent on the degree of suction, soil type and particle arrangement (Otter, 2011). This implies that as the degree of saturation increases and the suction reduces a reduction in stiffness as compared with the unsaturated state will occur. In terms of railway foundation design this is likely to result in increased deflections (Drumm et al., 1997). Assuming saturated conditions may therefore be a more conservative design approach than assuming unsaturated conditions. Saturated conditions are likely to prevail during extreme wet periods, resulting in a railway track foundation being completely submerged below the water table. The scenario of fully saturated conditions was investigated in this research.

2.4.2 Drainage conditions

In the laboratory soils are usually brought to failure under either drained or undrained loading conditions. In drained loading, the rate of loading is adjusted so as not to cause significant excess pore pressure accumulation at the furthest point from the drainage boundary.

In the field however, drainage conditions are not controlled artificially but rather are self-regulated by the permeability and the volumetric compressibility of the soil comprising the railway track foundation. The volumetric compressibility will dictate the amount of excess pore pressures generated as a result of PSR and the permeability, available resting periods and drainage path length will dictate how quickly these may be dissipated.

Most reported cyclic loading tests with and without PSR associated with pavement foundations have been performed under undrained conditions (Brown et al., 1975, Shahu et al., 1999; Gräbe & Clayton, 2009; Liu & Xiao, 2010; Ip et al., 2012). Undrained conditions were selected on the basis of investigating the susceptibility to the accumulation of excess pore pressures leading to a gradual softening of the foundation, which could then lead to mud pumping in the field. Ignoring any rest periods between

train passage is however likely to overestimate the rate of excess pore pressure accumulation and therefore overestimate the rate of track deterioration. It has been suggested that one way to simulate in situ resting periods would be to interrupt the undrained cyclic testing stage by introducing drainage periods (O'Reilly et al., 1991).

In some cases the justification for restricting any volume changes was based on the fact that the tested materials were predominantly fine grained and it was hypothesised that in the field these materials would not be completely drained and therefore some degree of excess pore pressure accumulation would be expected to occur. Recent investigations of the gradation of an in situ railway track foundation in South Africa showed that this varied significantly, alternating between mixes with dominant granular particles to mixes where the soil matrix was dominated by the fines (Gräbe, 2002). The in situ response of a clayey sand may be significantly different from that of a sandy clay. Undrained conditions investigate mainly the susceptibility to accumulate excess pore pressures under conditions where drainage may become restricted irrespective of the gradation of the foundation material. To simulate the in situ response where drainage is self-regulated, laboratory experiments could be carried out in which volume changes are allowed to occur and the tendency of the materials to accumulate any excess pore pressures at the furthest point from drainage is measured. For example Indraratna et al. (2009) reported that cyclic loading of a clay resulted in partly drained conditions

2.4.3 Effective Stress

Railway foundations are relatively shallow and may therefore be subjected to relatively low effective stresses. Recent field measurements revealed that railway foundation were confined to stresses typically in the range of 20kPa-60kPa (Liu (2006) cited in Liu & Xiao (2010)). Examples of effective stresses researched in the laboratory and in relation to railway track foundations include Indraratna et al. (2009) (40kPa), Miller et al. (2000) (14kPa, 35kPa), Shahu et al. (2000) (20kPa and 40kPa), Gräbe (2002) (30kPa), Momoya et al. (2005) (20kPa) and Otter (2011) (10kPa, 20kPa, 50kPa, 100kPa and up to 400kPa).

2.4.4 Cyclic Loading Frequency

The cyclic loading frequency of a soil element during train passage is related to train speed, axle spacing and bogie layout. The four axles under two adjacent bogies are usually regarded as a single load repetition (Li & Selig, 1996). For a given bogie layout and train speeds of 60-100km/h this may translate into cyclic loading frequencies of 2.0-3.0Hz (Gräbe, 2002; Liu & Xiao, 2010).

It is now accepted that at very small strain, the stiffness of soils is rate-independent. This implies that at very small strain, the stress strain response is essentially linear-elastic (Bolton & Wilson, 1989; Tatsuoka & Shibuya, 1992; Shibuya et al., 1997; Sorensen et al., 2010, Clayton, 2011). At higher strains beyond the elastic threshold strain, the stress-strain relation exhibits a non-linear response and increases with increasing strain rate (Tatsuoka & Shibuya, 1992; Lo Presti et al., 1997). The stress–strain response under cyclic loading can therefore be expected to be stiffer than under monotonic loading. Teachavorasinskun et al. (2002) reported that the stiffness varied between 10MPa in a compressive test at a stress rate of 0.05kPa/min to 35MPa under cyclic loading conditions equivalent to a stress rate of 320kPa/min. Sorensen et al. (2007) observed that the stiffness becomes more sensitive to the rate of loading at small strains (0.01% - 0.1%), while Teachavorasinskun et al. (2002) reported a rate sensitivity for strains in the region of 0.02% - 0.2%. At large strains however, the stiffness becomes independent of the strain rate (Teachavorasinskun et al., 2002).

Examples of reported cyclic frequencies for cyclic laboratory tests relevant to pavement foundations include 0.0167Hz (Shahu et al., 1999), 0.1Hz (O'Reilly et al., 1991), 0.8Hz (Miller et al., 2000), 1Hz (Leshchinsky & Rawlings, 1988); 1Hz (Loh & Nikraz, 2012), 2Hz (Frost et al., 2004), 2Hz (Liu & Xiao, 2010), 5Hz (Indraratna et al., 2009); 10Hz (Brown et al., 1975); 5Hz and 10Hz (Ip et al., 2012). None of the above studies involved PSR, which adds a significant degree of complexity to the experimental procedures. Furthermore, high loading frequencies are likely to result in a non-uniform distribution of

pore pressures throughout the specimen and create complications in the interpretation of data.

2.4.5 Number of loading cycles

It has already been discussed that for repeated loading magnitudes less than a critical threshold stress, the increment of additional plastic strain accumulating at the end of each cycle decreases with increasing number of loading cycles (Hyde, 1974). However although the additional plastic strain increment reduces substantially, it still contributes to a very small growth in permanent strain. Therefore to simulate in situ conditions realistically, a high number of load repetitions is desirable. A high number of loading repetitions also enables the investigation of the possibility of the occurrence of sudden fatigue type failures.

A literature review showed that the reported loading cycles relevant to railway track testing varied substantially between 100-900000 cycles. Examples of reported loading cycles in relation to cyclic laboratory tests relevant to pavement foundations include 100 cycles (Shahu et al., 1999); 2160 cycles (O'Reilly et al., 1991); 10000 cycles (Liu & Xiao, 2010); 100000 cycles (Leshchinsky & Rawlings, 1988); 100000 cycles (Brown et al., 1975); 150000 cycles (Loh & Nikraz, 2012); 900000 cycles (Ip et al., 2012). In some cases very high numbers of loading cycles were achieved by utilising high loading frequencies.

2.5 Knowledge gaps in the understanding of the significance of PSR on the stability of ballasted track foundations

The reviewed literature revealed that throughout their lifecycle railway track foundations are subjected to a range of stress changes and drainage conditions. The magnitude of vertical stress changes was shown to decrease with depth, whereas horizontal stress changes become more pronounced up to a certain depth below the sleeper and are further accentuated during train acceleration and braking. Cyclic changes in the magnitude of PSR are therefore likely to influence the long term performance of railway track foundations. Furthermore the susceptibility to accelerated deterioration under PSR may also depend on the gradation of the soil comprising the railway track foundation, as this may control the in situ drainage conditions.

Although numerical models are now available which detail the magnitudes of horizontal and vertical stress changes at different depths within railway track foundations, no comprehensive laboratory tests have been reported in which the influence of these magnitudes of cyclic changes on the rate of railway track deterioration under different drainage conditions were investigated. As a result our understanding of the significance of cyclic changes in the magnitude of PSR on the pore pressure, resilient stiffness and susceptibility to failure of railway track foundations under different drainage conditions is still uncertain. Thus a number of questions arise: How susceptible to accelerated degradation in resilient stiffness due to cyclic increases in PSR are soils with a dominant fines fraction? How do the fines affect the susceptibility to accelerated degradation in resilient stiffness under different drainage conditions? Further research is therefore required in order to improve our understanding of the significance of cyclic changes in PSR on the stability of railway track foundations.

2.6 Investigation of principal stress rotation in the laboratory

In the laboratory the most widely used method for studying the stress strain response of soils is the triaxial test (Hyde & Ward, 1985; Leshchinsky & Rawlings, 1988; Airey & Fahey, 1991; Erten & Maher, 1995; Hyodo et al., 1996; Yilmaz et al., 2004; Smith, 2006, Lackenby et al., 2007; Qadimi & Coop, 2007; Modoni et al., 2010; Yang & Sze, 2011; Loh & Nikraz, 2012). In the triaxial test a specimen can be brought to failure under an increasing cyclic or monotonic deviator stress. Depending on the rate of loading this can allow the response of soils from very small up to large strains to be explored. In terms of PSR effects, however, the triaxial test is very limited as only an interchange of the major and minor principal stress direction can be achieved.

A rotation of principal stress direction other than 90^o can be applied with the simple or modified shear apparatus (directional shear cell). Areas of difficulty in the use of this apparatus include its inability to reproduce a continuous rotation of the principal stresses, resulting in an inability to replicate the real in situ conditions; and the inability to obtain reliable on sample measurements of stress and strain (Arthur et al., 1977; Shaw & Brown, 1986). Although further modifications were made which enabled the application of a continuous rotation of principal stresses the issue of obtaining reliable on sample measurements of stress and strain remained unresolved (Arthur et al., 1979; Wong & Arthur, 1985; Shaw & Brown, 1986; Wong & Arthur, 1986). The ability to obtain on sample measurements of strain is critical in obtaining accurate stiffness values (Jardine et al., 1984; Clayton & Khatrush, 1986; Cuccovillo & Coop, 1997; Atkinson, 2000; Clayton & Heymann, 2001; Kuwano & Jardine, 2002; Clayton, 2011).

In the laboratory, the effects of PSR can be also studied using the Hollow Cylinder Apparatus (HCA). In the HCA a rotation in the direction of principal stresses can be achieved by applying an axial twist (torque), thereby inducing shear stresses on horizontal and complementary radial planes. However because the thickness of the specimen wall is finite, the application of the torque can result in a non-uniform stress

and strain distribution across the specimen wall, hence the suitability of the HCA to study PSR was criticised and questioned (Arthur et al., 1979; Saada & Townsend, 1981).

It was not until Hight et al. (1983) proposed a new framework for interpreting stress and strains in the Hollow Cylinder Apparatus that the suitability of the HCA was established. With the aid of numerical studies Hight et al. (1983) suggested that under certain circumstances, in particular relating to the specimen geometry, the non-uniformities in stress and strain may be reduced to acceptable levels. A literature review revealed that the majority of recent laboratory investigations involving PSR has been performed with the HCA (Symes et al., 1984; Symes et al., 1988; Shibuya et al., 1995; Zdravkovic & Jardine, 1997; Lee et al., 1999; Brown & Richardson, 2004; Nishimura et al., 2007; Georgiannou et al., 2008; Gräbe & Clayton, 2009; Kumruzzaman & Yin , 2010).

2.7 Conclusions

- Case studies have shown that premature failures of railway track foundations may not be prevented simply by increasing the overlying granular layer thickness (Burrow et al., 2007). Accelerated deterioration of railway track foundations may occur as a result of neglecting the in situ stress path, which involves complex stress changes in the horizontal as well as the vertical direction which result in PSR.

- This hypothesis is supported by laboratory investigations which suggested that cyclic rotations of the principal stress direction resulted in a higher rate of plastic strain accumulation than cycling the vertical stress only (Chan & Brown, 1994). Recent tests suggested that the effects of PSR on the rate of plastic strain accumulation were more pronounced for granular soils and less important for

soils containing significant amounts of fines (Gräbe 2002, Gräbe & Clayton, 2009).

- Most of the reported studies have focused on the effects of PSR on the rate of plastic strain accumulation. The rate of plastic strain accumulation, however, may not be the sole impact on the performance of railway track foundations. Although the rate and magnitude of plastic strain accumulation controls the railway track geometry, the magnitude of deformation is controlled by the soil stiffness which may either decrease or increase under the effects of repeated loading.

- Further uncertainties with regard to the significance of PSR on the stability of track foundations are associated with the relative lack of comprehensive numerical analysis detailing the magnitude of likely stress changes within a railway track foundation.

- In situ field measurements have shown that although vertical stress changes attenuate with depth, horizontal stress changes become more pronounced up to a certain depth below the sleeper base before they reduce with further depth increases. A comprehensive numerical analysis has been performed, which details the relationship between the vertical and horizontal stresses at different depths within a railway track foundation (Powrie et al., 2007).

- Other factors that may affect the response of railway track foundations during PSR include the degree of saturation, the in situ drainage conditions, the loading frequency and the number of loading cycles.

- Partly saturated conditions may have a beneficial effect on the soil's stiffness and may be more prevalent during extreme dry periods but less significant under relatively wet climate conditions.

- In the field, drainage conditions are not controlled artificially but rather are self-regulated by the permeability and the volumetric compressibility of the soil

comprising the railway track foundation. Depending on the soil type, undrained loading tests are therefore likely to overestimate the rate of excess pore pressure accumulation and hence the rate of track deterioration.

- Laboratory investigations have demonstrated that the stress-strain response of soils is sensitive to the rate of loading in the intermediate strain range 0.01%-0.2% (Sorensen et al., 2007). Although in situ conditions involve frequent load repetitions, in the laboratory testing at high loading frequencies is likely to result in a non-uniform distribution of excess pore pressures within the specimen causing complications in the interpretation of data. The ability to simulate a high number of load repetitions is associated with the selected test frequency, given the likely time constrains.

- Further high quality tests are required to improve our understanding of how cyclic changes in the magnitude of PSR, may influence the pore pressure, resilient Young's modulus and susceptibility to failure of soils under different drainage conditions. In this context a number of questions arise: How susceptible to accelerated deterioration as a result of cyclic increases in PSR are soils with a dominant fines fraction? How do the fines affect the susceptibility to cyclic increases in PSR under different drainage conditions?

- The triaxial apparatus poses some limitations in studying PSR effects, as only an interchange of the major and minor principal stress direction can be achieved. A rotation of principal stress direction other than 90^o can be applied with the simple or modified shear apparatus. The inability however to obtain on sample measurements of strain with this apparatus, is likely to limit the accuracy of stiffness measurements. In this context, the hollow cylinder apparatus is the most suitable apparatus in studying PSR effects in the laboratory, as it can be used to study rotations of principal stress direction other than 90^o and also enable local strain measurements. Uncertainties associated with stress-strain non-uniformities

across the wall of a hollow cylinder specimen can be limited to acceptable levels by the selection of appropriate specimen geometry (Hight et al., 1983).

Component description	Young's modulus E (MPa)	Poisson's ratio ν	Density ρ (kg/m^3)	Comments
Rail	210,000	0.3	7,850	$A=7.6125\times10^{-3}$ m^2 $J=2.70327\times10^{-5}$ m^4
Pad	6.9357	0.49	1,280	Assumed to be natural rubber E from Liegner (2002)
Sleeper	30,000	0.2	2,400	Reinforced concrete
Ballast	100	0.3	1,800	—
SSB	321	0.3	2,300	—
SB	296	0.3	2,200	—
A	143	0.3	2,100	—
B	118	0.3	2,100	—
Natural ground	27,000	0.25	2,300	—

(a)

Component description	Young's modulus (MPa)	Poisson's ratio	Unit weight (kN/m^3)	Remarks
Rail	210 000	0.3	76.93	Cross-section 78 mm wide × 153 mm deep
Sleeper	34 000	0.3	23.52	Cross-section 242 mm wide × 200 mm deep
Ballast	310	0.3	16.66	
Sub-ballast	130	0.49	22.54	
Prepared subgrade	100	0.49	19.6	
Natural ground	30	0.49	19.6	For Gibson soil, $E = 30 + mz, m = 4.5$

(b)

Table 2.1: Materials Properties for ballasted railway track foundations (a) From Priest et al. (2010) (b) From Powrie et al. (2007).

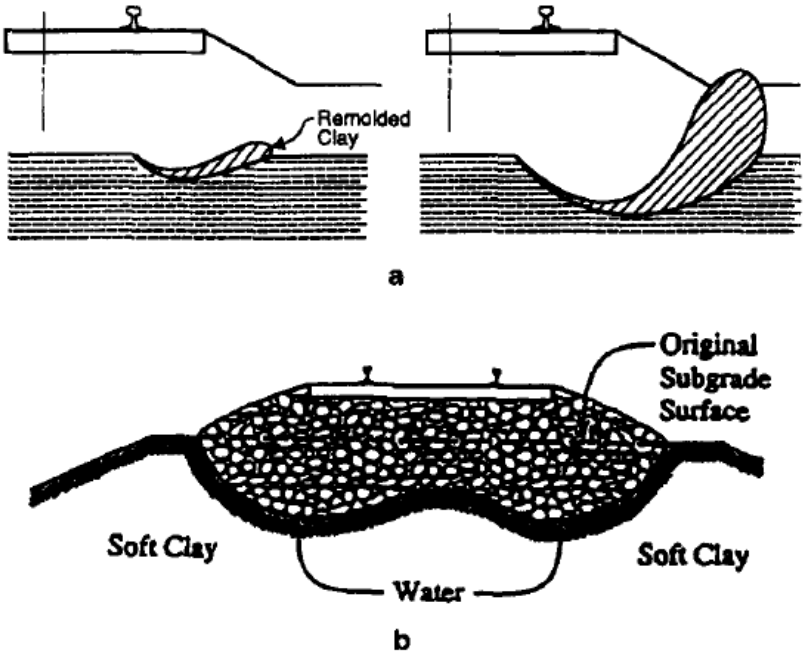

Figure 2.1: Types of railway track foundation (a) Progressive shear failure (b) Excessive plastic deformation resulting in the formation of ballast pockets. From Li & Selig (1998).

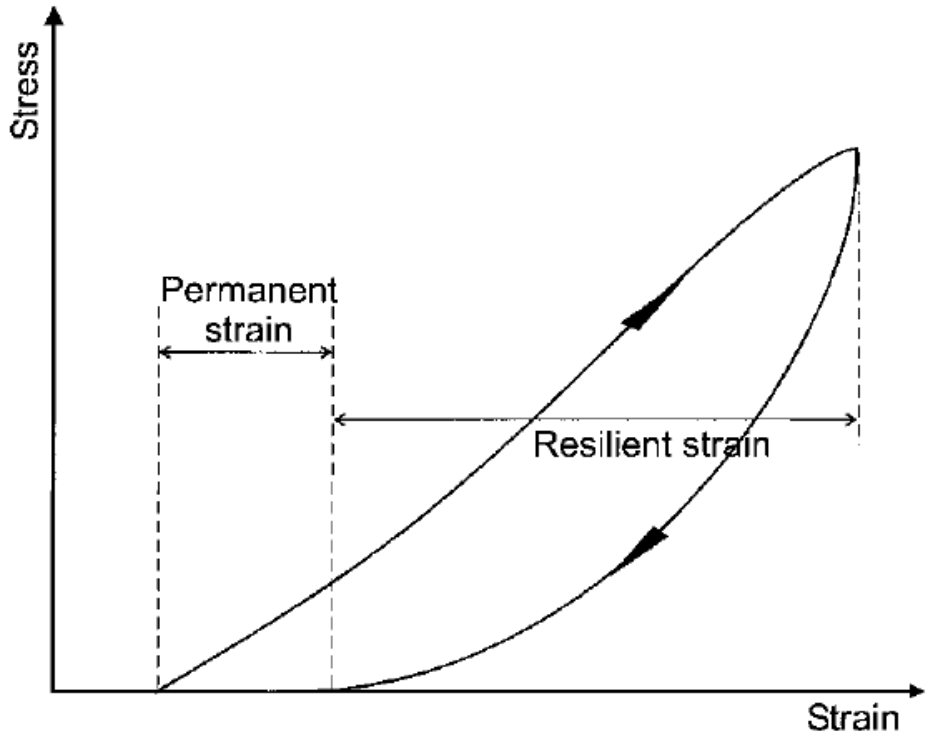

Figure 2.2: Strains during one cycle of load application. From Lekarp et al. (2000).

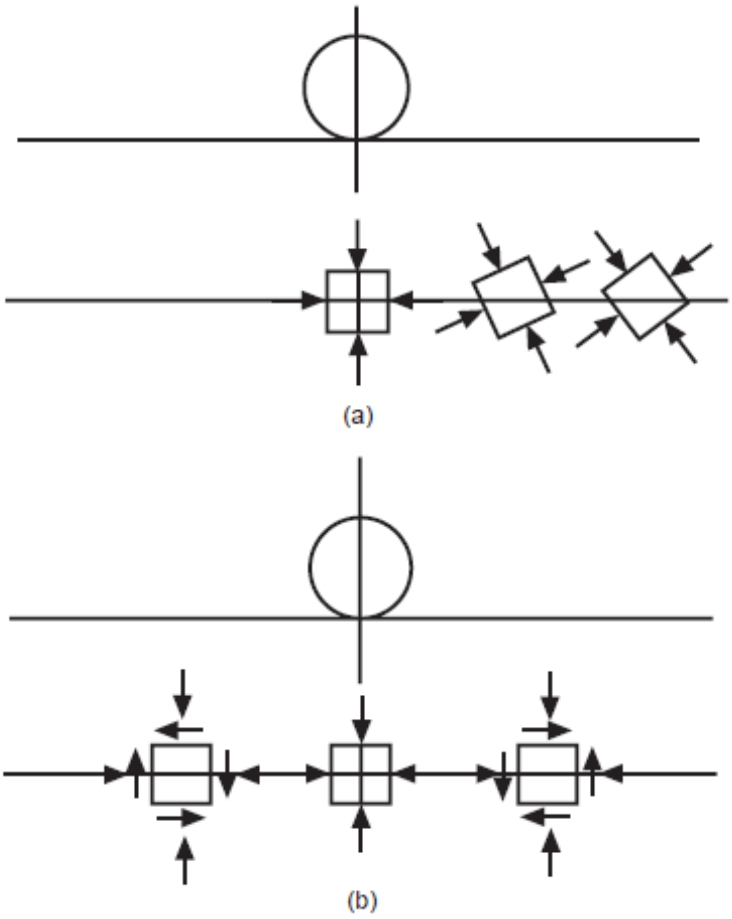

Figure 2.3: Stresses on a pavement element: (a) principal stresses - element rotates; (b) equivalent to shear stress reversal. From Brown (1996).

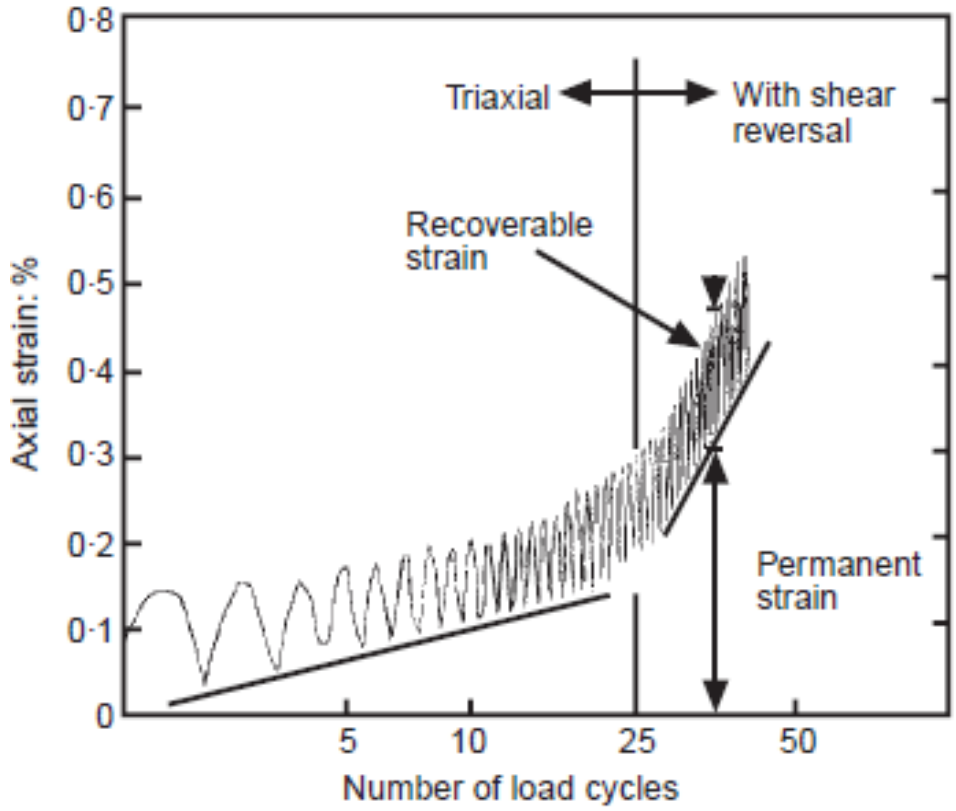

Figure 2.4: The effect of cyclic loading with and without PSR on the plastic strain accumulation of a dry crushed rock. From Chan & Brown (1994).

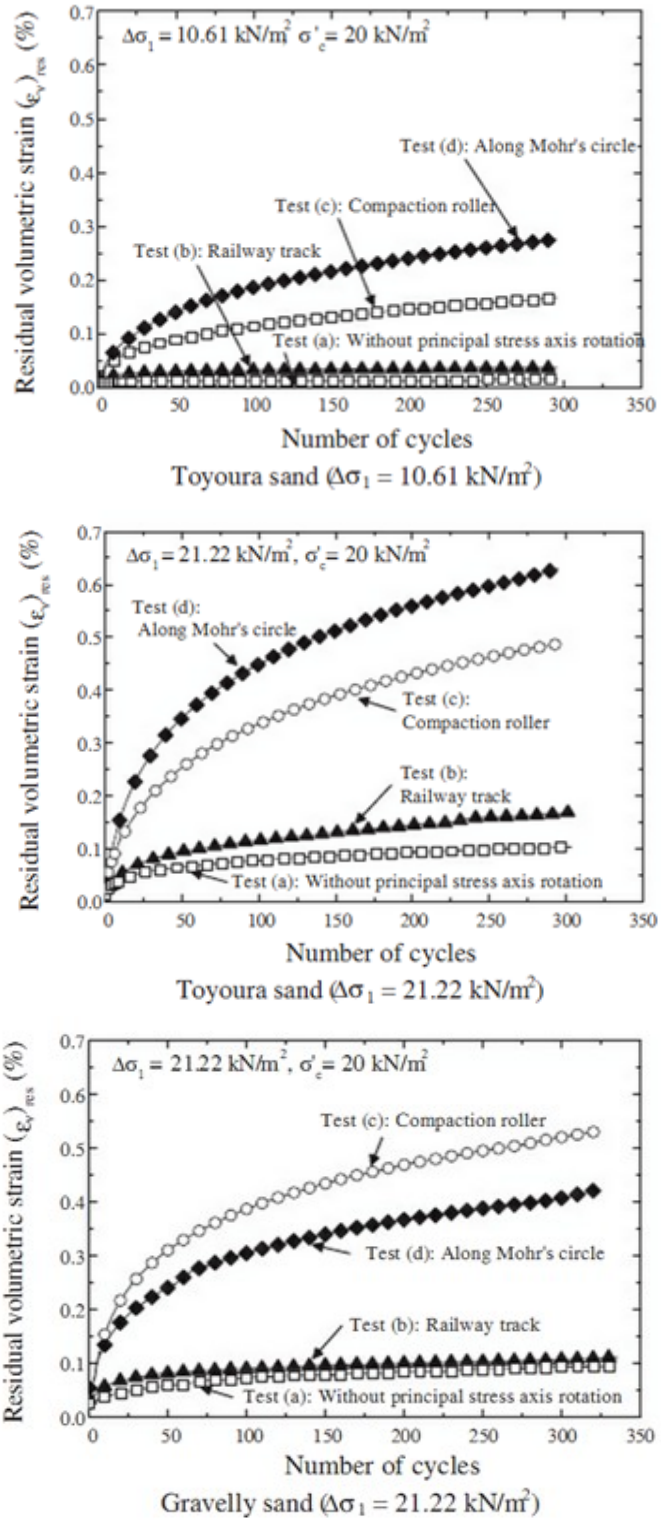

Figure 2.5: Residual volumetric strains under cyclic loading tests with and without principal stress rotation. From Momoya et al. (2007)

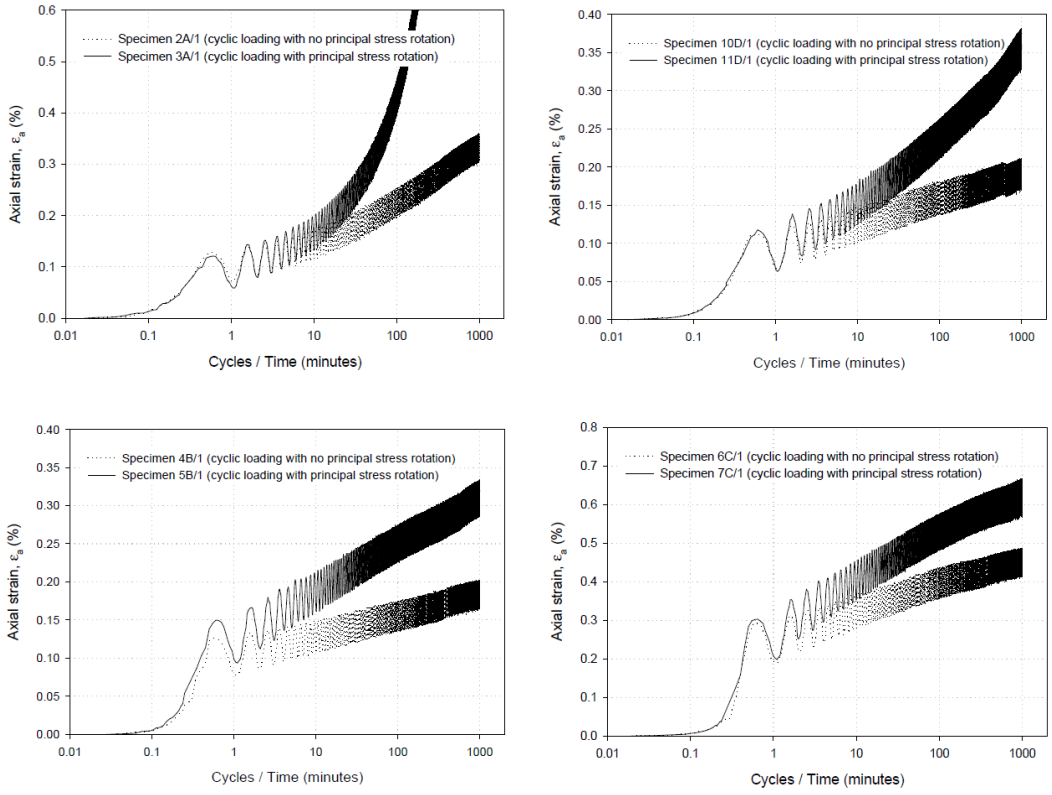

Figure 2.6: Axial strain accumulation of the 7%,11%,14%,24% clay mixes (corresponding to specimen A, D, B, C respectively) with and without principal stress rotation. From Gräbe (2002).

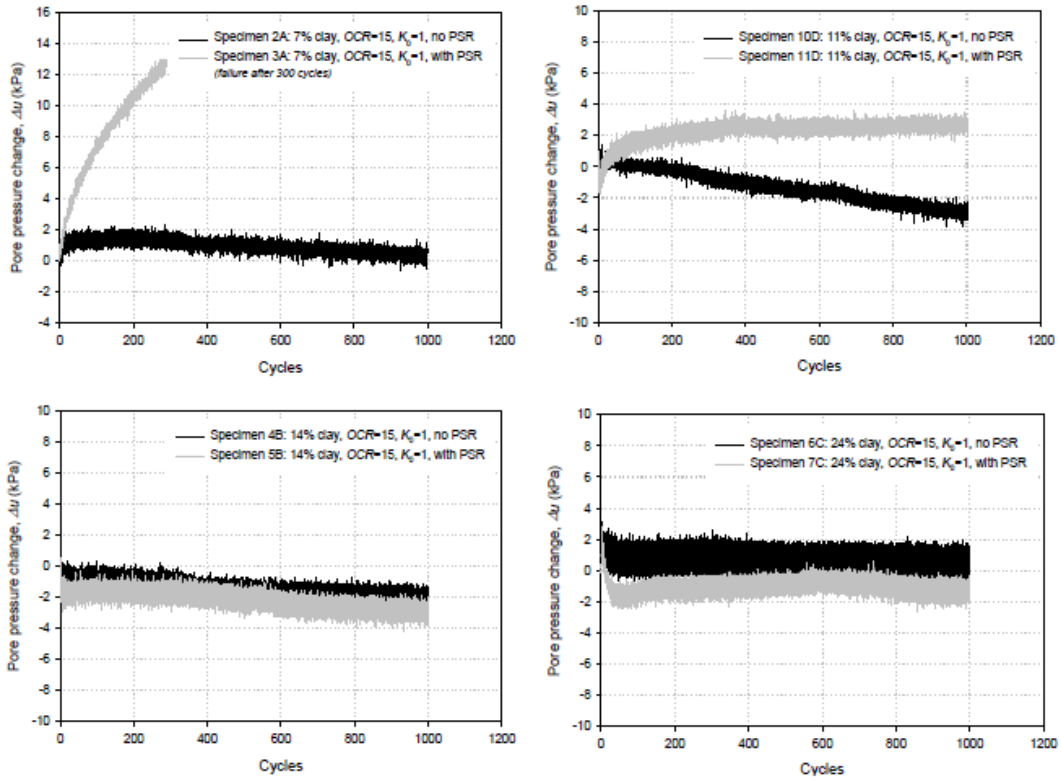

Figure 2.7: Excess pore pressure accumulation of the 7%,11%,14%,24% clay mixes with and without principal stress rotation. From Gräbe (2002).

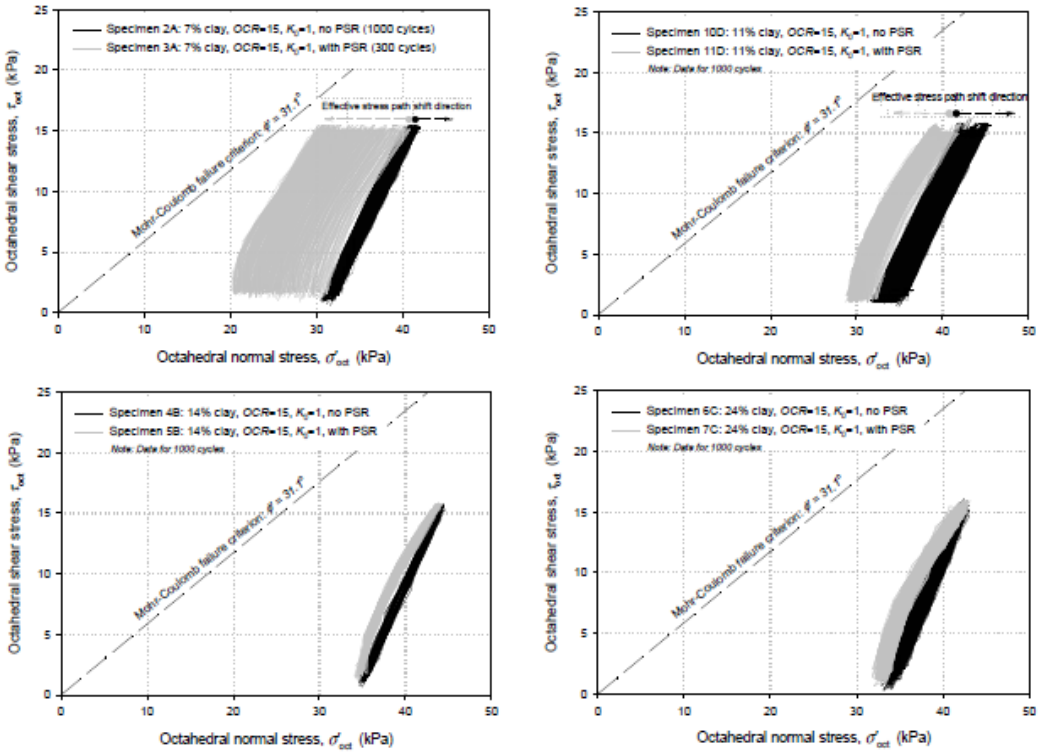

Figure 2.8: Stress path of the 7%,11%,14%,24% clay mixes with and without principal stress rotation. From Gräbe (2002).

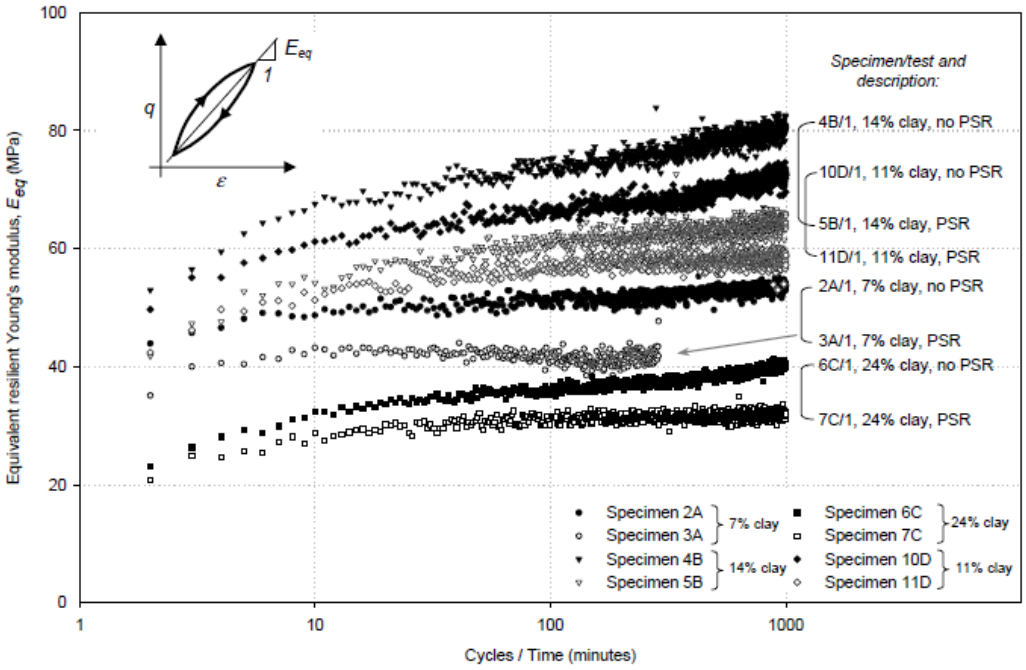

Figure 2.9: Equivalent resilient Young's modulus of the 7%,11%,14%,24% clay mixes with and without principal stress rotation. From Gräbe (2002).

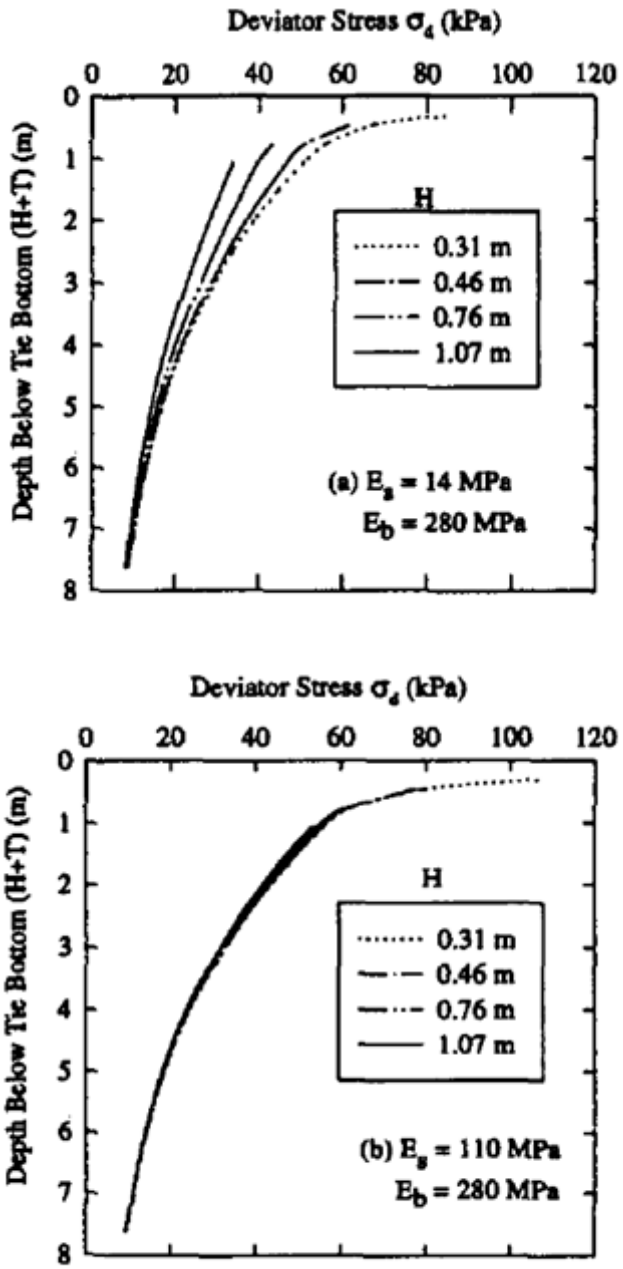

Figure 2.10: FEA using the GEOTRACK model of the distribution of deviator stress below the tie bottom for a (a) soft subgrade (b) stiff subgrade. From Li & Selig (1998).

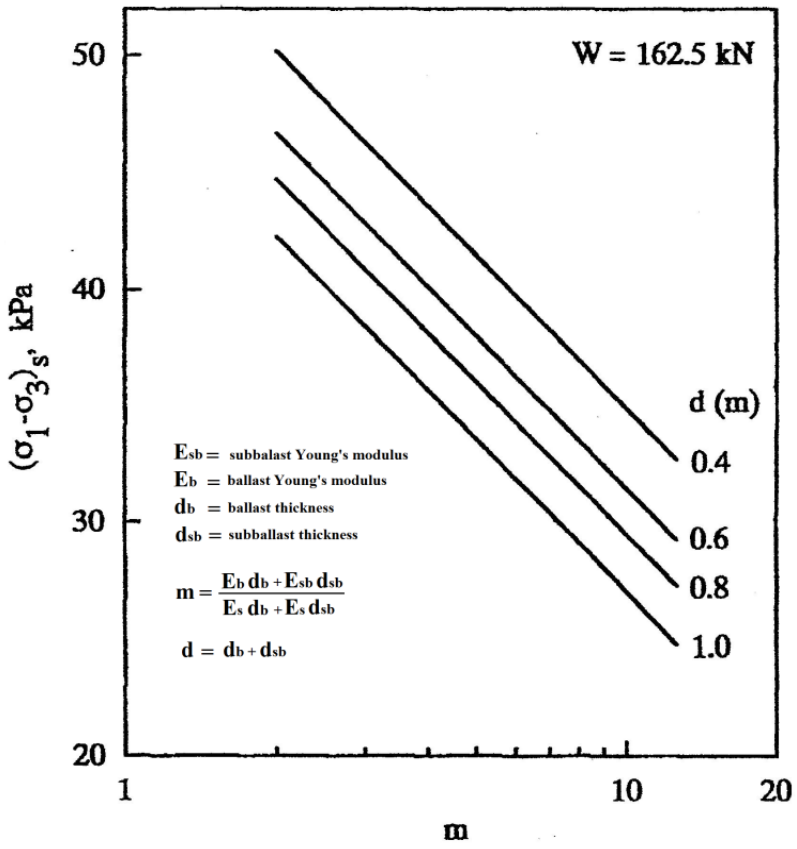

Figure 2.11: FEM showing the variation of deviator stress on top of the subgrade beneath the rail seat with the modular stiffness ratio m and the thickness of the ballast and subballast. Modified from Shahu et al. (2000).

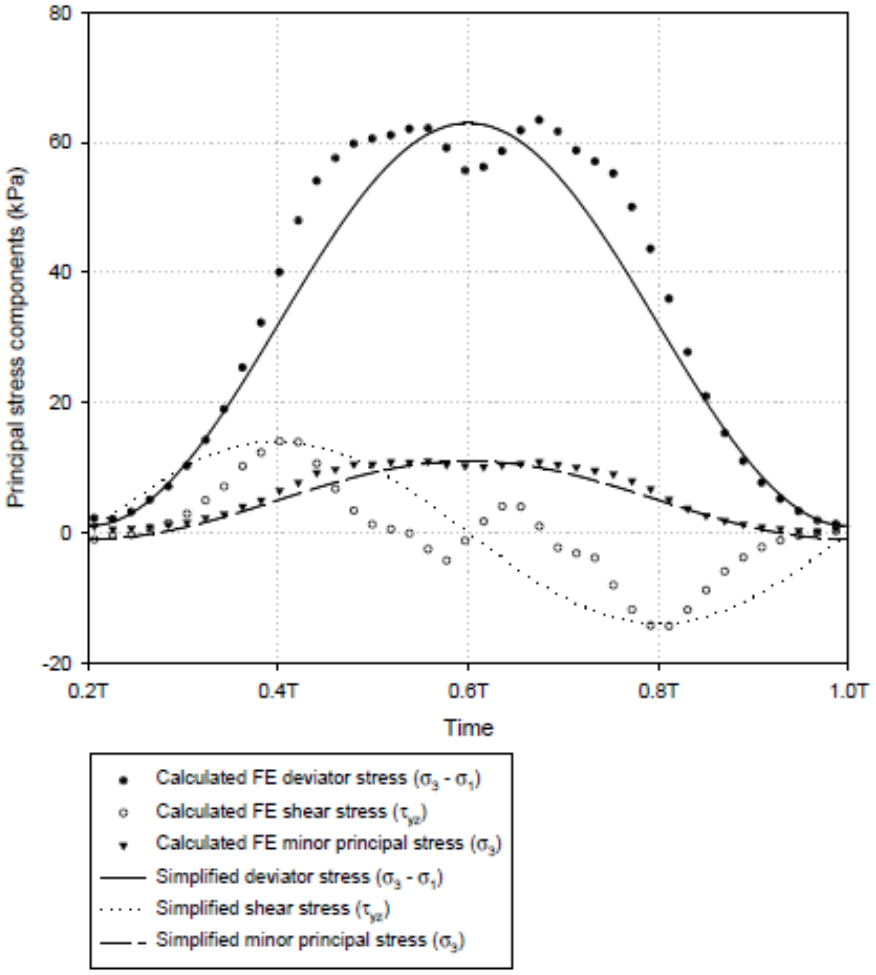

Figure 2.12: FEA of stress changes 0.5m below foundation level on the centre line of the railway track. From Gräbe (2002).

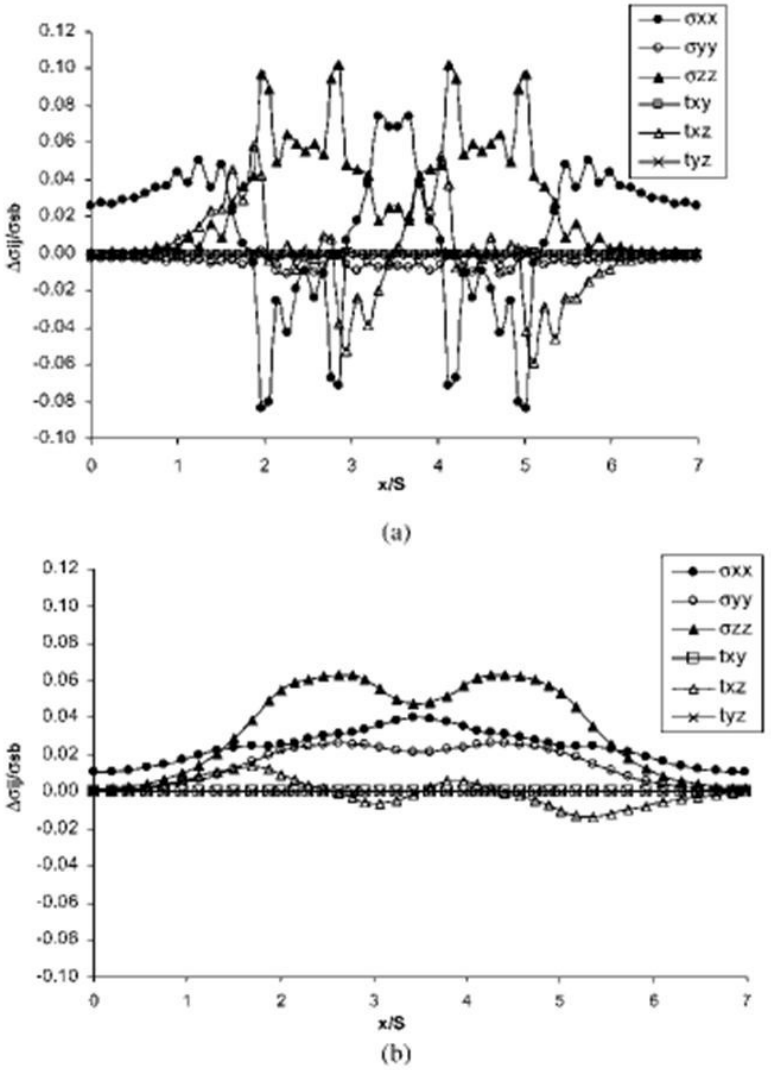

Figure 2.13: FEA of stress changes 0m and 0.7m below foundation level on the centre line of the railway track. From Powrie et al. (2007).

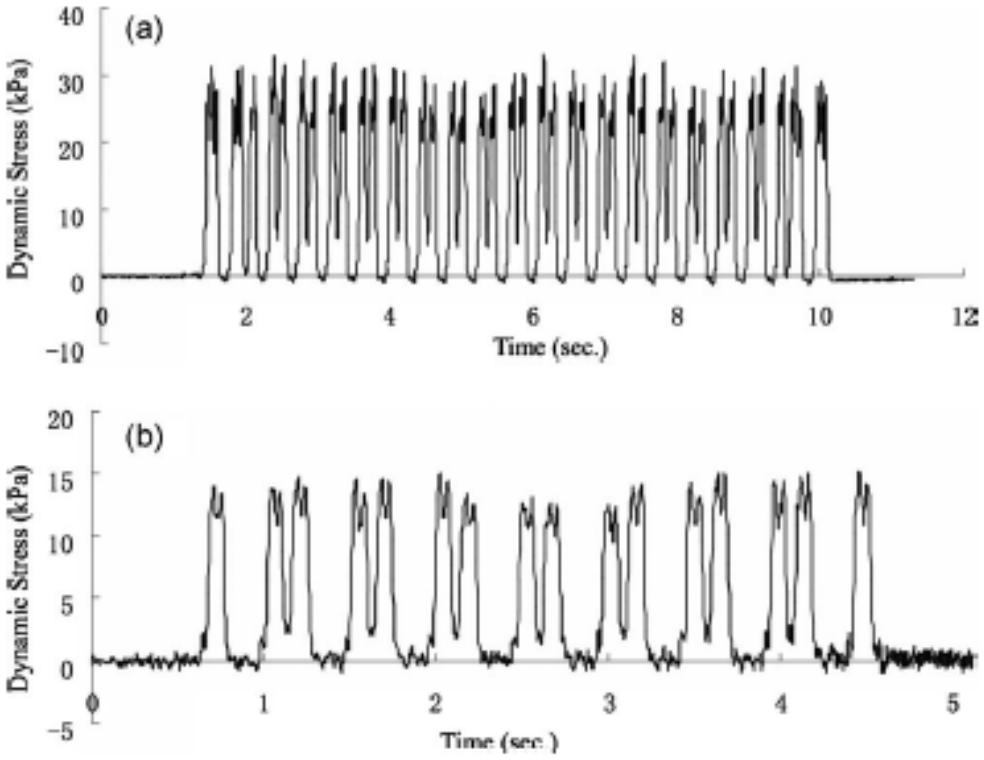

Figure 2.14: In situ stress change measurement on the sub-grade surface resulting from (a) 120km/h freight train (b) 200km/h driven vehicle set passenger train. From Liu & Xiao (2010).

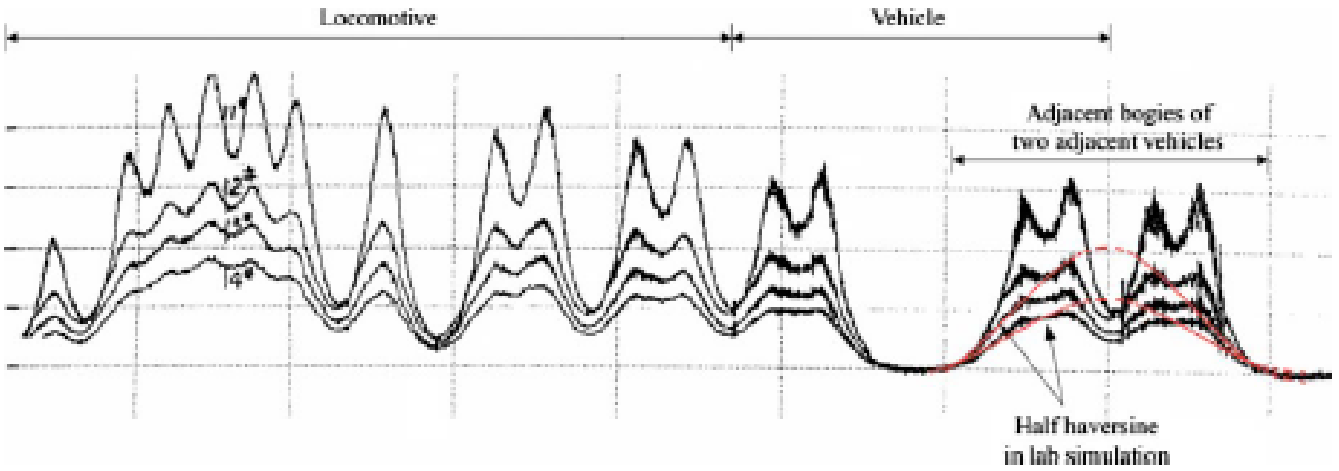

Figure 2.15: Stress pulse shape at different depths within the sub-grade. Note: point 11# was located on the sub-grade surface situated below 0.25m thick ballast and 0.40m thick medium coarse sand and points 12#, 13#, and14# were situated 0.25,0.50, and 0.80m,. From Liu & Xiao (2010).

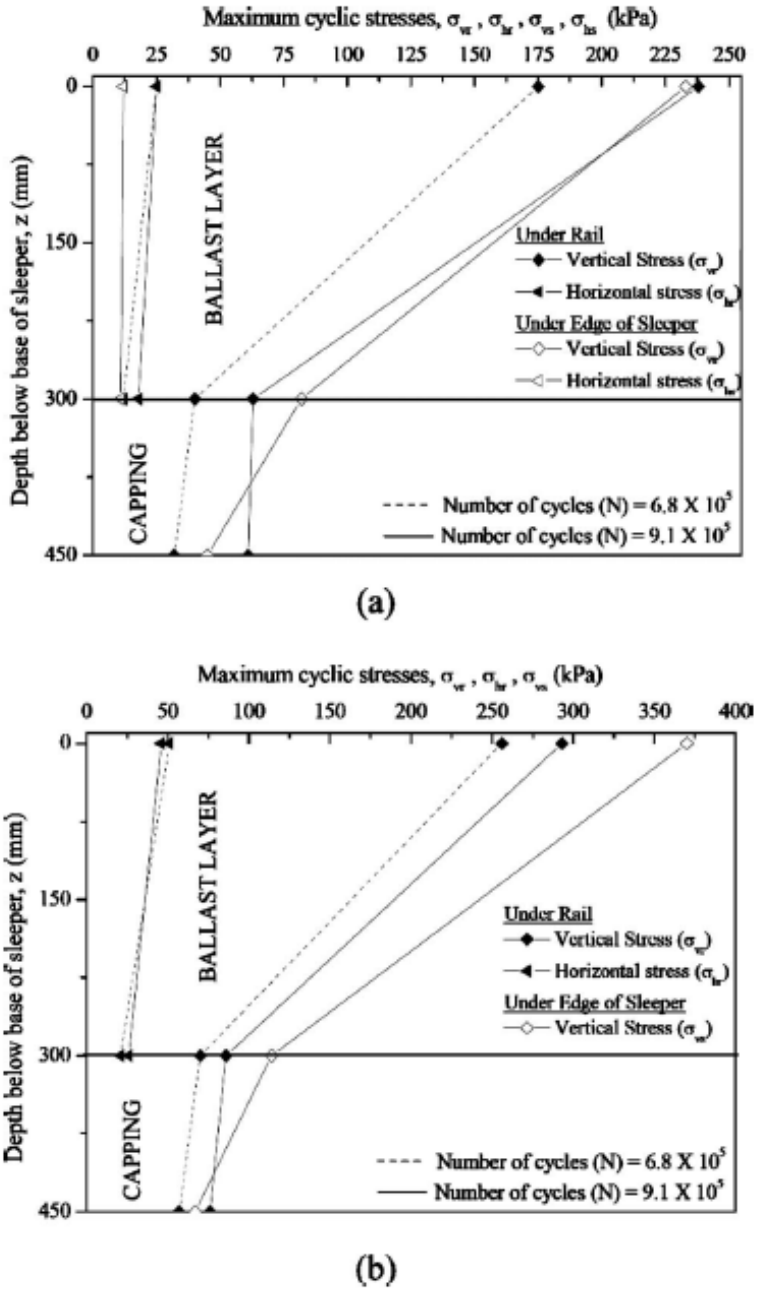

Figure 2.16: Vertical and horizontal maximum cyclic stresses obtained from field measurements during the passage (a) passenger train with 82 class locomotive (b) coal train with a 25 tons/axle configuration. From Indraratna et al. (2010).

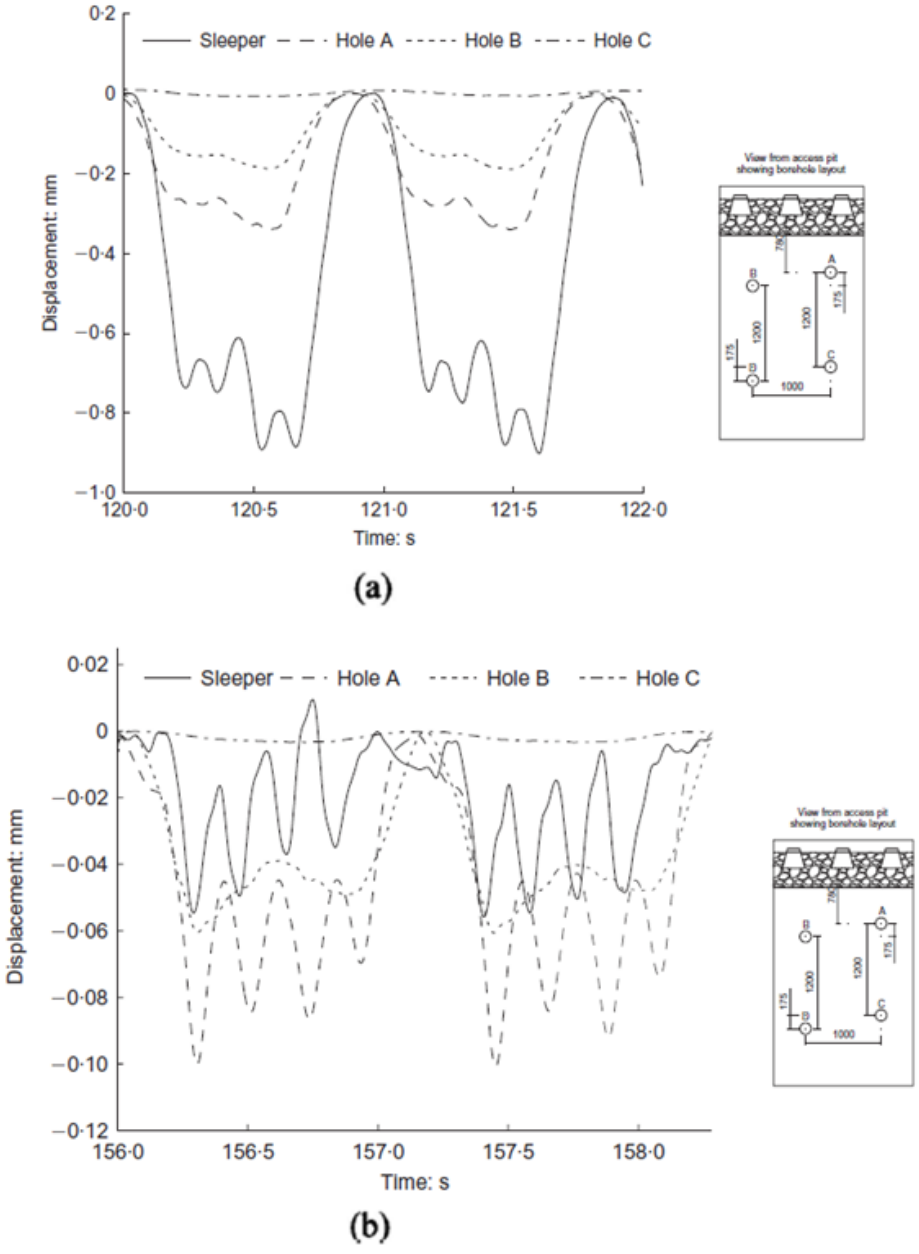

Figure 2.17: In situ measured (a) vertical and (b) horizontal displacement of the sleeper and boreholes located at the centre line of the railway track during the passage of 20tons axle loads. Modified from Priest et al. (2010).

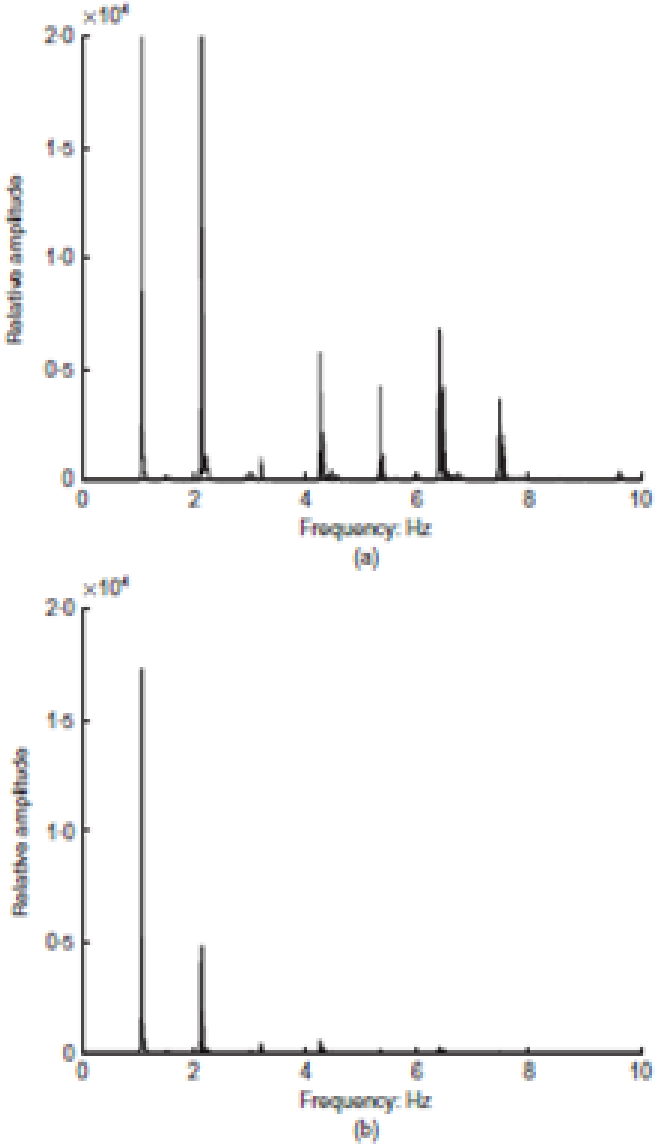

Figure 2.18: Power spectrum analysis obtained from vertical velocity data. (a) at the sleeper, illustrating the domineering 1Hz adjacent bogies loads (b)0.78m below the bottom of the sleeper illustrating the attenuation of 6Hz axle loads. From Priest et al. (2010).

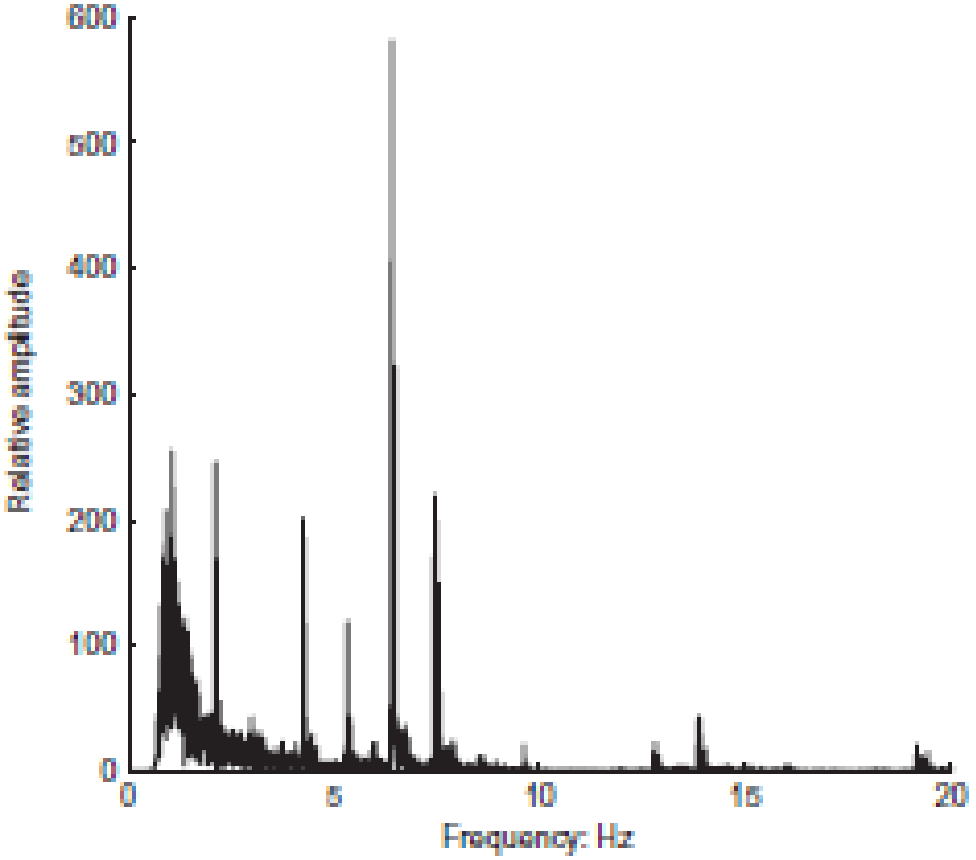

Figure 2.19: Power spectrum analysis of velocity data obtained from horizontal geophones attached to the sleeper illustrating the domineering 6Hz axle loads. From Priest et al. (2010).

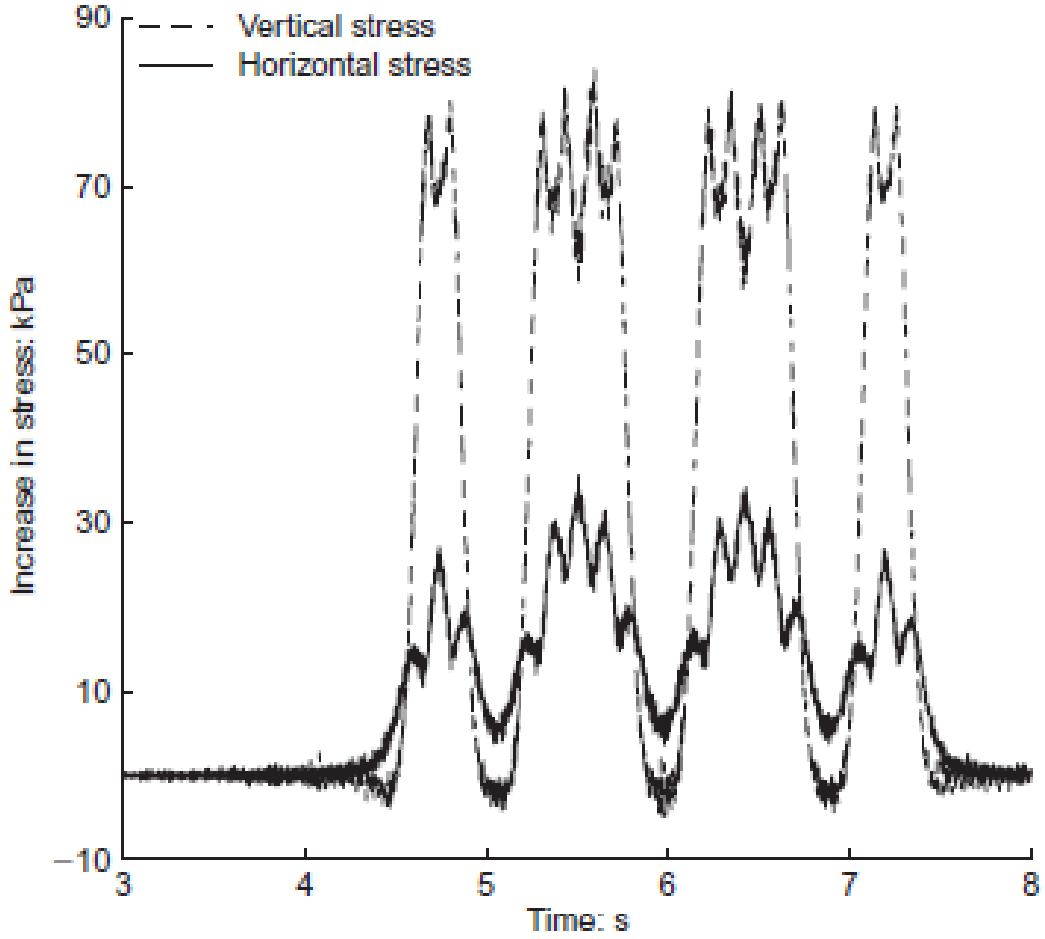

Figure 2.20: FEA of the vertical and horizontal stress changes back calculated from in situ displacement measurements for an element situated 0.8m below the bottom of the sleeper during the passage of a three-wagon train. From Priest et al. (2010).

Chapter 3

EXPERIMENTAL METHODS

The literature discussed in Chapter 2 identified the Hollow Cylinder Apparatus (HCA) as an appropriate tool to study principal stress rotation in the laboratory. This chapter begins with an introduction of the operational characteristics of the University of Southampton HCA before continuing with a detailed description of the data reduction techniques, which involve the use of average stress and strains. The mechanical characteristics of the materials investigated are then introduced, and the specimen preparation and testing techniques developed in this research are described.

3.1 Operational characteristics of the hollow cylinder apparatus

The apparatus used in this research was the Small Strain Hollow Cylinder Apparatus (SS-HCA), developed by Gräbe (2002) and GDS Instruments Ltd (Figure 3.1). In the HCA a hollow cylindrical specimen can be subjected to axial load F, torque T about a central

vertical axis and internal and external radial pressures p_i and p_o (Figures 3.2-3.3). The application of torque T induces shear stresses $\tau_{z\theta}$ on the horizontal planes and complementary shear stresses $\tau_{\theta z}$ on the vertical radial planes. The axial load F contributes to vertical stress σ_z and finally differences in the inner and outer cell pressures produces a gradient in radial stress σ_r.

The axial load is generated by the servomotor, which is attached to the base of the ball screw by a high stiffness zero backlash toothed belt drive (Figure 3.4). Rotation of the ball screw causes the ball nut to move axially, which is translated into axial motion in the ram. In addition to the axial movement, rotation is provided by the servomotor, attached to the shaft through a high stiffness zero backlash toothed belt drive. Control of the load/displacement and torque/rotation is achieved through high speed data acquisition and control cards. Load/displacement and torque/rotation values can be set to follow a sinusoidal waveform pattern. The SS-HCA can therefore be used to investigate the effects of cyclic rotations in principal stresses on the behaviour of soils.

3.2 Stress and strain in a hollow cylinder specimen

3.2.1 Data reduction methodology

The application of torque can be used to control the magnitude and orientation of principal stresses. However, because the thickness of the specimen wall is finite, the application of torque leads to variations of $\tau_{z\theta}$ across the hollow cylinder wall, which in turn may result in a non-uniform distribution of σ_z,σ_r,σ_θ. This is not the only potential source of stress non-uniformities. Differences between the inner and outer cell pressure can change the specimen's wall curvature, giving rise to variations in σ_r and σ_θ. Non–uniformities of stress and strain can also be introduced by the frictional restraint and stiffness of the end platens, which are necessary for the transmission of torque. Restraint on radial displacement at the ends of the specimen can develop radial shear stresses τ_{zr}

and complementary shears τ_{rz}. The presence of τ_{rz} would mean that σ_r would no longer be a principal stress throughout the test, however its effect decreases with distance from the end platens. Stress-strain non-uniformities may also arise due to second order P-δ effects. If the specimen is misaligned the axial load is applied eccentrically, creating a bending moment that causes stress non-uniformity.

Because of the varying stresses in the wall of the cylindrical specimen, tests in the HCA are interpreted using average stresses and strains. The equations for $\bar{\sigma}_z$ and $\bar{\sigma}_\theta$ are based on equilibrium considerations and the average strains $\bar{\varepsilon}_z$ and $\bar{\gamma}_{\theta z}$ are based on strain compatibility; thus the resulting expressions are always valid and independent of the constitutive law of the material. The expressions used for the remaining averages of stress and strain are derived assuming a linear elastic distribution of $\bar{\sigma}_r$, a uniform stress distribution for $\bar{\tau}_{z\theta}$ and a linear variation of radial displacement $\bar{\varepsilon}_r$ and $\bar{\varepsilon}_\theta$ across the wall (Hight et al., 1983).

$$\bar{\sigma}_z = \frac{F}{\pi\left(r_o^2 - r_i^2\right)} + \frac{\left(p_o r_o^2 - p_i r_i^2\right)}{\left(r_o^2 - r_i^2\right)} \tag{3.1}$$

$$\bar{\sigma}_\theta = \frac{\left(p_o r_o - p_i r_i\right)}{\left(r_o - r_i\right)} \tag{3.2}$$

$$\bar{\varepsilon}_z = \frac{\Delta H}{H} \tag{3.3}$$

$$\bar{\gamma}_{\theta z} = \frac{2\theta\left(r_o^3 - r_i^3\right)}{3H\left(r_o^2 - r_i^2\right)} \tag{3.4}$$

$$\bar{\sigma}_r = \frac{\left(p_o r_o + p_i r_i\right)}{\left(r_o + r_i\right)} \tag{3.5}$$

$$\bar{\tau}_{\theta z} = \frac{3T}{2\pi\left(r_o^3 - r_i^3\right)} \tag{3.6}$$

$$\bar{\varepsilon}_r = -\frac{\left(\Delta r_o - \Delta r_i\right)}{\left(r_o - r_i\right)} \tag{3.7}$$

$$\bar{\varepsilon}_\theta = -\frac{\left(\Delta r_o + \Delta r_i\right)}{\left(r_o + r_i\right)} \tag{3.8}$$

with r_o, r_i the inner and outer radii of the hollow cylinder specimen prior to any deformation, H the initial height, ΔH the axial displacement, θ the angular circumferential displacement and Δr_o, Δr_i the inner and outer radial displacement (Figure 3.3)

3.2.2 Stress corrections due to membrane restraint

The difference between the surrounding cell pressure and pore water pressure can cause the membrane to penetrate into the specimen's voids influencing the accuracy of the volumetric strain measurements. The magnitude of membrane penetration will depend on the soil's particle size distribution, density, magnitude of effective stress and can be significant for coarse grained soils. In this research the specimens were well graded, prepared at relatively high dry densities and tested at low effective stresses and as such membrane penetration effects were insignificant.

Additionally the membrane can restrain the lateral movement of particles, thereby affecting the axial load and torque carried by the specimen. Assuming the specimen retains a right cylinder geometry, the stress corrections due to membrane restraint for hollow cylinder specimens can be obtained by the theory of elasticity using a Poisson's ratio of 0.5 for rubber from the following equations (Tatsuoka et al., 1986).

$$\Delta\bar{\sigma}_z = -\frac{4}{3}\frac{E_m t_m}{{r_o}^2 - {r_i}^2}\left[r_o\left\{2\left(\bar{\varepsilon}_{zm}\right)_o + \left(\bar{\varepsilon}_{\theta m}\right)_o\right\} + r_i\left\{2\left(\bar{\varepsilon}_{zm}\right)_i + \left(\bar{\varepsilon}_{\theta m}\right)_i\right\}\right] \tag{3.9}$$

$$\Delta\bar{\sigma}_r = -\frac{2}{3}\frac{E_m t_m}{r_o + r_i}\left[\left\{\left(\bar{\varepsilon}_{zm}\right)_o + 2\left(\bar{\varepsilon}_{\theta m}\right)_o\right\} - \left\{\left(\bar{\varepsilon}_{zm}\right)_i + 2\left(\bar{\varepsilon}_{\theta m}\right)_i\right\}\right] \tag{3.10}$$

$$\Delta\bar{\sigma}_\theta = -\frac{2}{3}\frac{E_m t_m}{r_o - r_i}\left[\left\{\left(\bar{\varepsilon}_{zm}\right)_o + 2\left(\bar{\varepsilon}_{\theta m}\right)_o\right\} + \left\{\left(\bar{\varepsilon}_{zm}\right)_i + 2\left(\bar{\varepsilon}_{\theta m}\right)_i\right\}\right] \tag{3.11}$$

$$\Delta\bar{\tau}_{\theta z} = -2E_m t_m \frac{\left({r_o}^3 + {r_i}^3\right)}{\left({r_o}^3 - {r_i}^3\right)(r_o + r_i)}\bar{\gamma}_{\theta z} \tag{3.12}$$

with E_m and t_m the Young Modulus and average thickness of the membrane respectively, $\left(\bar{\varepsilon}_{zm}\right)_o$ and $\left(\bar{\varepsilon}_{zm}\right)_i$ the average axial strains in the outer and inner membranes and $\left(\bar{\varepsilon}_{\theta m}\right)_o$ and $\left(\bar{\varepsilon}_{\theta m}\right)_i$ the average circumferential strains in the outer and inner membranes respectively. The strains in the membranes can be calculated from

$$\left(\bar{\varepsilon}_{zm}\right)_o = {\varepsilon_{zm}}^* + \varepsilon_{zc} + \bar{\varepsilon}_z \tag{3.13}$$

$$\left(\bar{\varepsilon}_{\theta m}\right)_i = {\varepsilon_{\theta m}}^* + \varepsilon_{\theta c} + \bar{\varepsilon}_\theta \tag{3.14}$$

with ${\varepsilon_{zm}}^*$ and ${\varepsilon_{\theta m}}^*$ the initial membrane strains at the setting up of the specimen, and ε_{zc} and $\varepsilon_{\theta c}$ the axial and radial strains during consolidation and finally $\bar{\varepsilon}_z$ and $\bar{\varepsilon}_\theta$, the average axial and circumferential strains during torsional shear.

Assuming that the average axial strain of the specimen since set-up is equal to the axial strains of the inner and outer membranes $\left(\bar{\varepsilon}_{zm}\right)_o = \left(\bar{\varepsilon}_{zm}\right)_i = \left(\bar{\varepsilon}_{zm}\right)$ and that the circumferential strains of the inner and outer membranes are equal to the circumferential

strains of the adjacent radial section of the specimen $\left(\bar{\varepsilon}_{\theta m}\right)_o = \left(\bar{\varepsilon}_{\theta m}\right)_i = \left(\bar{\varepsilon}_{\theta m}\right)$, equations 3.9-3.11 can be simplified to (Gräbe, 2002)

$$\Delta\bar{\sigma}_z = -\frac{4}{3}\frac{E_m t_m}{r_o - r_i}\left[\left\{2\left(\bar{\varepsilon}_{z m}\right) + \left(\bar{\varepsilon}_{\theta m}\right)\right\}\right] \tag{3.15}$$

$$\Delta\bar{\sigma}_r = 0 \tag{3.16}$$

$$\Delta\bar{\sigma}_\theta = -\frac{2}{3}\frac{E_m t_m}{r_o - r_i}\left[\left\{2\left(\bar{\varepsilon}_{z m}\right) + 4\left(\bar{\varepsilon}_{\theta m}\right)\right\}\right] \tag{3.17}$$

Based on the above corrections, for each stress component the true stresses $\bar{\sigma}_{z_{cor}}$, $\bar{\sigma}_{\theta_{cor}}$, $\bar{\tau}_{\theta z_{cor}}$ and the corresponding principal stresses may therefore be obtained as

$$\bar{\sigma}_{z_{cor}} = \bar{\sigma}_z + \Delta\bar{\sigma}_z \tag{3.18}$$

$$\bar{\sigma}_{\theta_{cor}} = \bar{\sigma}_\theta + \Delta\bar{\sigma}_\theta \tag{3.19}$$

$$\bar{\tau}_{\theta z_{cor}} = \bar{\tau}_{\theta z} + \Delta\bar{\tau}_{\theta z} \tag{3.20}$$

3.2.3 Generalised stress space parameters

Based on the stress corrections due to membrane restraint the magnitude of total principal stresses can be obtained as

$$\sigma_1 = \left(\frac{\bar{\sigma}_{z_{cor}} + \bar{\sigma}_{\theta_{cor}}}{2}\right) + \sqrt{\left(\frac{\bar{\sigma}_{z_{cor}} - \bar{\sigma}_{\theta_{cor}}}{2}\right)^2 + \bar{\tau}_{\theta z_{cor}}^{\,2}} \tag{3.21}$$

$$\sigma_2 = \overline{\sigma_r} \tag{3.22}$$

$$\sigma_3 = \left(\frac{\bar{\sigma} z_{cor} + \bar{\sigma} \theta_{cor}}{2} \right) - \sqrt{\left(\frac{\bar{\sigma} z_{cor} - \bar{\sigma} \theta_{cor}}{2} \right)^2 + \bar{\tau} \theta z_{cor}^{\,2}} \tag{3.23}$$

The orientation of the major principal total stress σ_1 to the vertical α will change according to Equation (3.24) with α varying between 0^o and 90^o (Hight et al., 1983).

$$\alpha = \frac{1}{2} tan^{-1} \frac{\left(2\bar{\tau} \theta z_{cor} \right)}{\left(\bar{\sigma} z_{cor} - \bar{\sigma} \theta_{cor} \right)} \tag{3.24}$$

The intermediate principal stress parameter, which gives the relative magnitude of σ_2 with respect to σ_1 and σ_3, may be calculated using Eq. (3.25), with b taking values between 0 and 1. For the specific case of equal internal and external pressures as is the case in this research, the relationship between the intermediate principal stress parameter and the orientation of the major principal stress to the vertical reduces to Eq. (3.26).

$$b = \frac{(\sigma_2 - \sigma_3)}{(\sigma_1 - \sigma_3)} \tag{3.25}$$

$$b = sin^2 \alpha \tag{3.26}$$

In this research inner and outer pressures were kept equal so as to avoid stress strain non-uniformities arising from changes in the specimen wall curvature. Although cycling the surrounding pressure of the specimen may be a more realistic representation of train

loading, data presented by Gräbe (2002) suggest that this had an insignificant effect on the resilient response of the investigated materials. Finally the mean effective stress *p'* and deviator stress *q* can be calculated as (Wood, 1984; Powrie, 2004)

$$p' = \frac{\sigma'_1 + \sigma'_2 + \sigma'_3}{3} \tag{3.27}$$

$$q = \frac{1}{\sqrt{2}}\sqrt{(\sigma'_1 - \sigma'_2)^2 + (\sigma'_1 - \sigma'_3)^2 + (\sigma'_2 - \sigma'_3)^2} \tag{3.28}$$

with σ'_1 , σ'_2 and σ'_3 the effective principal stresses.

3.2.4 Instrumentation for the measurement of stress-strain

To obtain realistic stiffness values, axial strains are measured locally on the specimen so as to exclude bedding errors associated with the misalignment of specimen ends and also to exclude strains associated with apparatus compliance (parts of the apparatus compressing under increasing axial load) (Jardine et al., 1984; Clayton & Khatrush, 1986; Cuccovillo & Coop, 1997; Atkinson, 2000; Clayton & Heymann, 2001; Simpson, 2010).

Although local instrumentation for the measurement of strains is relatively widespread in triaxial tests (Cresswell & Powrie, 2004; Gasparre, 2005; Bhandari, 2009; Alvarado et al., 2012) use of local instrumentation in the HCA is less common. A review of different strain measurement methodologies reported by different researchers in the context of HCA test is provided in Table 3.1. In this research local instrumentation was used for the measurement of strains (Table 3.1 and Figure 3.5). Measurements of axial strain were obtained from two LVDTs mounted at opposite positions over the central half of the

specimen. In addition displacement was also measured globally through the axial actuator motor shaft encoder. The global axial strain $\varepsilon_{z_{glo}}$ was calculated as the change in height of the specimen ΔH measured by the actuator motor shaft encoder divided by the initial height of the specimen H.

$$\varepsilon_{z_{glo}} = \frac{\Delta H}{H} \tag{3.29}$$

The average local axial strain ε_{local} was calculated as the average of readings from the LVDTs positioned on opposite sides of the specimen. The axial strain was obtained by dividing the measured displacement ΔH_{local} by the spacing of the brackets holding the LVDT H_{local} (Figure 3.6).

$$\varepsilon_{local} = \frac{\Delta H_{local}}{H_{local}} \tag{3.30}$$

The change in the outer diameter of the specimen was measured by an LVDT attached to a radial caliper. Due to the arrangement of the caliper geometry (pinned at one end) the change in the outer diameter was calculated as half the recorded displacement measured by the LVDT (Figure 3.6) (Bhandari, 2009). The change in the inner r_i radius was calculated by assuming the specimen retained a cylindrical shape during deformation.

$$r_i = r_{i_O}\sqrt{\frac{1+(\Delta V_i/V_i)}{1+(\Delta H/H)}} \tag{3.31}$$

with r_{i_O}, V_i and H the initial inner radius, inner volume and specimen height respectively and ΔV_i and ΔH the change in inner volume and specimen height.

Circumferential displacements were measured semi-locally (platen to platen) by the radial actuator shaft encoder. The Force F and Torque T were measured through the combined Load and Torque cell located at the top of the specimen. The inner and outer cell pressure and the applied back pressure were controlled and measured by GDS Ltd Pressure Controllers. Pore pressures were measured at the top and bottom of the specimen by high resolution Druck Pressure Transducers.

3.2.4.1 Calibration of the instrumentation

Calibration of a transducer is the process of correlating the output mV with the actual physical quantity trying to be measured. The objective of the calibration is to determine how accurately a true value is measured. The calibration details of all the instrumentation utilised in this research are presented in Table 3.3 and Figures 3.7-3.15. The LVDTs were calibrated over their design range with the use of a micrometer. The Load Cell as well as the Druck Pressure Transducers were calibrated against a Budenberg dead weight tester. This apparatus operates on the principle of balancing the pressure between a piston loaded by dead weights and the pressure at the outlet port. The Torque Transducer was calibrated using a purpose built torque calibration frame following the procedure described in detail by Gräbe (2002).

3.2.5 Stress-strain non-uniformities and hollow cylinder geometry

Stress-strain non-uniformities across the wall of a hollow cylinder specimen arising from wall curvature, end restraint and the application of torque are geometry dependent. In an infinitely tall and thin hollow cylinder these effects would be minimised. A number of studies have been reported, which investigated the effects of changes in the hollow cylinder geometry on the non-uniform distribution of stress and strain. Based on the

assumption of a thin elastic cylindrical shell, Saada & Townsend (1981) established the following set of geometric criteria to minimise non-uniformities

$$\left.\begin{array}{l} \dfrac{H}{\sqrt{\left(r_o{}^2 - r_i{}^2\right)}} \geq 5.44 \\ \dfrac{r_i}{r_o} \geq 0.65 \end{array}\right\} \tag{3.32}$$

Hight et al. (1983) questioned the validity of these criteria arguing that it assumes a central zone free from end restraint effects, which is of the same length as the zone influenced by the end restraint effects. The effect of end restraint on the non-uniform stress distribution was investigated analytically by Hight et al. (1983). The linear elastic numerical analysis demonstrated that the distribution of $\sigma_\theta$and $\sigma_z$was more sensitive to height than to changes in the inner and outer diameter of the specimen. On the other hand, experimental results from Lade (1981) reported that little improvement in terms of stress-strain uniformity was achieved by changing the ratio of the specimen height to the mean diameter beyond 1.5. Sayao & Vaid (1991) performed numerical analysis to investigate the relationship between different hollow cylinder geometries and the stress non uniformities arising from curvature and end restraint, and established the following geometric criteria, for limiting non-uniformities.

$$\left.\begin{array}{l} r_o - r_i = 20 - 26mm \\ 0.65 \leq \dfrac{r_i}{r_o} \leq 0.82 \\ 1.8 \leq \dfrac{H}{2r_o} \leq 2.2 \end{array}\right\} \tag{3.33}$$

A summary of hollow cylinder geometries used by different researchers and their conformity to the geometric criteria set out by Saada & Townsend (1981) and Sayao & Vaid (1991) is presented in Table 3.3. As can be seen the selected specimen dimensions in this research were in good agreement with both Saada & Townsend (1981) and Sayao & Vaid (1991) criteria.

3.3 Experimental Methodology

3.3.1 Material properties

The sand-clay mixes investigated in this research were selected so as to replicate the gradation of the railway track foundation material used in the South African Coal Line. The South African Coal Line is a well documented case study, including laboratory investigations field measurements and numerical analysis (Gräbe, 2002; Gräbe et al., 2005; Gräbe & Clayton, 2009; Priest et al., 2010; Otter, 2011)

Four different mixes were investigated which had varying amounts of Leighton Buzzard sand fraction B (LBSFB), fraction C (LBSFC), fraction D (LBSFD), Hymod Prima Clay (HPC) and Oakamoor HPF5 silica flour silt. Scanning electron micrographs of the particle shape of some of the constituent materials are presented in Figure 3.16. As can be observed, the sand fractions had a rounded to sub-rounded particle shape and the Hymod Prima Clay the characteristic platy shaped form.

The aggregate composition and quantities of the different sand-clay mixes as a percentage of the total dry mix weight along with the Atterberg values of the different mixes are presented in Tables 3.4-3.6. The HPF4 silt used by Gräbe (2002) was no longer commercially available for this research, so the HPF5 silt was selected as the closest fit to the gradation of HPF4. The grading curves of the investigated mixes reveal that a good fit with the grading envelope of the coal line material was achieved (Figure 3.17).

3.3.2 Specimen preparation method

In this research the specimens were prepared by compaction to replicate the in situ material placement processes. During compaction the efficiency of the particle packing can be controlled by the number of compaction layers, the number of blows applied per layer, the moisture content and weight of the hammer. In the laboratory, the two most

common compaction methods are the under-compaction technique (Ladd, 1978) and the modified Proctor technique (BS1377-4, 1990). In the modified Proctor compaction technique a constant compaction effort is applied throughout the height of the specimen. As a result the bottom layers tend to be subjected to a higher compaction energy than the top layers, which may give rise to a non-uniform density distribution throughout the specimen. In the under-compaction technique the lower layers are initially subjected to a lower compactive effort and are then further densified as subsequent layers are applied and compacted.

In the past it had been suggested that the under-compaction technique may be more suitable for achieving a uniform density distribution throughout the specimen. However recent radiographic analysis of specimens prepared using the under-compaction technique revealed that density varied throughout the height of the specimen, suggesting that some degree of density variation throughout the specimen may have to be accepted (Frost & Park, 2003). Furthermore a non-uniform density distribution is likely to be more pronounced at very low dry densities and may be less important at higher dry densities such as those prepared in this research. In this research therefore a sand-clay mix at a given clay content was prepared using a constant compaction effort for each layer.

The Proctor compaction curves for the different sand-clay mixes are shown in Figure 3. 18 (Otter, 2011). The modified Proctor technique, BS1377:4 (1990), specifies the construction of specimens in a 1L mould of 105mm diameter, and 115.5mm height. Variations in the compaction curve between different users are to be expected. In this context the Proctor curves served as an initial reference point to extrapolate the required compaction energy to form specimens with a height of 200mm and a diameter of 100mm at a given dry density.

The selected dry density to which the specimens were compacted was dictated by the optimum dry density achieved for the 7% clay mix. The other mixes at 11%,14%,24% clay content were prepared to match this target density so as to allow comparisons between the different materials to be made. Selection of the achieved optimum dry

density of the 7% clay was made on the basis of replicating the in situ process where granular materials are compacted to the optimum dry density. As the clay content increases the Proctor compaction curves flatten out with no well defined optimum dry density, so the clay content is less likely to influence in situ compaction processes.

To achieve a given dry density the compaction energy between different sand-clay mixes at different clay contents was adjusted. For example the 11% clay was compacted in 6 layers with 25 blows per layer, whereas the 24% clay was compacted in 12 layers with 50 blows per layer. The dry densities and corresponding void ratios achieved for the different sand-clay mixes are detailed in Chapter 4.

After compaction a specimen was transferred to a soil lathe to create a hollow cylindrical specimen with an internal diameter of 60mm. The specimen, contained in the three part split mould with a jubilee clip, was carefully placed on the base of the soil lathe. After the verticality of the specimen had been checked and corrected, the upper plate of the soil lathe was lowered and brought into contact with the specimen so as to secure the specimen into position throughout the drilling process. The drilling of the specimen was executed using a bottom - up approach, so as to allow the excess soil to be removed by gravity from the bottom.

3.3.3 Hollow cylinder specimen set up

Before the start of every test the inner and outer membranes were carefully inspected for possible punctures. Furthermore, and owing to the complicated and multiple drainage arrangements in the HCA, all the pipes were put under a high pressure to detect possible leakages. Figure 3.19 illustrates the components of the hollow cylinder set up. A detailed description of the sequence of steps followed in the specimen set up procedure is given below:

- Two 100 diameter O-rings were stretched over the base pedestal and lower top cap.
- The lower membrane holder was positioned onto the bottom surface of the base pedestal, whose internal surface was covered in a thin layer of silicon grease.
- The upper membrane holder and attached O-ring were threaded through the inner membrane and then secured into place on the base pedestal by 4 screws, which compressed the O-ring and created an air tight seal between the inner membrane and the base pedestal.
- The porous disk with inset blades was fastened onto the base pedestal with 6 screws. The hollow cylinder specimen which was still contained within a 3 part split mould and jubilee clip was carefully threaded through the inner membrane and then positioned onto the lower porous disk on the base pedestal.
- After the verticality of the specimen had been checked and corrected the 3 part split mould was temporarily removed, so as to place the outer membrane around the specimen.
- The lower top cap and attached porous stone were placed onto the top of the specimen.
- The inner membrane was then stretched and folded over the lower top cap and secured into position by 2 O-rings. Throughout this process the specimen was still contained within a 3 part split mould and jubilee clip, so as to minimize disturbance to the specimen.
- A thin layer of silicon grease was applied to the O-ring of the upper top cap, before the latter was placed on top of the lower top cap and secured into position with 9 screws.
- The split mould was removed from the specimen and replaced with a longer one, to contain the specimen as well as the base pedestal and upper cap so as to avoid disturbance to the specimen during the transfer to the HCA.
- The specimen was transferred to the HCA and carefully placed in the HCA and positioned onto the HCA base platen, in such a way so as to align the fixing holes in the lower pedestal with the corresponding holes in the HCA base platen. To

prevent sliding of the base pedestal on the HCA base platen during rotation, the 2 parts were fastened together with 4 screws.

- The specimen was then rotated using the control software, so as to align the fixing holes in the top cap with those in the load cell. Once aligned the top cap was brought into contact with the load cell and secured into position using 4 screws.
- The next step involved the mounting of all the local instrumentation on the specimen. Checks were made throughout to ensure that all transducers were correctly aligned.
- Before lowering the HCA cell a thin layer of silicon grease was applied to the O-ring on the base of the HCA to help create a water tight seal. Once the HCA cell was in place it was secured into position with 6 nuts.
- The valve on the top of the HCA was undone and the tap connecting the top of the inner cell of the hollow cylinder was opened so as to allow the removal of air during filling. Silicon oil was then used to fill the outer and inner chamber of the hollow cylinder specimen.

3.3.4 HCA Testing Procedure

Specimens were formed unsaturated therefore the first step of the testing procedure was to saturate the specimens. The saturation process evolved around two parameters. The time required for water to flow into the soil and compress the air under a given back pressure, which is a permeability problem, and the time required for the bubbles of air to dissolve into the surrounding pore water after they have been compressed, which is a diffusion problem.

A-two stage saturation strategy was adopted. First, carbon dioxide CO_2 was percolated through the specimen to replace the air with a gas of greater solubility and subsequently de-aired water was flushed through the specimen (Lacasse & Berre, 1988). Given that the

permeability of the specimen reduced significantly as the clay content increased it is possible that the carbon dioxide and the de-aired water may have percolated through the perimeter of the specimen rather than through the void space between the particles. Therefore this initial stage was only an augmenting saturation stage and the main saturation stage was based on elevating the pressure of the pore fluid so as to force the CO_2 and any remaining air into solution.

This was achieved by simultaneous elevations of the surrounding pressure and back pressure, so as to maintain the effective stress and not cause any consolidation of the specimen. Once relatively high back pressures in excess of 670kPa were achieved, sufficient time for any air bubbles to compress and dissolve into the surrounding pore water was allowed. During this time the amount of water flowing into the specimen was monitored, and as soon as the water volume inflow stabilised, the surrounding pressure was raised by 50kPa and the corresponding pore pressure change was recorded. A B-value value in excess of 0.97 was taken to indicate sufficient saturation depending on the soil stiffness (Black & Lee, 1973).

All the saturated sand clay mixes were isotropically consolidated to an effective stress of 33kPa, to match the low confining stresses typically measured in railway track foundation in the field (Liu (2006) cited in Liu & Xiao (2010)). The cyclic tests involved simultaneous cyclic changes in the magnitude of the deviator stress and shear stress. Each sand clay mix at 7%,11%,14%,24% clay content was subjected to gradual increases in the magnitude of PSR up to failure so as to explore the widest possible spectrum of changes in PSR typically expected within the foundation layer of the railway track. The stress path was based on the numerical analysis reported by Powrie et al. (2007) as this was identified as the most comprehensive analysis in quantifying the likely stress changes at different depths within a railway track foundation. A detailed description of the investigated stress paths is given in the results Chapter 4. In all the tests reported in this thesis, the axial stress was cycled 90^o degrees out of phase with the torsional shear stress at a cyclic frequency of 0.0083Hz, as this was the frequency at which a consistent response of the software could be achieved. It is accepted that the in situ cyclic loading

frequency of railway track foundations may be considerably higher than 0.0083Hz, and even if the software restrictions could be resolved testing at very high cyclic frequencies may have resulted in a non-uniform pore pressure distribution throughout the specimen.

Researcher	Axial strain measured	Circumferential displacement measured
Present study	Locally	Platen to platen
Cai et al. (2012)	Non Locally	Platen to platen
Georgiannou et al. (2008)	Non Locally	Platen to platen
Dutinne et al. (2007)	Locally	Locally at 1/3 and 2/3 of the specimen height
Chaudhary et al. (2004)	Non Locally	Platen to platen
Gräbe (2002)	Locally	Platen to platen and in some tests locally at 1/3 and 2/3 of the specimen height
Sivathayalan & Vaid (2002)	Non Locally	Platen to platen
Shibuya et al. (1995)	Non Locally	Platen to platen
Ampadu & Tatsuoka (1993)	Non Locally	Platen to platen
Alarcon et al. (1986)	Non Locally	Platen to platen
Tatsuoka et al. (1986)	Non Locally	Platen to platen

Table 3.1: Details of how axial and circumferential strains were measured by different researchers in the HCA.

Transducer	Measurement	Design Range	Calibration Range	Accuracy[2]
Load Torque Cell	Axial load Torque	10kN 100Nm	3kN 8.48Nm	0.0041kN 0.03Nm
Pressure Transducer	Outer Cell Pressure	1000kPa	1000kPa	0.46kPa
Pressure Transducer	Inner Cell Pressure	1000kPa	1000kPa	0.47kPa
Pressure Transducer	Back Pressure	1000kPa	1000kPa	0.28kPa
Pressure Transducer	Pore Pressure	1000kPa	1000kPa	0.34kPa
LVDT	Axial Displacement	±5mm	±5mm	17μm
LVDT	Axial Displacement	±5mm	±5mm	10μm
LVDT	Radial Displacement	±5mm	±5mm	9.7μm

Table 3.2: Details of the instrumentation used in this research and their calibrated accuracy.

[2] The accuracy of the instrumentation was determined assuming a Gaussian distribution of the errors, which gave a confidence level of 95% that the difference between a measured value and the true value would be within the specified accuracy.

Researcher	H(mm)	$2r_o$(mm)	$2r_i$(mm)	$\frac{r_i}{r_o}$	$\frac{H}{\sqrt{{r_o}^2 - {r_i}^2}}$	$r_o - r_i$	$\frac{H}{2r_o}$
Present study	200	100	60	0.6	5	20	2
O'Kelly & Naughton. (2009)	200	100	71	0.71	5.68	14.5	2
Georgiannou et al. (2008)	140	70	40	0.57	4.87	15	2
Duttine et al. (2007)	120	200	160	0.8	2	20	0.6
Nishimura et al. (2006)	200	100	60	0.6	5	20	2
Chaudhary et al. (2004)	200	100	60	0.6	5	20	2
Lee et al. (1999)	230	98	78	0.79	7.75	10	2.34
Shibuya et al. (1995)	120	70	30	0.42	3.79	20	1.71
Turner & Kulhawy. (1992)	142.2	71.1	50.8	0.71	5.71	10.15	2
Alarcon et al. (1986)	200	71	38	0.53	6.69	16.5	2.81
Hight et al. (1983)	254	254	203	0.79	3.32	25.5	1
Iwasaki et al. (1978)	100	100	60	0.6	2.5	20	1

Table 3.3: Hollow cylinder geometries used by different researchers.

	Sand (%)	Silt (%)	Clay (%)
Material A	78	14	8
Material D	73	16	11
Material B	68	18	14
Material C	54	22	24

Table 3.4: Percentage of sand, silt and clay for materials A to D (as a percentage of total sample weight). Materials composition is based on representing the range of material encountered following a survey of the COALlink line (Gräbe, 2002). Reproduced from Gräbe (2002).

	Leighton Buzzard Sand Fraction B (%)	Leighton Buzzard Sand Fraction C (%)	Leighton Buzzard Sand Fraction D (%)	HPF5 Silt (%)	Hymod Prima Clay (%)
Material A	51	11	11	19	8
Material D	47	10	10	21	13
Material B	43	9	9	23	16
Material C	32	7	7	27	27

Table 3.5: Different aggregates for materials A to D, (as a percentage of total sample weight) as formulated by Gräbe (2002). Reproduced from Gräbe (2002).

	Plasticity Index (%)	Liquid Limit (%)	Plastic Limit (%)
Material A	9	23	14
Material D	15	29	14
Material B	16	30	14
Material C	19	36	17

Table 3.6: Atterberg values of the different sand-clay mixes. Reproduced from Otter (2011).

	Plasticity Index (%)	Liquid Limit (%)	Plastic Limit (%)
Material A	11	25	14
Material D	14	28	14
Material B	17	31	14
Material C	21	37	16

Table 3.7: Atterberg values of the different sand-clay mixes. Reproduced from Gräbe (2002).

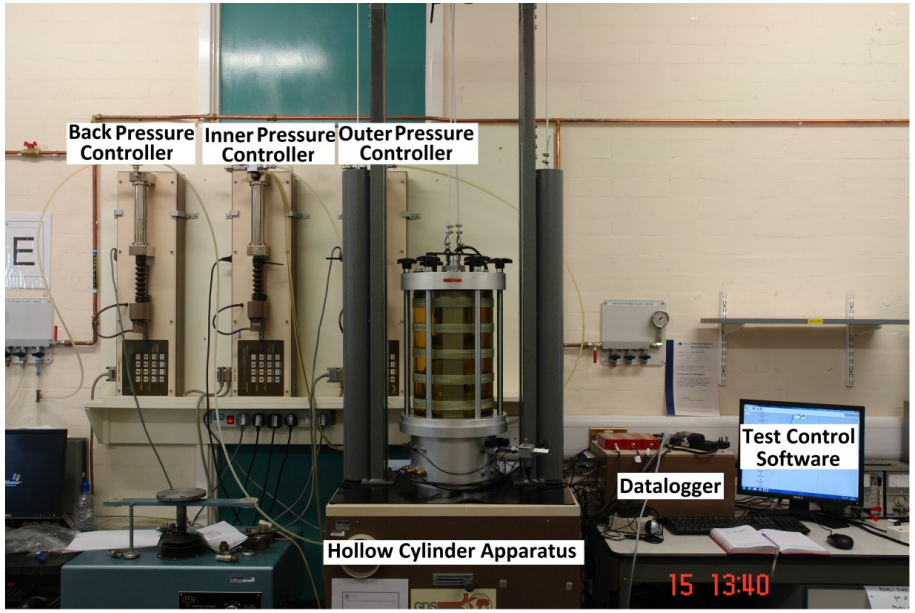

Figure 3.1: The GDS Small Strain Hollow Cylinder Apparatus (SS-HCA).

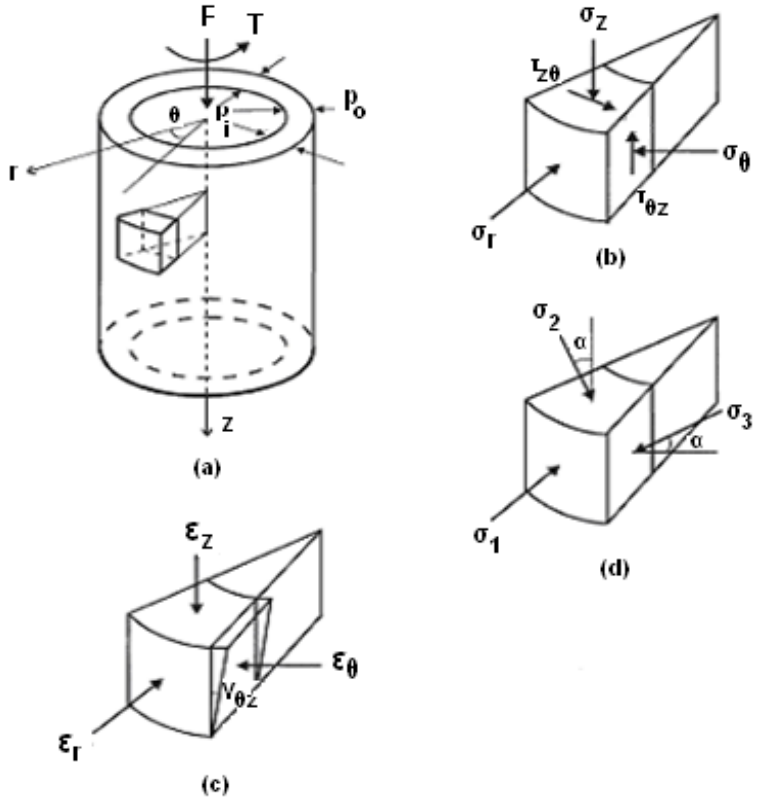

Figure 3.2: Stress and strain (a) of the hollow cylinder specimen, (b) on an element in the specimen wall, (c) principal strains on an element in the specimen wall, (d) principal stresses on an element in the specimen wall. Modified from Zdravkovic & Jardine (2001).

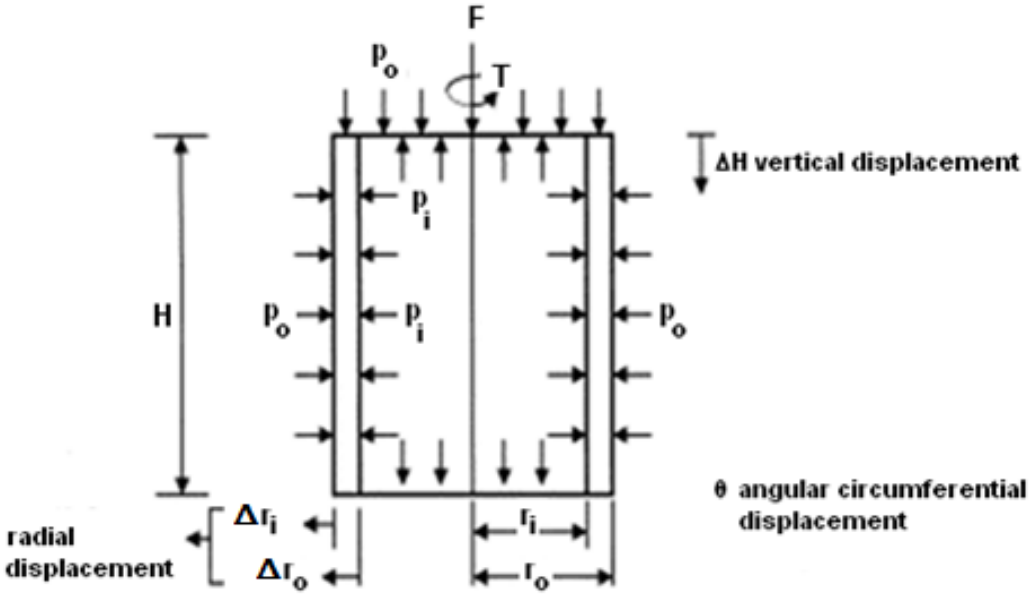

Figure 3.3: Schematic definition of average stress and strains components. Modified from Hight et al. (1983).

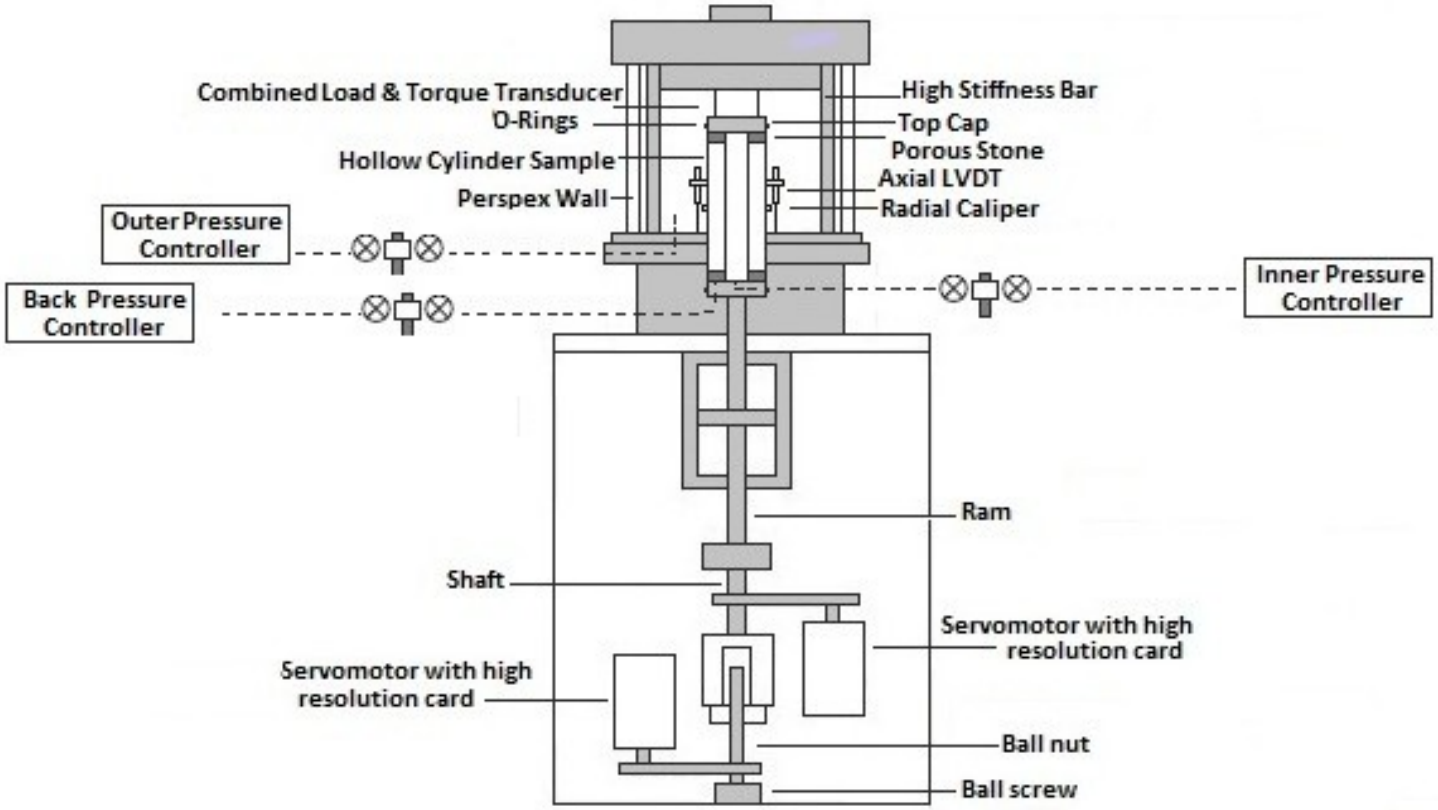

Figure 3.4: Detailed schematic layout of the GDS Small Strain Hollow Cylinder Apparatus (SS-HCA) and local instrumentation.

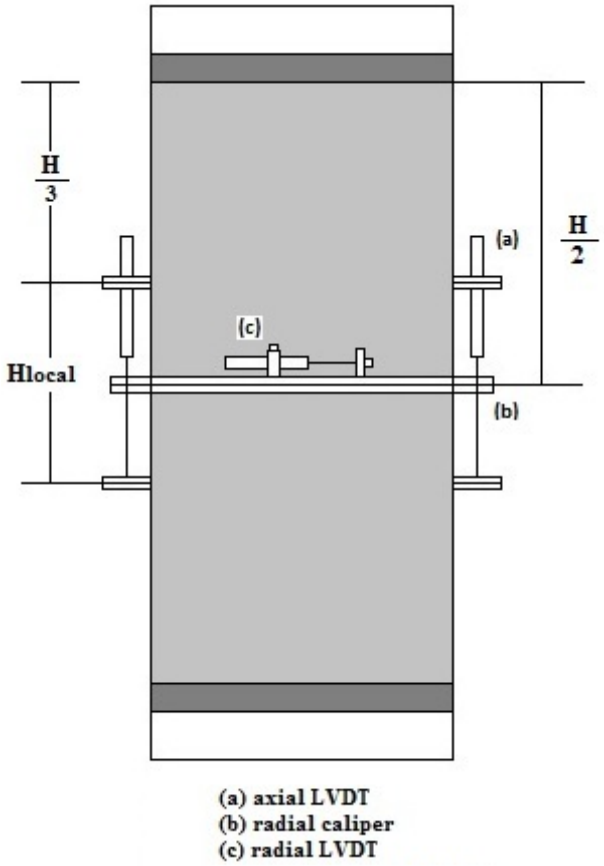

Figure 3.5: Front view of the specimen showing LVDT measuring local axial strains as well as radial caliper with attached LVDT measuring changes in the outer diameter.

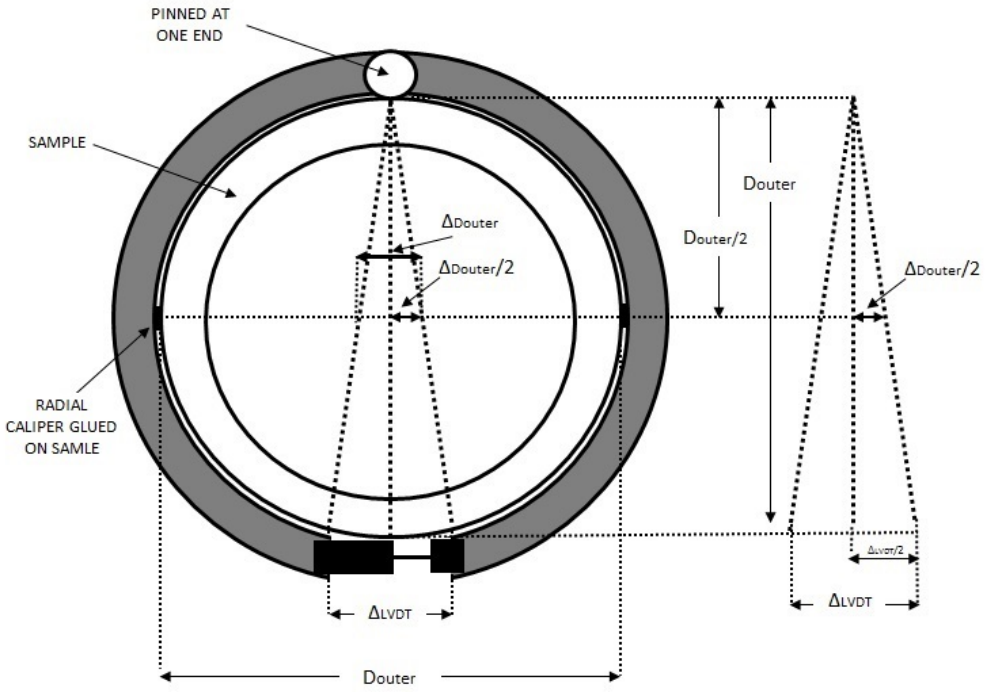

Figure 3.6: Geometric illustration of how outer diameter changes are derived based on the LVDT readings of the radial calliper.

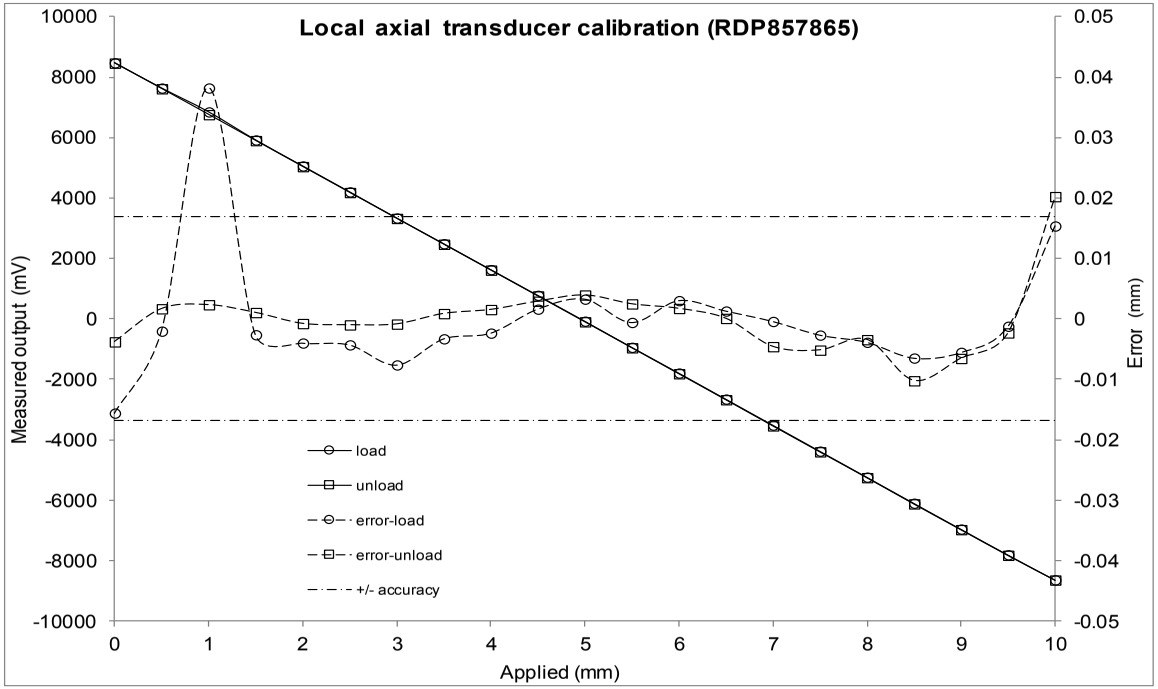

Figure 3.7: Calibration results of the local axial LVDT RPD85785.

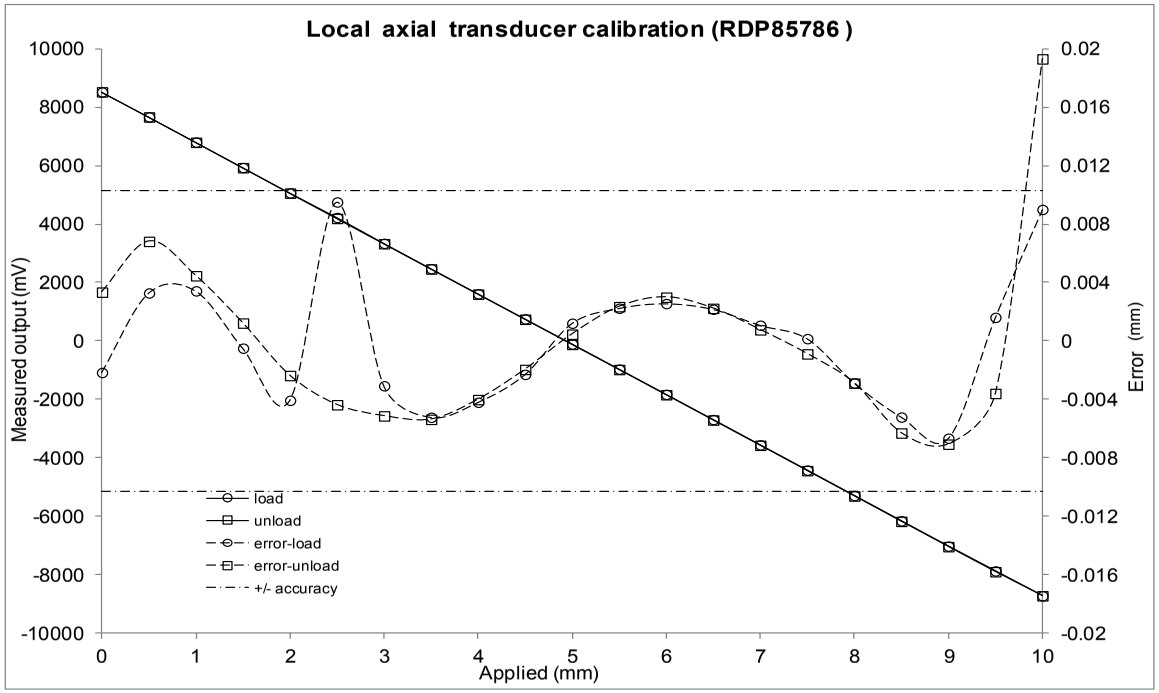

Figure 3.8: Calibration results of the local axial LVDT RPD85786.

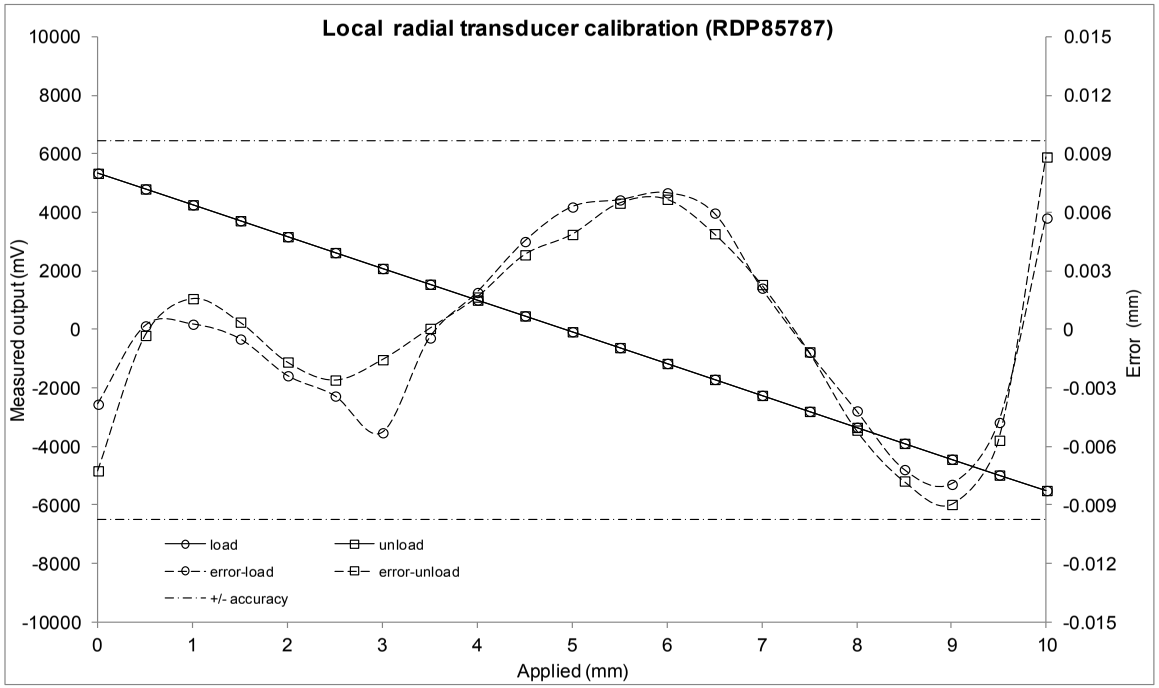

Figure 3.9: Calibration results of the radial LVDT RPD85787.

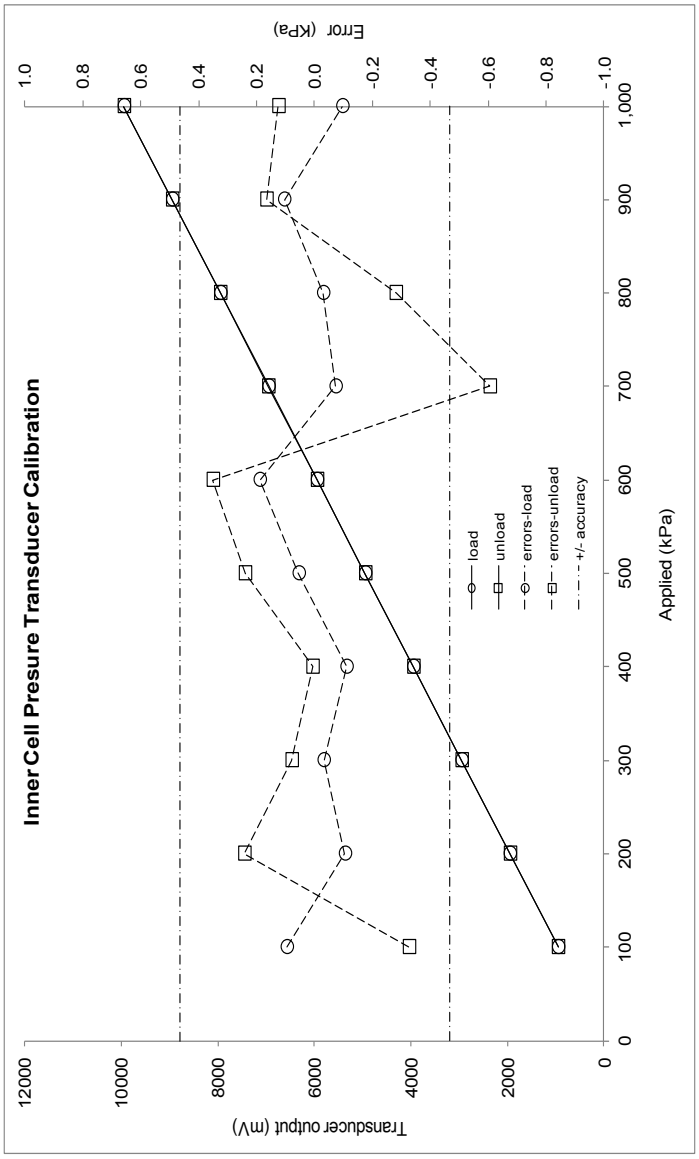

Figure 3.10: Calibration results of the inner cell pressure transducer.

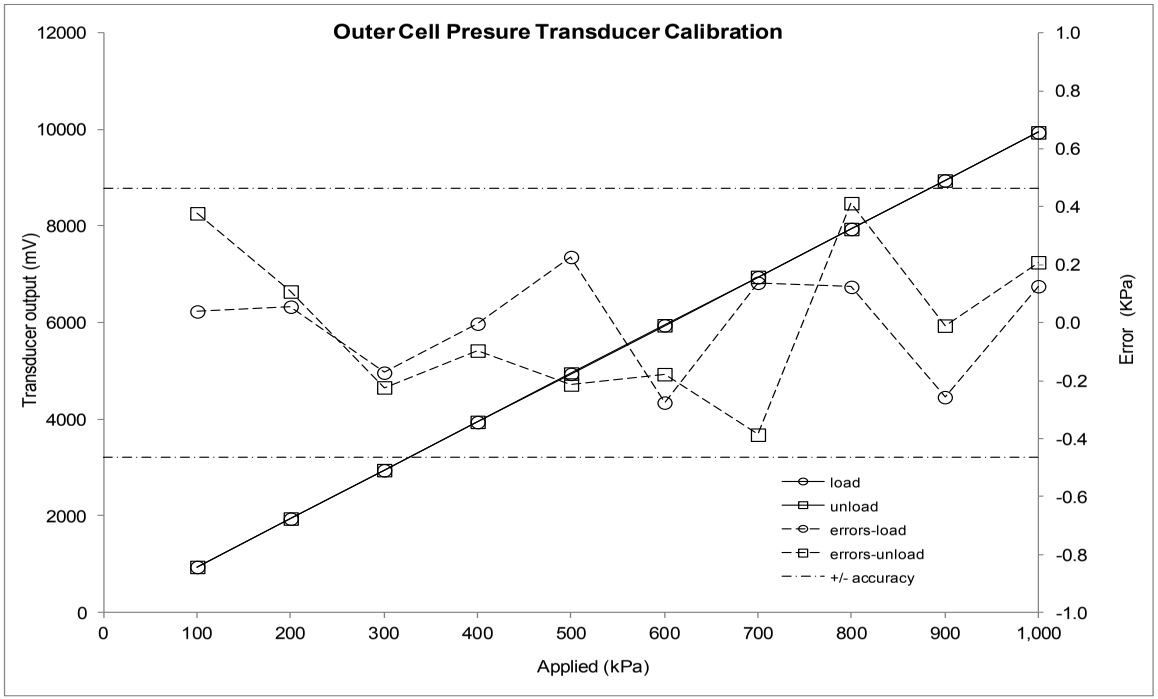

Figure 3.11: Calibration results of the outer cell pressure transducer.

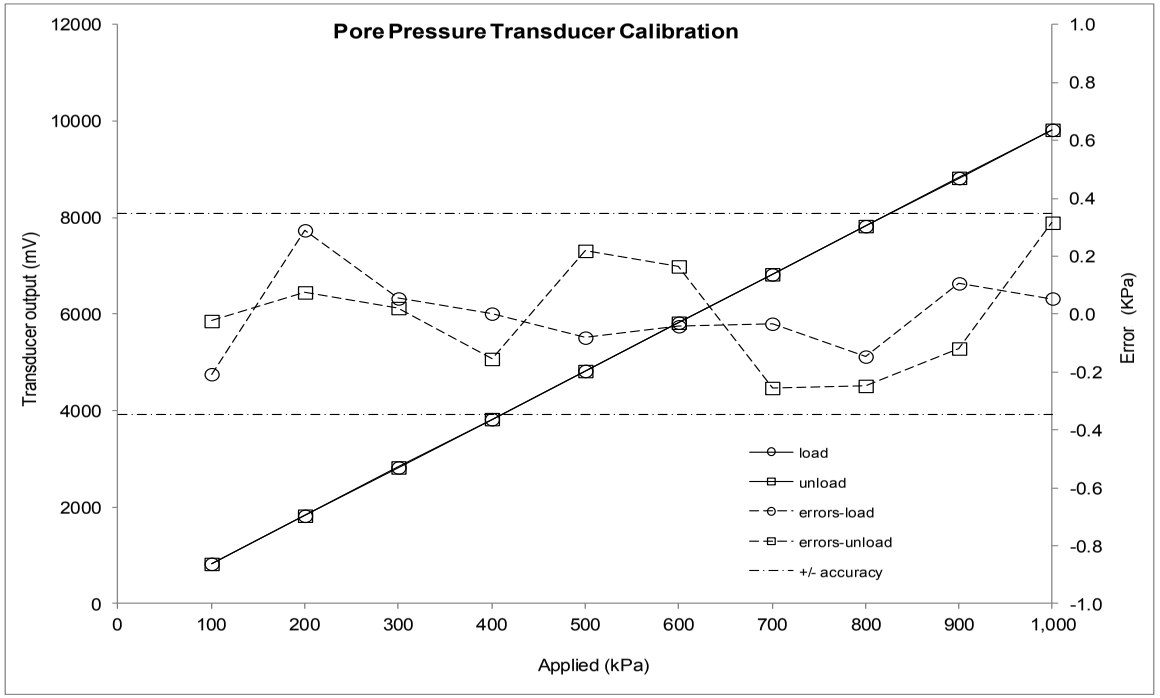

Figure 3.12: Calibration results of the pore pressure transducer.

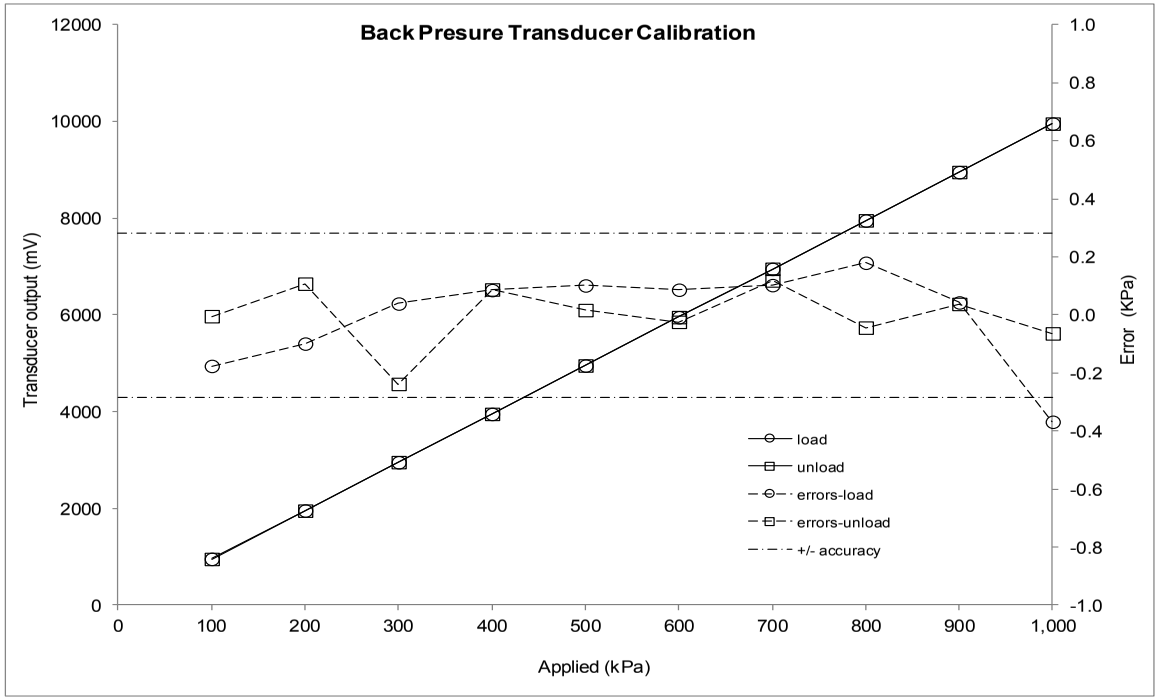

Figure 3.13: Calibration results of the back pressure transducer.

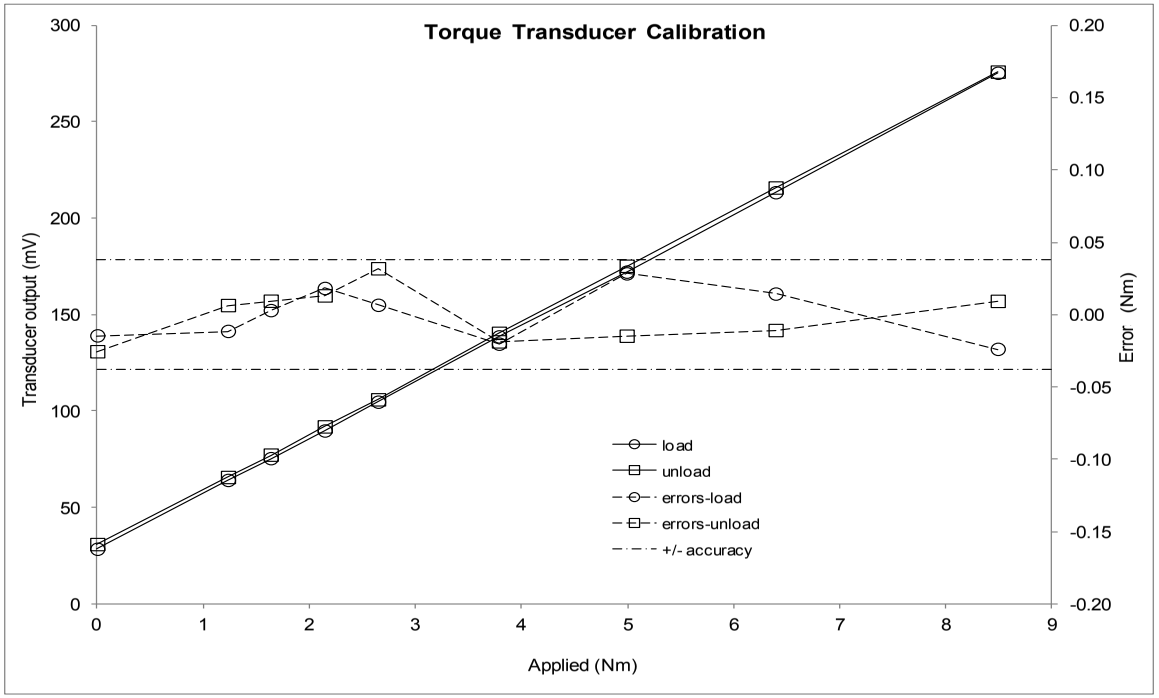

Figure 3.14: Calibration results of the torque transducer.

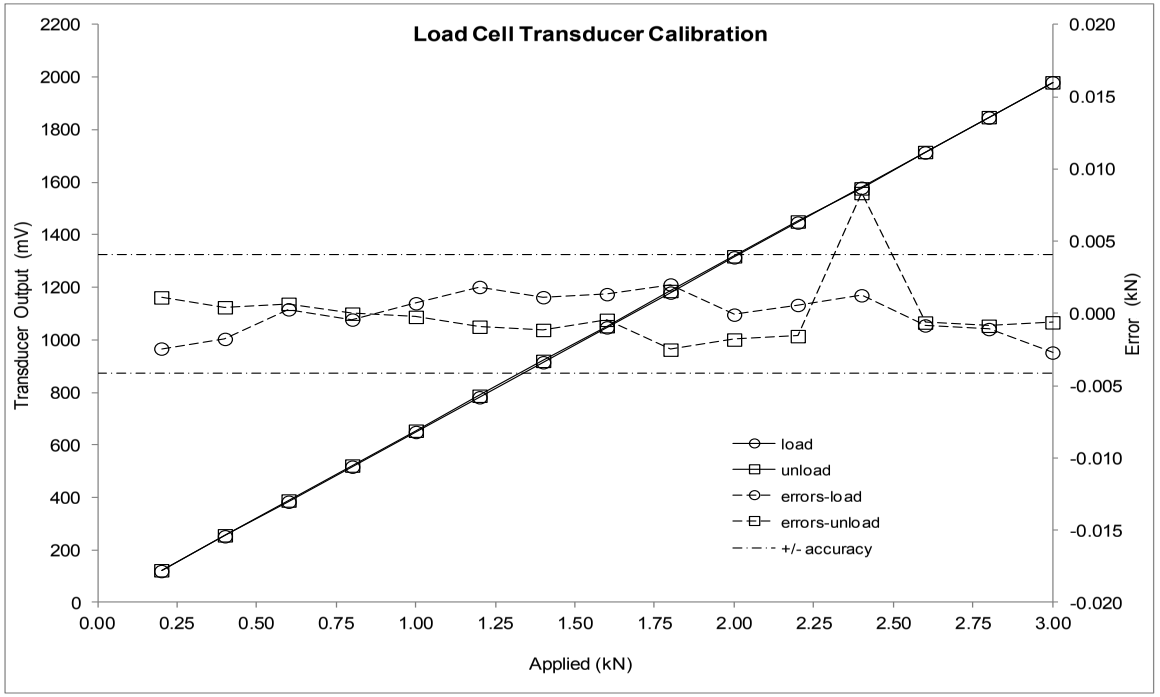

Figure 3.15: Calibration results of the load cell transducer.

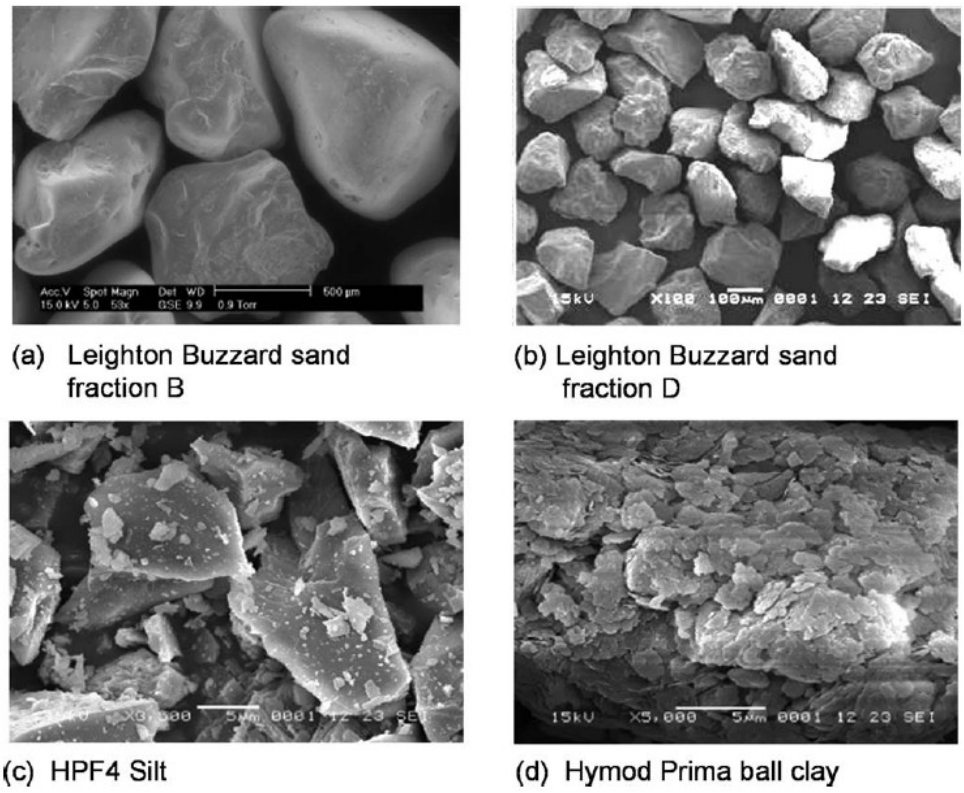

Figure 3.16: Scanning electron micrographs of constituent materials of the investigated sand-clay mixes. From Clayton & Gräbe (2009).

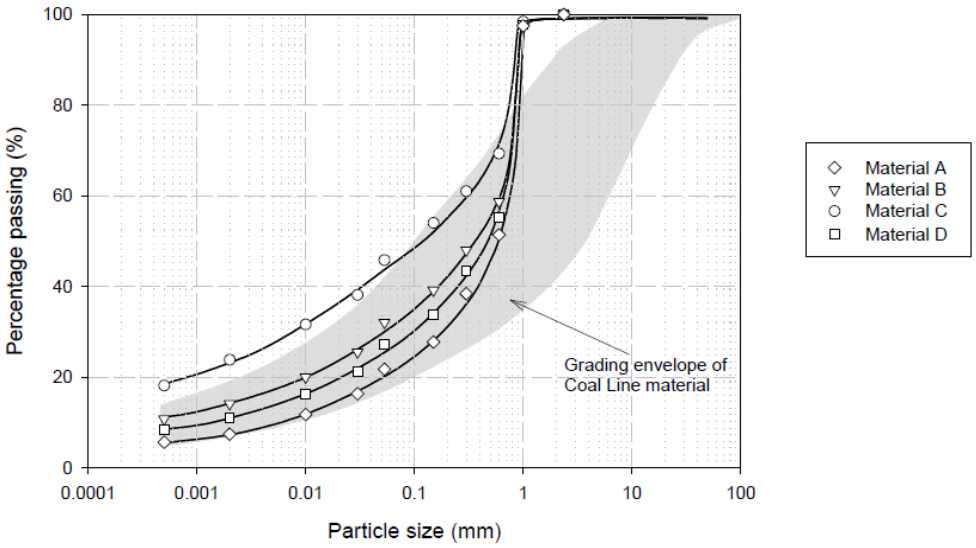

Figure 3.17: Particle size distribution of the sand-clay mixes and of the actual coal line material. (Material A 7% clay, Material D 11% clay, Material B 14% clay, Material C 24% clay). From Gräbe (2002).

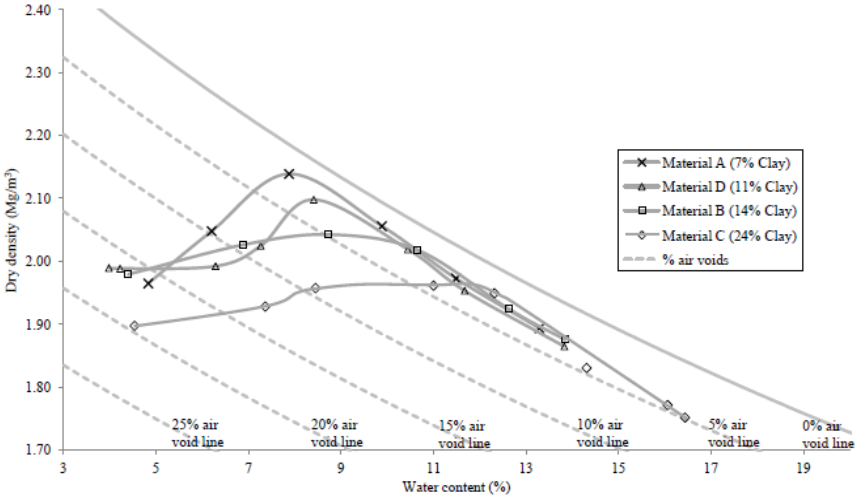

Figure 3.18: Proctor compaction curves. From Otter (2011).

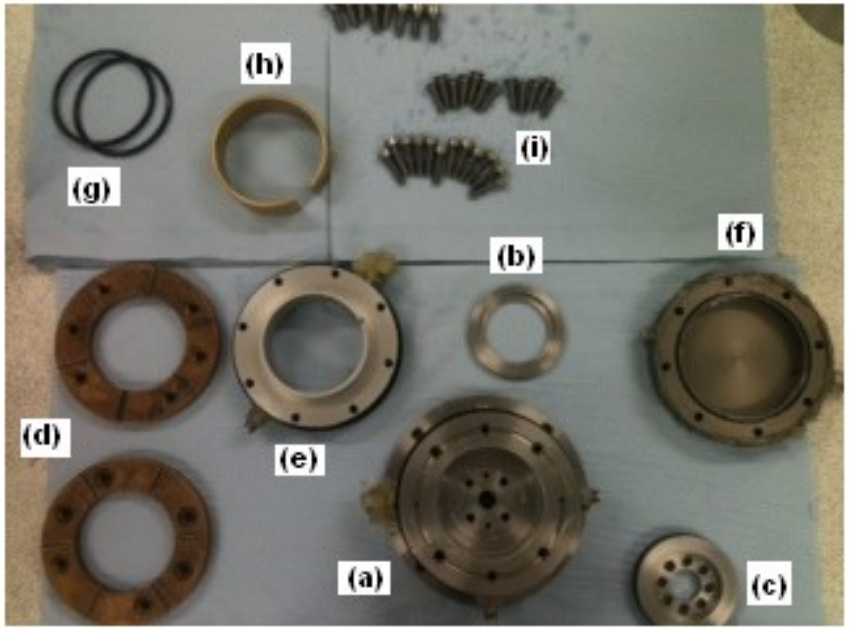

Figure 3.19: Components of the hollow cylinder specimen set up preparation.

Chapter 4

DISCUSSION OF EXPERIMENTAL RESULTS

This chapter presents and discusses the results of the laboratory tests conducted to improve our understanding of the influence of cyclic changes in the magnitude of PSR on the pore pressure, stiffness and susceptibility to failure of railway track foundation soils under different drainage conditions. The results are analysed in the context of relevant published data before concluding with a discussion of the implications of this research on railway foundation design.

4.1 Defining a basis of comparison between different sand-clay mixes

The addition of fines to a sand may substantially alter the mechanical characteristics of the sand and therefore the selection of an appropriate basis for comparison between sands

with varying fines content becomes of critical importance. The most commonly used parameter to assess the mechanical response of different soils is the efficiency with which particles are packed together. In terms of sand mixes which include a significant amount of fines, the literature review revealed that this efficiency is usually quantified either by means of the global void ratio e, relative density D_r or the inter-granular void ratio e_G and skeleton void ratio e_{sk}. The global void ratio e is defined as the ratio of the volume of voids to the volume of solids in a soil element and considers the voids formed by both sand and fine particles (Figure 4.1).

$$e = \frac{V_{voids}}{V_{sand} + V_{fines}} \tag{4.1}$$

with V_{voids}, V_{sand}, V_{fines} the volume of voids, sand and fines respectively.

The relative density D_r indicates the relative value of a given global void ratio e, with respect to the global maximum and minimum void ratios e_{max} and e_{min}, for a given soil

$$D_r = \frac{e_{max} - e}{e_{max} - e_{min}} x100 \tag{4.2}$$

The concept of the inter-granular void ratio e_G (Mitchell, 1976) for a mixed soil is based on the idea that up to a certain fines content, the fines do not actively participate in the force transmission and thus should be treated as voids

$$e_G = \frac{V_{voids} + V_{fines}}{V_{sand}} \tag{4.3}$$

When the specific gravities of the coarser and finer fractions of the soil are the same, the intergranular void ratio is usually referred to as the skeleton void ratio e_{sk} (Shen et al., 1977, Kuerbis et al., 1988).

The concept of the inter-granular void ratio e_G, however may not sufficiently represent the effect of fines on the mechanical response of the host sand. Pitman et al. (1994) investigated the effects of adding kaolin or silica fines on the mechanical response of Ottawa sand. They observed that the undrained shear strength of the sand mix with 20% silica was higher than that with 10% silica, despite the higher inter-granular void ratio of the 20% silica mix. This suggests that the silica fines do not act simply as voids, but rather contribute to the shear strength of the mix. When the sand was mixed with kaolin, the undrained shear strength of the specimen with 20% fines was higher than that of the 10% fines, but now the granular void ratio in the specimen with 20% fines was lower than that of the specimen with 10% fines, and both of them had a lower granular void ratio than the clean sand (without any fines). As there were no data at the same granular void ratio however, it is not possible to conclude whether the higher strength was due to the packing of sand or to the presence of fines.

Carraro et al. (2009) reported the results of a series of drained triaxial tests on Ottawa sand mixed with either nonplastic silt or kaolin clay. At the same inter-granular void ratio, increasing the silt content increased the drained shear strength. The shear strength of the mixes was greater than that of the clean sand, despite the clean sand being denser. This implies that the silt had a beneficial effect on the strength of the mix. When the same sand was mixed with 2% clay it exhibited a reduction in the drained shear strength despite the fact that it had a denser packing compared to the clean sand. Further additions of clay up to 11% however did not impart further reductions in shear strength despite the fact that the mixes were prepared at higher granular void ratios compared to the clean sand. This may suggest that the clay had a beneficial contribution to the shear strength.

On the other hand Thevanayagam & Mohan (2000) reported that when sand was mixed with silica, at the same inter-granular void ratio, the sand-silica mixes exhibited a similar strength to the clean sand. This suggests that the silica fines had little influence on the strength of the host sand. This effect however was not observed when the sand was mixed with kaolin. Adding kaolin to the sand reduced the strength of the mixture below that of the clean sand.

In order to take into account the different ways the fines may contribute to the mechanical response of the host sand, Thevanayagam et al. (2002) modified the expression for the inter-granular void ratio e_G and proposed an alternative expression the equivalent granular void ratio e_{Ge}, which is based on the actual global void ratio e, the fines content f_c and the portion of fines c that contribute in the inter-particle contact forces

$$e_{Ge} = \frac{e+(1-c)f_c}{e-(1-c)f_c} \tag{4.4}$$

with c bounded between 0 and 1 that is, $0 < c < 1$. When c=0 the fines act exactly like voids, and when c=1 the fines are indistinguishable from the host sand particles. The equivalent granular void ratio e_{Ge} however is not a core parameter as it requires the results of the laboratory tests to determine the c parameter.

In this research the data were interpreted using the global and inter-granular void ratio expressions. The concept of relative density was not considered as appropriate for a soil with widely differing solid phases, since e_{max} and e_{min} will in general vary with the percentage of finer particles. The dry densities and corresponding global and inter-granular void ratios of the various sand-clay mixes tested in this research are presented in Table 4.1. As can be observed from Table 4.2 the specific gravity of the constituent particles was similar and the specific gravity of all the mixes was found to be the same

and equal to 2.64 (Gräbe, 2002; Otter, 2011). The global void ratio was calculated through Eq. (4.5)

$$e = \frac{V_{voids}}{\frac{M_{sand}}{G_{s\,sand}\rho_{water}} + \frac{M_{silt}}{G_{s\,silt}\rho_{water}} + \frac{M_{clay}}{G_{s\,clay}\rho_{water}}} \tag{4.5}$$

with M_{sand}, M_{silt} *and* M_{clay} the mass of the sand, silt and clay, G_{ssand}, G_{ssilt} *and* G_{sclay} the specific gravity of the sand, silt and clay particles and ρ_{water} the density of the water. In the unsaturated state, after the specimen compaction $V_{voids} = V_{air} + V_{water.}$ Alternatively the global void ratio may also be calculated through Eq. (4.6)

$$e = \frac{G_{s\,mix} \times \rho_{water}}{\rho_{dry}} - 1 \tag{4.6}$$

with G_{smix} the specific gravity of the mixes, ρ_{dry} the dry density of the mixes and ρ_{water} the density of the water. Calculating the global void ratio using the specific gravity of the constituent particles or calculating the global void ratio using the dry density and the specific gravity of the mixes gave similar results. Furthermore due to the saturation strategy which involved simultaneous elevations of the cell pressure and back pressure, so as to maintain the effective stress and not cause any consolidation of the specimen it is reasonable to assume that insignificant changes to the global void ratio occurred.

Finally the granular void ratio was calculated through Eq. 4.7 making similar assumptions to the above.

$$e_G = \frac{V_{voids} + \frac{M_{silt}}{G_{s\,silt}\rho_{water}} + \frac{M_{clay}}{G_{s\,clay}\rho_{water}}}{\frac{M_{sand}}{G_{s\,sand}\rho_{water}}} \tag{4.7}$$

4.2 Investigated stress paths

4.2.1 In situ versus laboratory drainage path

In the field, drainage conditions are likely to be self-regulated by the amount of clay present in the volume of the sand and the size of the loaded zone. The speed of any excess pore pressure dissipation will be controlled by the permeability, the volumetric compressibility, the drainage path length and the rest period between each train passage. The volumetric compressibility will dictate the amount of excess pore pressure generated as a result of PSR and the permeability, drainage path length and available drainage time will control the rate of any excess pore pressure dissipation.

Assuming that the train load can be regarded as uniformly distributed over the track which acts as a strip footing of width B≈2.4m, then the resulting stress distribution can be obtained approximately from Figure 4.2. As can be observed the drainage conditions vary spatially as the loading is non-uniformly distributed through the depth and any generated excess pore pressures will cause the water to flow both horizontally and vertically to the nearest unloaded zone. For example at a depth of 0.5m one part of the excess pore pressure may move horizontally along a drainage path length of approximately 1.5m where the stress will have reduced by 90%. Another part of the excess pore pressure may cause a vertical flow along a drainage path length of 1.5m where 90% of the stress will have attenuated.

In the laboratory however the flow of the water is unidirectional. Simulation of in situ drainage conditions in the laboratory therefore poses a number of challenges. In the laboratory the assumption is made that the soil behaves as an element and that the load is uniformly distributed, with no spatial variation in stress distribution. Another difficulty is associated with how to simulate rest periods between each train passage since this would require the interruption and resetting of PSR test stages which would pose a further challenge when a high number of loading cycles is required.

PSR tests were therefore carried out both under conditions where the mixes were free to drain and under undrained conditions, so as to investigate the range of possible drainage conditions likely to occur in the field. Undrained tests investigated the worst case scenario and examined which sand-clay mix would be more likely to accumulate significant excess pore pressures. Free to drain tests investigated the susceptibility to PSR when the rate of any excess pore pressure dissipation was controlled by the volumetric compressibility, the permeability of the different sand-clay mixes and the drainage path length. Although the frequency of loading applied in these free to drain tests was slow compared with in situ conditions, this was compensated for, qualitatively, by the fact that no rest periods were considered and the drainage path in the specimen was longer than in the field. In the free to drain tests the specimen was allowed to drain from the bottom and excess pore pressures were measured at the furthest point from drainage at the top of the specimen. The drainage path length was therefore approximately 200mm.

4.2.2 Cyclic stress changes

All the tests reported in this thesis involved the application of cyclic changes in the axial stress and shear stress. The magnitude of applied cyclic changes in shear stress $\tau_{\theta z}$ started from the lowest values indicated by the numerical analysis by Powrie et al. (2007) near the bottom of a railway track foundation under the passage of a 25.5 ton/axle freight train ($|\Delta\tau_{\theta z}|$=8.5kPa), and was thereafter increased in increments until failure occurred. The axial stress magnitude was kept constant so as to correlate the axial strain, pore pressure and stiffness changes with cyclic changes in PSR only. A cyclic axial stress amplitude of $|\Delta\sigma_z|$=30kPa was selected to capture the relative ratio of shear stress to axial stress, which is more pronounced at a depth below the foundation layer. In terms of absolute values the selected magnitude of axial stress corresponds approximately to the mid depth of railway track foundations during the passage of freight trains (Powrie et al., 2007). For the investigated depths, the railway track foundation in a wet climate is likely to be saturated, without the beneficial effect of stiffness increases associated with suction (Otter, 2011).

The effect of increasing the clay content on the cyclic response during undrained PSR was investigated in tests series UAT8.5, UDT8.5-UDT11.5, UBT8.5-UBT14.5, UCT8.5-UCT14.5 (Table 4.3). The first letter of every test series denotes the drainage type; U for undrained and F for free to drained tests. The letter that follows denotes the type of material, and T and the number that follows, denote the magnitude of cyclic shear stress imposed on the specimen.

Before the undrained tests stage the specimens were subjected to a free to drain cyclic PSR preloading stage, to eliminate the effects of specimen preparation. In Table 4.3 these tests are referred to as FAT8.5PR-FAT11.5PR, FDT8.5PR-FDT11.5PR, FBT8.5PR-FBT11.5PR, FCT8.5PR-FCT11.5PR, where the suffix PR denotes the preloading stage. The free to drain preloading phase may also simulate the in situ effect of a rolling compactor wheel during preparation of the railway track foundation.

The pore pressure response at the furthest point from the drainage boundary revealed that with 7%-14% clay content present in the pore space of the sand, the combination of generated volume changes and permeability of the mixes lead to insignificant excess pore pressure accumulation (Figure 4.3). For these clay contents the pore pressure changes at the furthest point from drainage essentially followed the pattern changes of the back pressure controller. With 24% clay present in the voids however, the rate of dissipation was dominated by the substantially reduced permeability and significant excess pore pressures started to accumulate (Figure 4.4).

Increasing the clay content increased the volumetric stability of the sand-clay mixes, as it reduced the volumetric contraction during PSR (Figure 4.5). As the specimens compressed and rearranged into a denser packing, the measured stiffness registered a small increase (Figure 4.6). The resilient Young's modulus was calculated as the magnitude of the deviator stress change divided by the resilient axial strain during a load cycle.

4.3 Observations during undrained cyclic loading

4.3.1 Discussion of the effects on excess pore pressure generation

After the cyclic conditioning stage each PSR test stage was carried out undrained (UAT8.5, UDT8.5-UDT11.5, UBT8.5-UBT14.5, UCT8.5-UCT14.5). The aim of these tests was to investigate the susceptibility of different soils to generate significant excess pore pressures as a result of cyclic increases in the rotation of principal stresses. Pore pressures were allowed to dissipate only at the end of each undrained test stage, before the start of a new stage. This was to allow the influence of increasing the applied shear stress at each stage to be assessed separately.

The development of excess pore pressures at increasing magnitudes of applied shear stress for sands containing varying amounts of clay is illustrated in Figure 4.7. The results suggest that even small additions of clay can have a significant effect in reducing the pore pressure response of a sand.

The most granular mix exhibited the strongest susceptibility to generate excess pore pressures, which led to a significant reduction in effective stress. After approximately 700 cycles the effective stress had reduced by 57%. Increasing the clay content beyond 11%, resulted in insignificant residual pore pressures accumulation for the same incremental increases in PSR. It should be noted that halfway through the testing of the 11% specimen, owing to a complication in the communication channel between the hardware and software interface, the deviator stress remained constant and equal to 15kPa rather than being cycled between 0 and 30kPa, whereas the cyclic shear stress continued to be applied between the desired predefined values. At this point the 7% clay had already developed a significant excess pore pressure of +14kPa representing a loss of approximately 50% of the initial effective stress of 33kPa, whereas the specimen with the 11% clay content had not accumulated any excess pore pressures.

Thereafter the 11% 14% and 24% clay mixes were subjected to an increase in the magnitude of PSR by increasing $\tau_{\theta z}$ up to ±11.5kPa. This triggered a rapid pore pressure accumulation in the specimen having 11% clay, whereas the 14% and 24% clay specimens exhibited insignificant pore pressure accumulation. This verifies the observations as to the beneficial role of fines in decreasing excess pore water pressure generation. . Finally the specimen with 14% and 24% clay contents were subjected to a further increase in $\tau_{\theta z}$ up to ±14.5kPa. Under this stress combination the specimen with 14% clay rapidly accumulated significant excess pore pressures, whereas the excess pore pressure generation in the specimen with 24% clay was less significant. In the 24% clay mix the excess pore water pressure rose quickly from the very first load cycle and thereafter oscillated within a constant range with little further accumulation.

Although the sand-clay mixes were compacted to relatively high dry densities, the excess pore pressures generated during principal stress rotation were not insignificant. After an initial rapid increase in excess pore pressure, the rate of pore pressure accumulation gradually decreased and the pore pressures stabilised as the mixes registered a loss of effective stress ranging from 27% - 57% of the initial value.

4.3.2 Discussion of the effects on plastic strain accumulation

The accumulated permanent strain during cyclic increases in shear stress is illustrated in Figure 4.8. It can be seen that an increase in clay within the pore space of the sand increased the cyclic threshold strain at which the rate of increase in plastic strain accelerated. This agrees with previous observations made on fine grain materials (Hsu & Vucetic, 2006; Hazirbaba & Rathje, 2009). The threshold strain increased from 0.05% to 0.12%, 0.36% and 0.42% as the clay content increased from 7% to 11%, 14% and 24% respectively. The data suggest that the mixes were very sensitive to even small changes in the magnitude of PSR once the cyclic strain threshold was exceeded. In terms of railway track foundation maintenance and design, this implies that a currently stable railway track

foundation may not necessarily be suitable to accommodate heavier traffic loads. The ability to respond in a resilient manner when subjected to cyclic increases in PSR is related to the cyclic threshold strain of the specific soil type comprising the railway track foundation.

4.3.3 Discussion of the effects on resilient stiffness

Changes in stiffness for the different specimens during PSR excursions are illustrated in Figure 4.9. The resilient Young's modulus was calculated as the magnitude of the deviator stress change divided by the resilient axial strain during a load cycle.

Changes in stiffness were associated with the cyclic threshold strain for each sand-clay mix. During loading with PSR below the cyclic threshold strain, no appreciable increase in pore pressure or change in stiffness was measured. Once the threshold strain had been passed, significant reductions in stiffness were observed. The results suggest that cyclic rotations in the direction of principal stresses can have a deleterious impact on the stability of railway track foundations, as they not only accelerate the rate of plastic strain accumulation, but also cause significant degradation in the resilient stiffness.

The stiffness measured in the laboratory tests in this research was lower than that back calculated from in situ displacement measurements on the same materials (Figure 4.10) (Priest et al., 2010). This may indicate that at the time of the field measurements the in situ soil might have been under suction. Recent laboratory investigations into the effect of suction on the stiffness of the same soils tested in this research, have shown that in unsaturated conditions the small strain stiffness increased by up to 550% and 900% % for the 11% and 24% clay, compared with a dry specimen (Otter, 2011).

4.3.4 Discussion of the effects in the general stress space

The stress path followed by the soils approaching and during failure is illustrated in Figures 4.11 - 4.12. As expected, the gradual reduction in effective stress due to increased pore pressures caused a migration of the stress path. The shape of the stress paths varied with clay content. For the mix dominated by the granular fraction, the stress path was more concave than for the mixes at higher clay contents. The relationship between q/p' and axial strain mobilised by the different specimens is shown in Figure 4.13. As can be observed q/p' invariably increased with increasing magnitude of PSR. The mixes dominated by the sand fraction mobilised a higher q/p' at smaller axial strains.

4.4 Observations during free to drain cyclic loading

Test series FAT8.5-FAT23.5, FDT8.5-FDT26.5, FBT8.5- FBT29.5 (Table 4.3), were designed to investigate the role of increasing the clay content during cyclic increases in PSR, under conditions where the rate of any excess pore pressure dissipation was controlled by the permeability and volumetric compressibility of the mixes. The aim of these tests was to simulate in situ conditions where the drainage is self-regulated by the amount of fines present in the volume of the sand. Although the cyclic loading frequency in these tests was lower than that in the field, this was compensated for, qualitatively, by the fact that no rest periods were considered and the drainage path in the specimen was longer than in the field.

The pore pressure response of the different specimens is illustrated in Figures 4.14-4.16. The measurement was obtained at the top of the specimen, which was at the furthest point from the drainage boundary at the base of the specimen. Increasing the clay content did not affect the rate of excess pore pressure generation, when the specimens were subjected to cyclic increases in PSR below failure. The pore pressure at the furthest boundary followed the back pressure controllers, which oscillated typically between ±1kPa.

Failure was driven by the inability to dissipate the generated volumetric contractions at a sufficiently high rate so as not to cause significant excess pore pressure accumulation. Increasing the clay content from 7%-11%-14%, increased the cyclic stress changes the mixes were able to sustain before failure. During failure the susceptibility to PSR was controlled by the tendency to accumulate excess pore pressures. This confirms the results of the undrained dataset, which suggested that the sandier mixes are more susceptible to cyclic changes in principal stress rotation.

4.4.1 Discussion of the effects on volumetric and axial strains

The volumetric contractions observed for the different specimens are presented in Figure 4.17. Increasing the clay content of the materials reduced the susceptibility to cyclic changes in PSR by increasing the volumetric stability of the mixes. The sand clay mixes at higher clay contents generated less volumetric contractions when subjected to the same stress changes.

As the clay content increased, the mixes were able to sustain higher cyclic changes in PSR before failure. For cyclic changes in the magnitude of PSR below failure, the rate of volumetric and axial strain accumulation was more pronounced during the first 100 cycles for each PSR increase (Figures 4.17-4.18). Thereafter, the rate of strain accumulation substantially reduced, and a characteristic flattening out of strain was observed. At this stage the mixes were stable over a high number of loading applications and no fatigue failures were observed.

4.4.2 Discussion of the effects on resilient stiffness and on the mobilised q/p' ratio

The stiffness measured throughout the free to drain tests is illustrated in Figure 4.19. The stiffness changes were more pronounced during the first 700 cycles and thereafter small increases in stiffness were recorded, as the mixes consolidated and the particles rearranged into a denser packing. During failure, where the rate of volumetric contraction caused a partial dissipation of excess pore pressures, a weakening of the sand-clay mixes was observed as a result of the reduction in effective stress.

The cyclic changes in the magnitude of PSR covered the widest spectrum of possible stress changes expected within a railway track foundation. The increase in stiffness observed during loading suggests that for free to drain cyclic changes in PSR below failure, cyclic loading may have a beneficial effect.

The q/p' ratio mobilised with increasing axial strain excursions is presented in Figure 4.20. As can be observed the sandier mix mobilised higher q/p' at smaller strains. All of the investigated mixes mobilised a similar q/p' ratio of approximately 1.25 near failure.

4.5 Comparison of results with previous work on the effects of increasing the fines content in a host sand

The role of increasing the fines content in the volume change behaviour of sand has attracted systematic research interest over the last decades, not least because this topic has a broad field of application since most natural soils contain some degree of fines. However the observations made by different researchers vary (Koester, 1994; Amini & Qi, 2000; Salgado et al., 2000; Ni et al., 2004; Murthy et al., 2007; Bahadori et al., 2008;

Papadopoulou & Tika, 2008; Carraro et al., 2009; Hazirbaba & Rathie, 2009; Yang & Wei, 2012).

Some researchers observed that the fines increased the tendency for excess pore pressure generation whereas others reported the opposite. A third group of researchers observed that the effect of fines changed at a threshold fines content. Below this threshold the addition of fines in the volume of the sand increased the tendency for excess pore pressure generation, but this trend was reversed as the fines threshold was exceeded (Dezfulian, 1982; Law & Ling, 1992; Chameau & Sutterer, 1994; Finn et al., 1994; Pitman et al., 1994; Vaid, 1994; Zlatovic & Ishihara, 1995; Thevanayagam et al., 1996; Lade & Yamamuro, 1997; Amini & Qi, 2000; Polito & Martin, 2001; Monkul & Yamamuro, 2011).

The importance of the pore pressure response on the susceptibility to failure under cyclic increases in PSR was evident in this research. Even in the free to drain tests, failure was ultimately driven by the accumulation of significant excess pore pressures. The presence of moderate amounts of clay was observed to have a beneficial effect on the rate of excess pore pressure accumulation. This observation agrees with field testing observations, which demonstrated that sands with significant fines contents were less susceptible to significant excess pore accumulation (Tokimatsu & Yoshimi, 1983; Seed et al., 1983; Seed et al., 1985).

Figure 4.21 plots the excess pore pressure ratio against the global and inter-granular void ratio of the different sand-clay mixes which were investigated as part of this research. The excess pore pressure ratio corresponds to an axial strain excursion of 0.5%. When the global void ratio is used as a basis for comparison, the results indicate that the reduction in the tendency for excess pore pressure accumulation is linked to the presence of fines, since this is the only changing variable as similar densities for the different mixes were considered.

When the intergranular void ratio is used to interpret the results, the data suggest that despite the host sand becoming looser a reduction in the rate of excess pore pressure accumulation occurred (Figure 4.22). Clearly the concept of the intergranular void ratio is not sufficient in interpreting the reduction in the tendency for excess pore pressure generation with increasing fines content. The experimental results imply that the addition of fines had a beneficial effect, which cannot be correlated with the host sand alone. In terms of the equivalent inter-granular void ratio e_G proposed by Thevanayagam et al. (2002), the results suggest that the b parameter takes a value equal to 1 as the fines fully participate in the load transfer mechanism of the host sand.

To analyse further and understand the effect of fines on the excess pore pressure generation of sands, the results of this research were put into context with previous published data. Figure 4.23 plots the excess pore pressure ratio as a function of the logarithm of axial strain for sands containing various amounts of fines. A wide variety of fines content is included ranging from clean sands up to sands containing significant amounts of fines. The global void ratios of the mixes vary, along with the type of fines used. The beneficial effects of fines on the pore pressure generation are evident. The loose sand without any addition of fines generated the highest excess pore pressures. The addition of only 5% fines to the same sand caused a 20% reduction in the excess pore pressure ratio as compared to the clean sand at otherwise similar conditions (Monkul & Yamamuro, 2011). Despite the different absolute excess pore pressure ratios generated by the different mixes, the data indicate that a common pattern between sands containing various amounts of fines can be established. As can be observed, the rate of pore pressure increase with axial strain for sands containing different fines contents is similar and independent of the volume of fines present in the host sand. The gradual addition of fines in the pore space of the sand however causes a downward, almost parallel, shift in the amount of generated excess pore pressures as a ratio of the initial effective stress in the mixes.

4.6 Implications for railway foundation design

The results of this research indicate that cyclic changes in PSR can have a deleterious effect on the stability of railway track foundations. It was found that PSR not only increases the rate of plastic strain accumulation but can also reduce the resilient stiffness of soils. The susceptibility of different soils to accelerated deterioration as a result of PSR is related to the cyclic stress threshold for the specific soil. Cyclic changes in PSR beyond the cyclic shear threshold can result in a rapid acceleration in the generated excess pore pressures and significant stiffness degradation.

The different sand-clay mixes were observed to be very sensitive to even small increases in PSR once this threshold was exceeded. However, for cyclic increases in the principal stress directions below the cyclic threshold, the mixes exhibited a stable response for a high number of loading applications and no sudden fatigue type failures were observed. In railway track foundation design, this requires a very careful consideration of the design loads in terms of the cyclic shear threshold for the specific type of soil under consideration. The consequences on the stability, serviceability and safety of railway track infrastructure can be severely and rapidly compromised once the cyclic changes in PSR exceed the cyclic threshold of the specific soil under consideration.

The results also suggest that the gradation of the soil comprising the railway track foundation can significantly influence the rate of railway track deterioration. In the field drainage conditions are self-regulated by the amount of volumetric contraction generated through the cyclic changes in PSR and the permeability of the sand-clay mixes. The results suggest that under free to drained conditions, small increases in clay content up to 14% clay may have a beneficial effect on the stability of railway track foundations, reducing the generated volumetric contractions and increasing the stiffness of the mixes. For further increases in clay content up to 24%, the beneficial effects of increasing the volumetric stability are likely to be outweighed by the significantly reduced permeability, which may result in significant excess pore pressure accumulation.

The undrained dataset also confirmed that sand-clay mixes with low clay contents are more susceptible to accelerated deterioration as a result of PSR. Increasing the clay content was observed to reduce the rate of excess pore pressure generation and increased the cyclic strain threshold the mixes were able to sustain before rapid stiffness degradation occurred.

The measured stiffness of all the sand-clay mixes investigated in this research was lower than that back calculated from in situ displacement measurements on the same materials (Priest et al., 2010). This may be associated with the fact the mixes in this research were saturated whereas in situ the soil may have been in suction. Suction in soils has been shown to increase its strength and stiffness with the increase dependent on the degree of suction, soil type and particle arrangement (Otter, 2011). Assuming saturated conditions may therefore be considered a more conservative design approach than unsaturated conditions, but may in some cases significantly increase the design and maintenance costs. It may therefore be worthwhile exploring how suction changes could affect the susceptibility of different soils to accelerated deterioration as a result of cyclic changes in the direction of principal stresses.

Test	Material	Dry density (Mg/m^3)	Global void ratio	Inter-granular void ratio
UA	A	2.15	0.23	0.69
UD	D	2.12	0.25	0.87
UB	B	2.12	0.25	1.05
UC	C	2.10	0.26	1.75
FA	A	2.14	0.23	0.69
FD	D	2.12	0.25	0.87
FB	B	2.11	0.25	1.06

Table 4.1: Dry densities, global and intergranular void ratios of the investigated sand-clay mixes.

	Specific Gravity
LBSFB	2.65[a]
LBSFC	2.65[b]
LBSFD	2.65[b]
Silica Flour Silt HPF5	2.60[c]
Hymod Prima Ball Clay	2.65[d]
Material A	2.64[e]
Material D	2.64[e]
Material B	2.64[e]
Material C	2.64[e]

[a]Clayton et al. (2004), [b]Noureddine et al. (2006) and Otter (2011) based on published values, [c]Adwan Chemicals (2013) and Otter (2011) based on published values, [d] Imerys performance minerals (2013) and Otter (2011) based on published values, [e]Gräbe (2002) determined following BS 1377-2 (1990) and Otter (2011) back calculated based on published values for aggregate constituents and their percentage weight for each material.

Table 4.2: Specific gravity of aggregate constituents and the different investigated sand-clay mixes.

Table 4.3: An analytical summary of all the PSR tests investigated in this research (a) Undrained dataset (b) Free to drain dataset

(a) Undrained dataset

Test	Material	$\Delta\tau_{\theta z}$	Number of cycles
UAT8.5	A	$\Delta\tau_{\theta z}$ =+8.5 → −8.5kPa	729
UDT8.5	D	$\Delta\tau_{\theta z}$ =+8.5 → −8.5kPa	710
UDT11.5		$\Delta\tau_{\theta z}$ =+11.5 → −11.5kPa	321
UBT8.5	B	$\Delta\tau_{\theta z}$ =+8.5 → −8.5kPa	710
UBT11.5		$\Delta\tau_{\theta z}$ =+11.5 → −11.5kPa	710
UBT14.5		$\Delta\tau_{\theta z}$ =+14.5 → −14.5kPa	345
UCT8.5	C	$\Delta\tau_{\theta z}$ =+8.5 → −8.5kPa	710
UCT11.5		$\Delta\tau_{\theta z}$ =+11.5 → −11.5kPa	710
UCT14.5		$\Delta\tau_{\theta z}$ =+14.5 → −14.5kPa	276

(b) Free to drain dataset

Test	Material	$\Delta\tau_{\theta z}$	Number of cycles
FAT8.5PR	A	$\Delta\tau_{\theta z}$ =+8.5 → −8.5kPa	710
FAT11.5PR		$\Delta\tau_{\theta z}$ =+11.5 → −11.5kPa	710
FDT8.5PR	D	$\Delta\tau_{\theta z}$ =+8.5 → −8.5kPa	708
FDT11.5PR		$\Delta\tau_{\theta z}$ =+11.5 → −11.5kPa	700
FBT8.5PR	B	$\Delta\tau_{\theta z}$ =+8.5 → −8.5kPa	712
FBT11.5PR		$\Delta\tau_{\theta z}$ =+11.5 → −11.5kPa	710
FCT8.5PR	C	$\Delta\tau_{\theta z}$ =+8.5 → −8.5kPa	700
FCT11.5PR		$\Delta\tau_{\theta z}$ =+11.5 → −11.5kPa	700

Test	Material	$\Delta\tau_{\theta z}$	Number of cycles[3]
FAT8.5	A	$\Delta\tau_{\theta z}$ =+8.5 → −8.5kPa	720
FAT11.5		$\Delta\tau_{\theta z}$ =+11.5 → −11.5kPa	718
FAT14.5		$\Delta\tau_{\theta z}$ =+14.5 → −14.5kPa	720
FAT17.5		$\Delta\tau_{\theta z}$ =+17.5 → −17.5kPa	721
FAT20.5		$\Delta\tau_{\theta z}$ =+20.5 → −20.5kPa	720
FAT23.5		$\Delta\tau_{\theta z}$ =+23.5 → −23.5kPa	103
FDT8.5	D	$\Delta\tau_{\theta z}$ =+8.5 → −8.5kPa	705
FDT11.5		$\Delta\tau_{\theta z}$ =+11.5 → −11.5kPa	715
FDT14.5		$\Delta\tau_{\theta z}$ =+14.5 → −14.5kPa	721
FDT17.5		$\Delta\tau_{\theta z}$ =+17.5 → −17.5kPa	708
FDT20.5		$\Delta\tau_{\theta z}$ =+20.5 → −20.5kPa	707
FDT23.5		$\Delta\tau_{\theta z}$ =+23.5 → −23.5kPa	713
FDT26.5		$\Delta\tau_{\theta z}$ =+26.5 → −26.5kPa	57
FBT8.5	B	$\Delta\tau_{\theta z}$ =+8.5 → −8.5kPa	722
FBT11.5		$\Delta\tau_{\theta z}$ =+11.5 → −11.5kPa	720
FBT14.5		$\Delta\tau_{\theta z}$ =+14.5 → −14.5kPa	720
FBT17.5		$\Delta\tau_{\theta z}$ =+17.5 → −17.5kPa	727
FBT20.5		$\Delta\tau_{\theta z}$ =+20.5 → −20.5kPa	721
FBT23.5		$\Delta\tau_{\theta z}$ =+23.5 → −23.5kPa	720
FBT26.5		$\Delta\tau_{\theta z}$ =+26.5 → −26.5kPa	716
FBT29.5		$\Delta\tau_{\theta z}$ =+29.5 → −29.5kPa	306

Table 4.3: (continued) (b) Free to drain dataset

[3] Each test stage was terminated when the rate of plastic strain accumulation was insignificantly small and a characteristic ’flattening out’’ of strains was observed. For cyclic stress changes below the critical shear threshold stress, this was observed to occur well within 700 cyclic load applications.

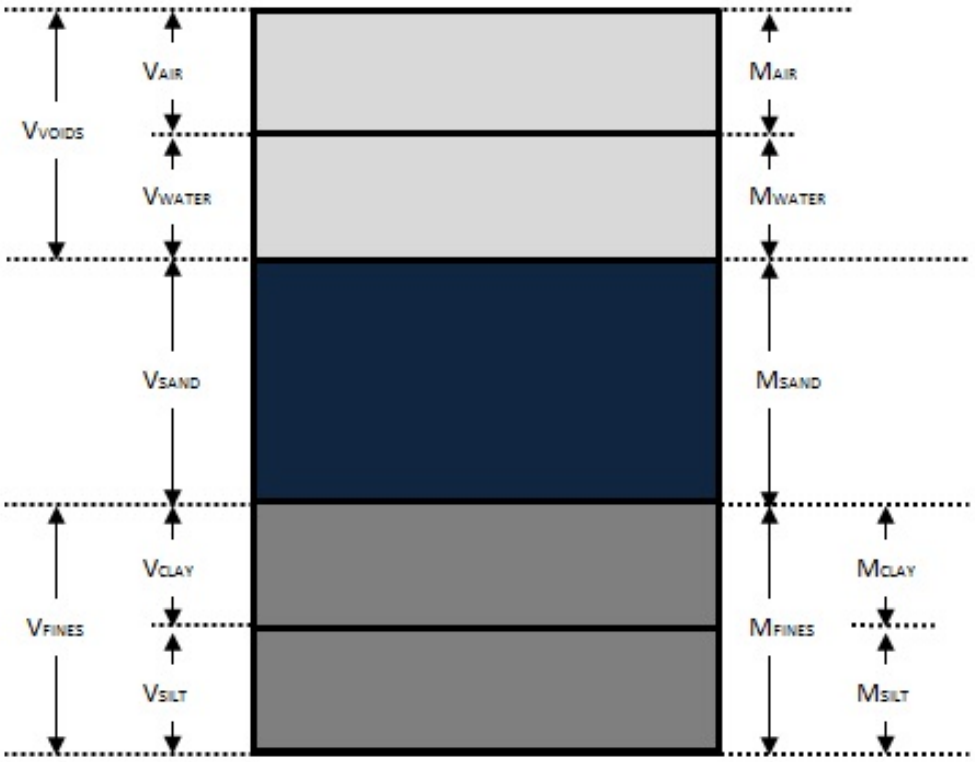

Figure 4.1: Phase relation of a sand containing fines

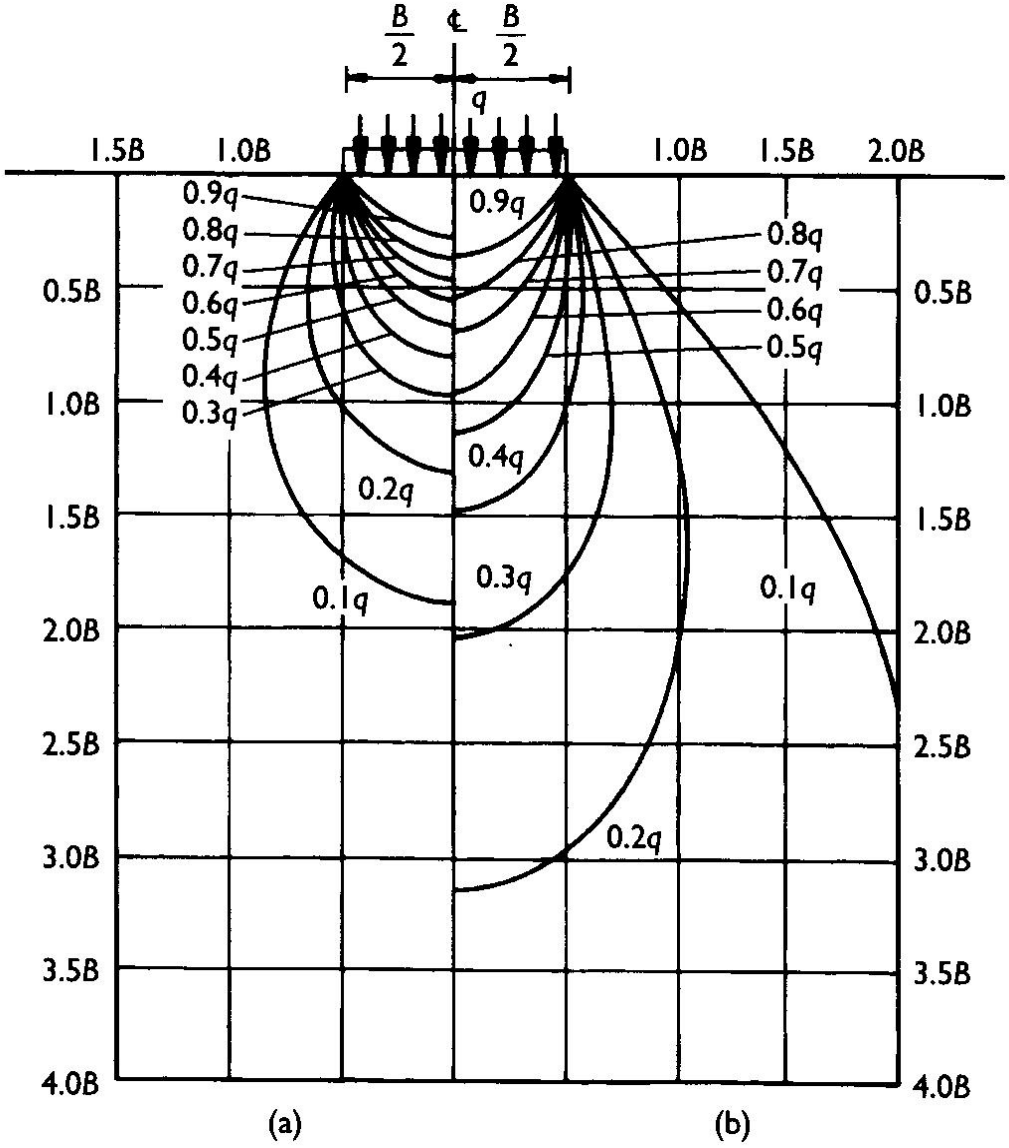

Figure 4.2: Contours of increase in vertical stress (a) below a circular footing of diameter B, and (b) below a strip footing of width B subjected to a uniform vertical surcharge q. From Powrie (2004) redrawn after Whitlow (1995).

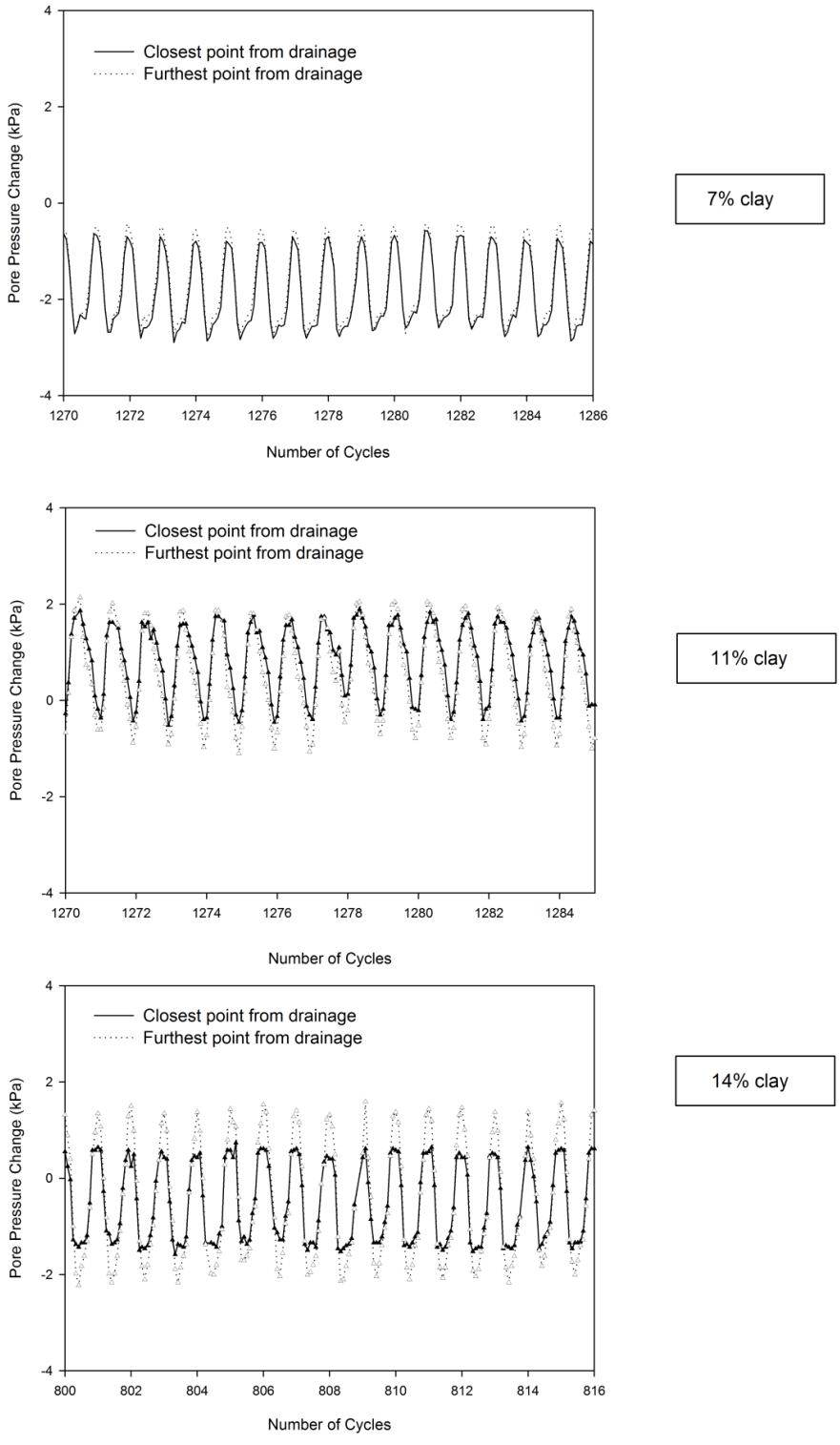

Figure 4.3: Pore pressure response at the furthest and closest point from drainage during cyclic preloading with PSR for the 7%,11%,14% clay content mixes.

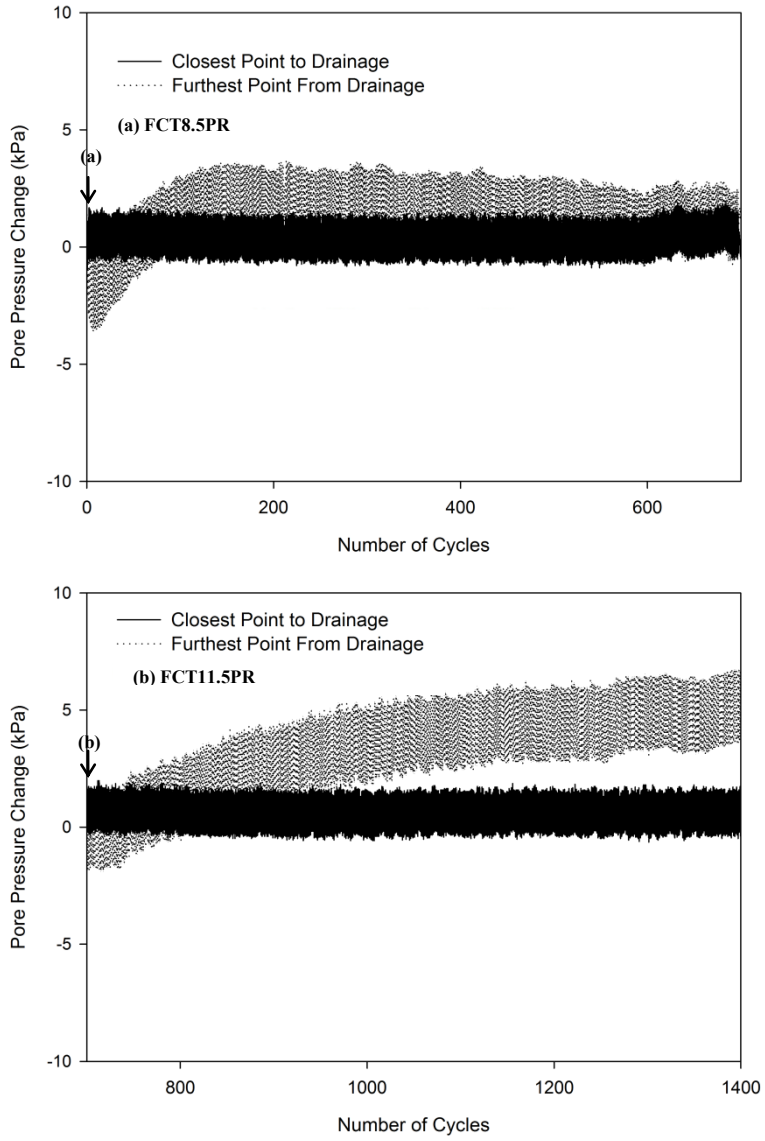

Figure 4.4: Pore pressure response at the furthest and closest point from drainage during cyclic preloading with PSR for the 24% clay content mix.

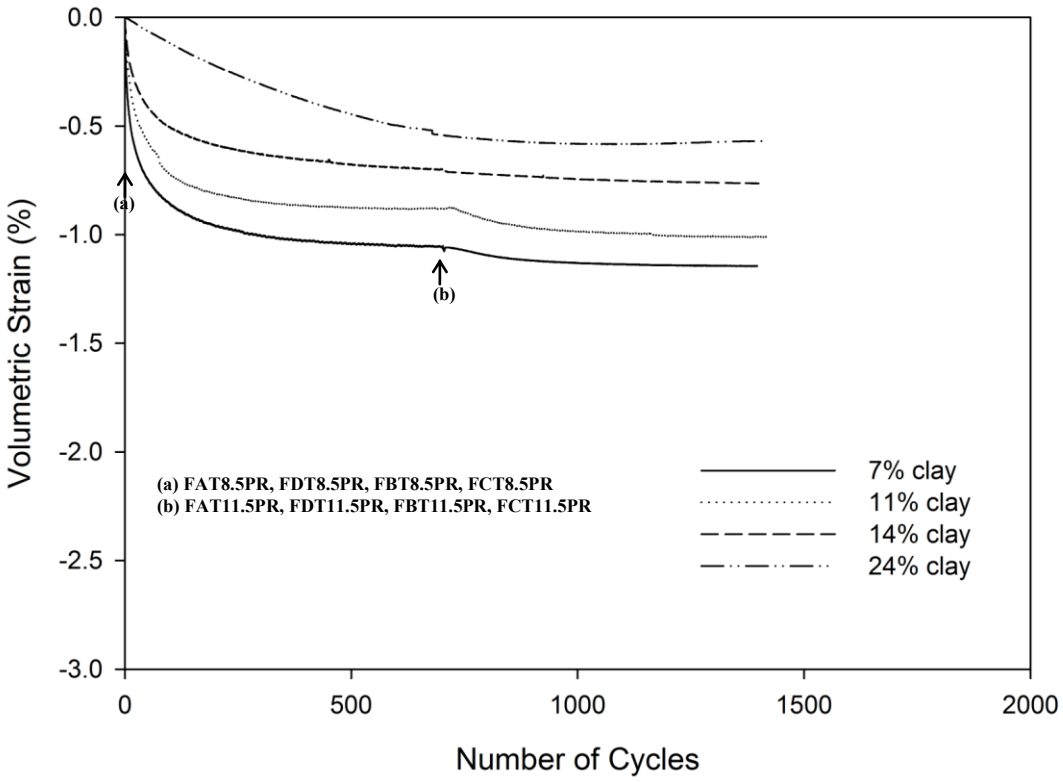

Figure 4.5: Volumetric strains of the 7%,11%,14% and 24% clay content mixes during cyclic preloading with PSR.

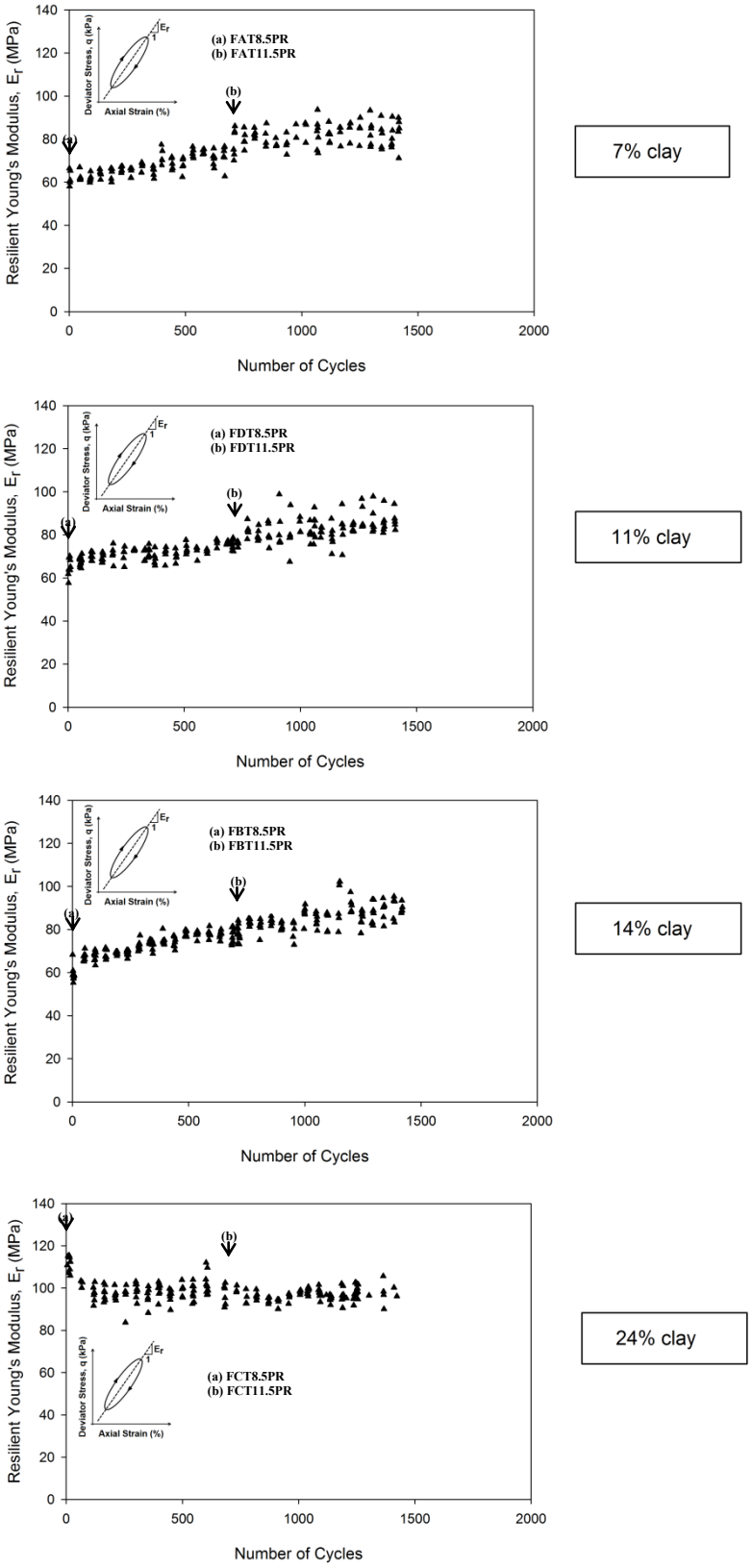

Figure 4.6: Resilient Young's modulus of the 7%,11%,14% and 24% clay content mixes during free to drain cyclic preloading with PSR.

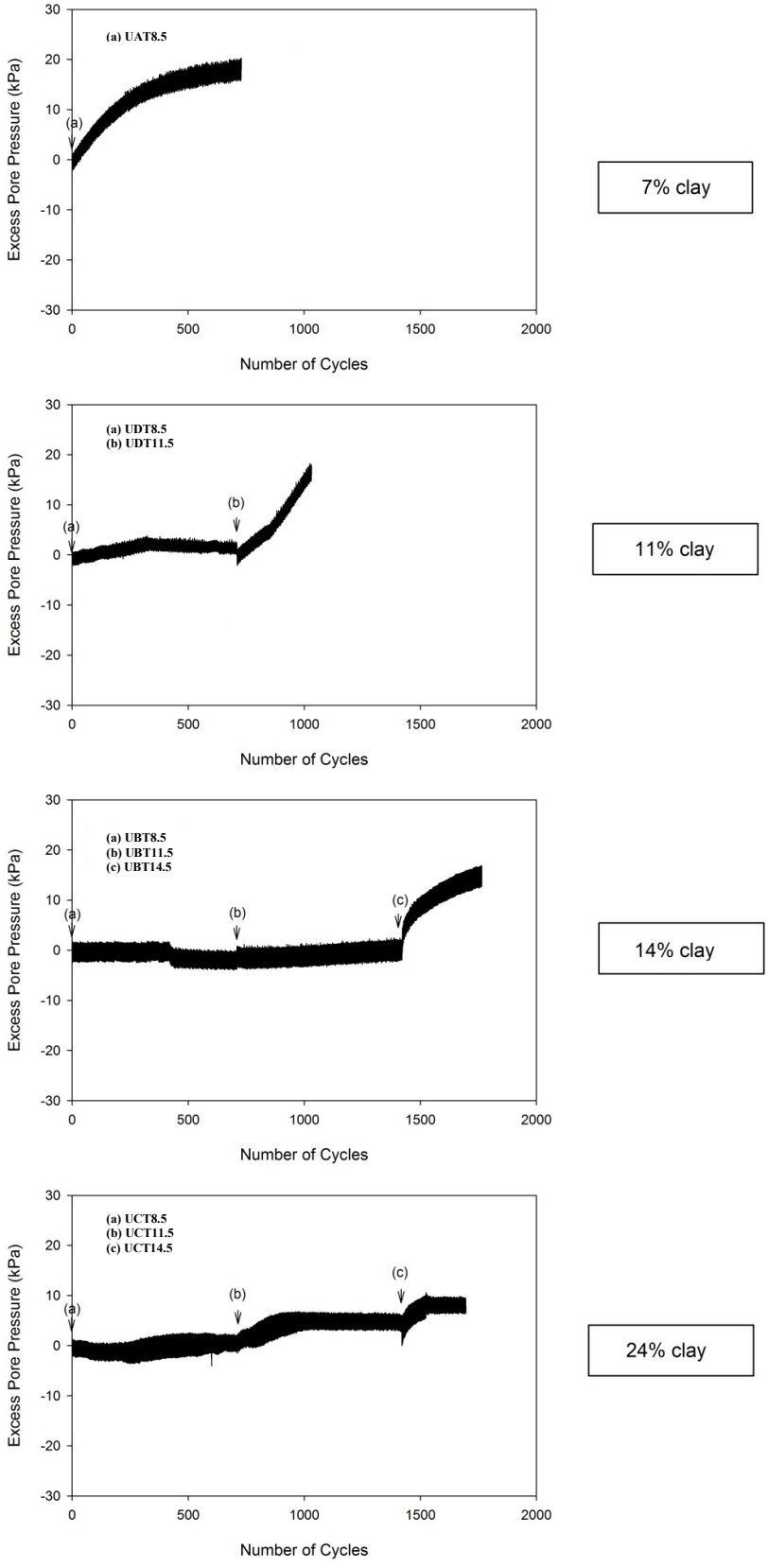

Figure 4.7: Excess pore pressure accumulation during undrained cyclic PSR of the 7%,11%,14% and 24% clay content mixes.

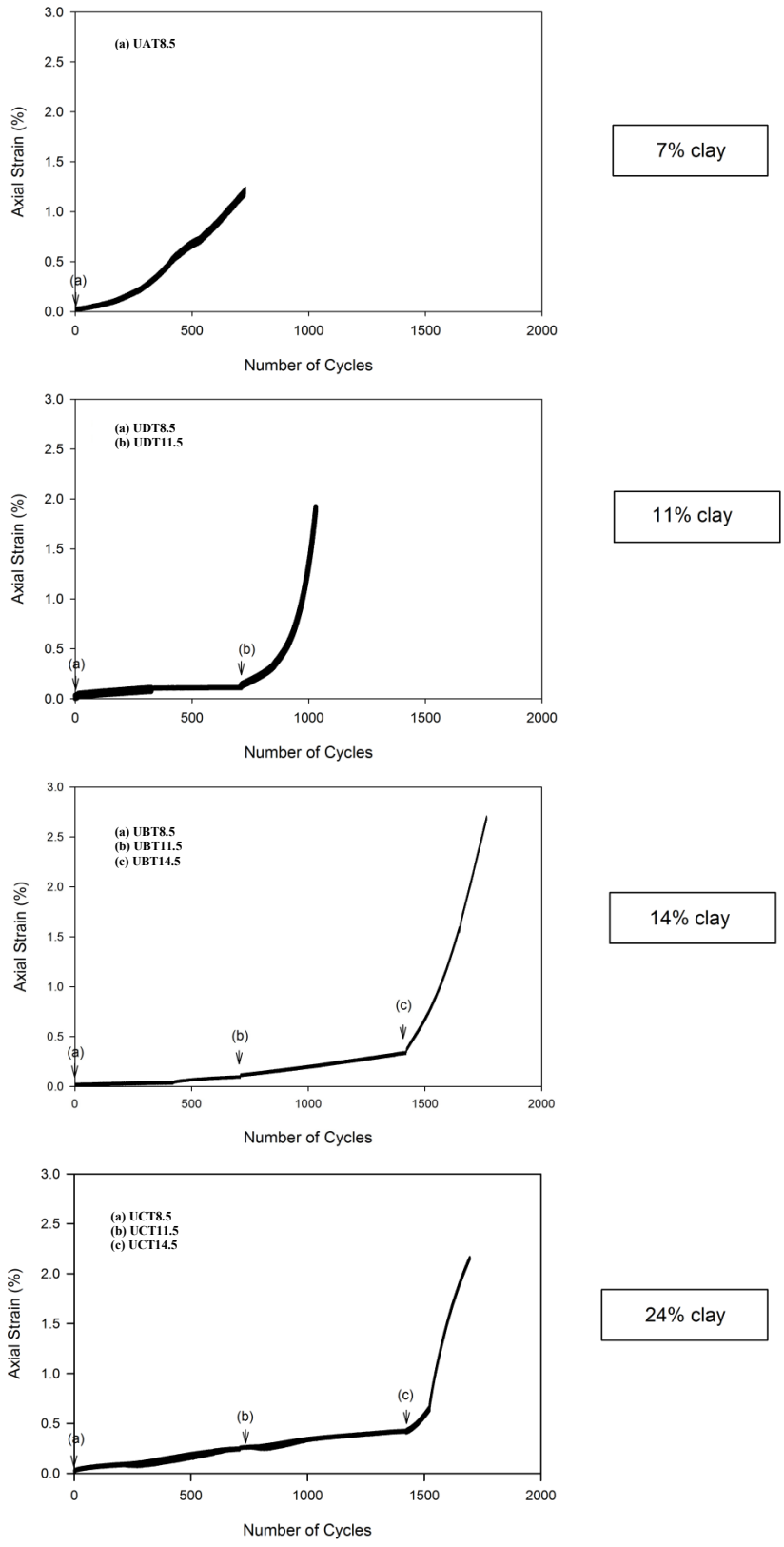

Figure 4.8: Axial strain accumulation during undrained cyclic PSR of the 7%,11%,14% and 24% clay content mixes.

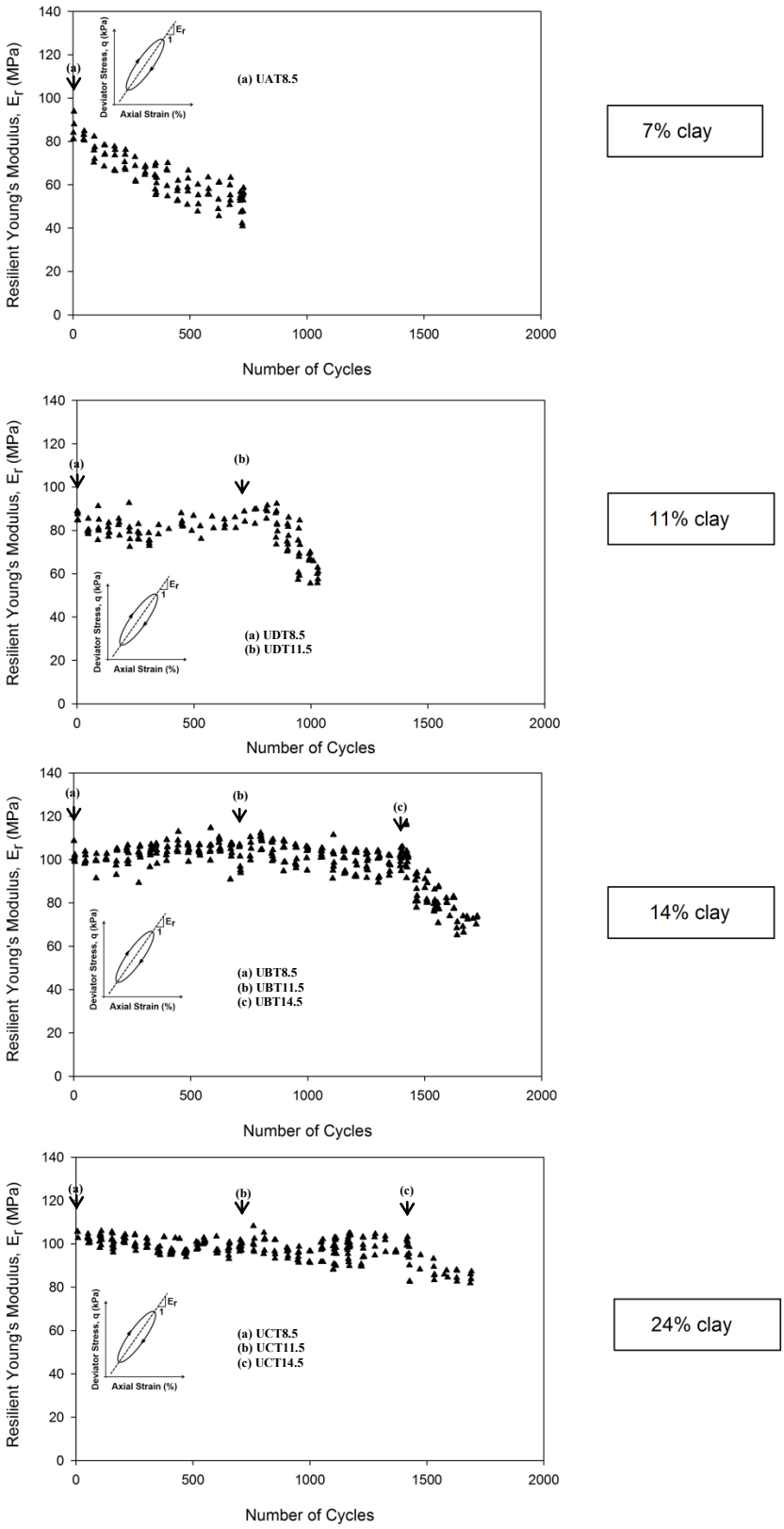

Figure 4.9: Resilient Young's modulus of the 7%,11%,14% and 24% clay content mixes during undrained cyclic PSR.

Component description	Young's modulus: MPa	Poisson's ratio	Density: kg/m^3	Remarks
Rail	210 000	0·3	7850	$A = 7{\cdot}6125\times10^{-3}$ m^2 $I = 2{\cdot}70327\times10^{-5}$ m^4
Pad	6·9357	0·49	1280	Assumed natural rubber (Liegner, 2002)
Sleeper	30 000	0·2	2400	Reinforced concrete
Ballast	100 (29·1)	0·3	1800	
SSB	321 (611)	0·3	2300	
SB	296 (297)	0·3	2200	
A	143 (113)	0·3	2100	
B	118 (48)	0·3	2100	
Natural ground	27 000 (894)	0·25	2300	

Note: Values of Young's modulus given in parentheses are initial values obtained from Shaw (2005). Values not in parentheses are calculated values obtained using trial and error such that model displacements correspond to measured displacements.

Figure 4.10: Back-calculated stiffness values of the South African railway track foundation based on field displacement measurements. From Priest et al. (2010).

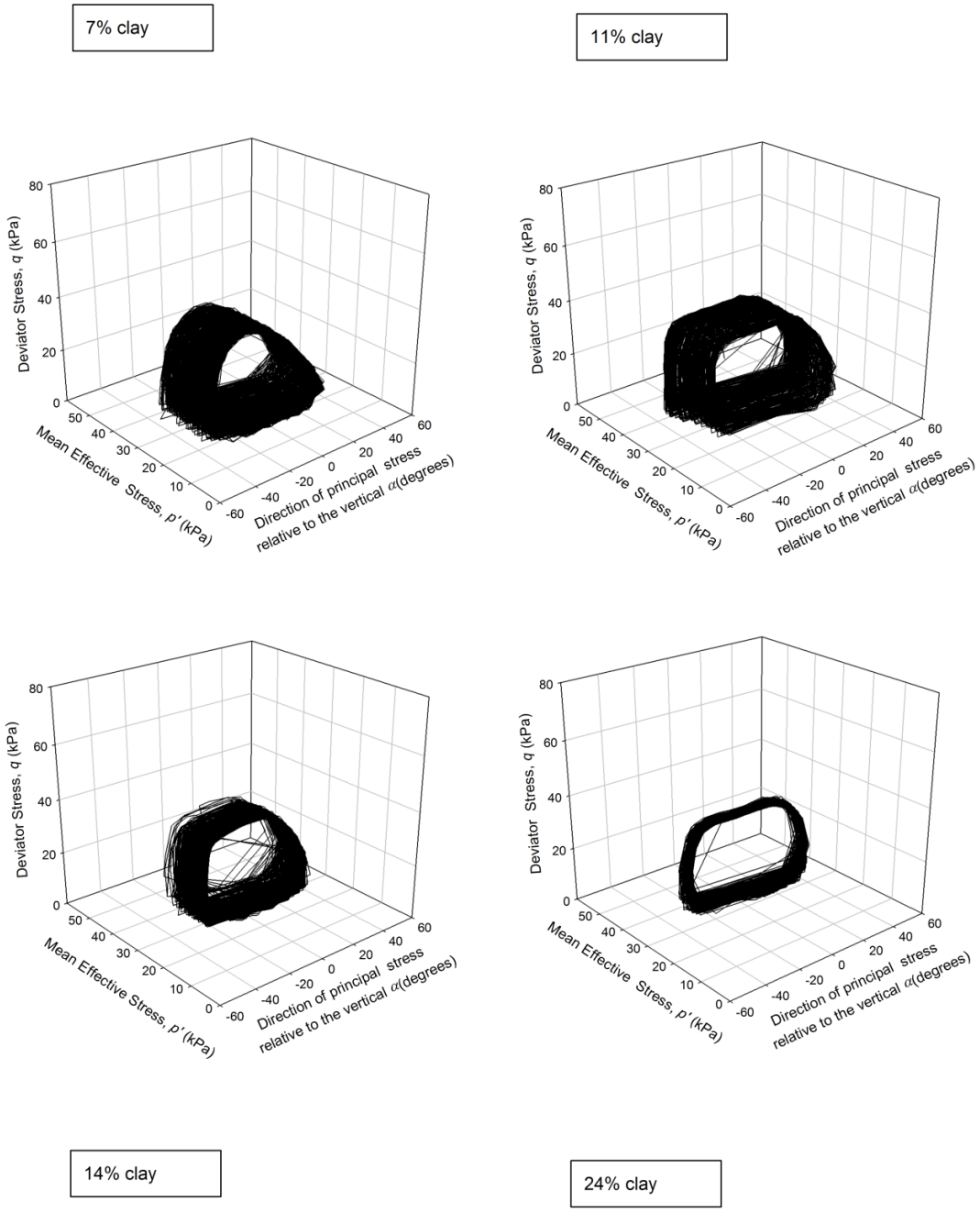

Figure 4.11: Stress paths of the 7%,11%,14% and 24% clay content mixes in the general stress space during failure under undrained cyclic PSR.

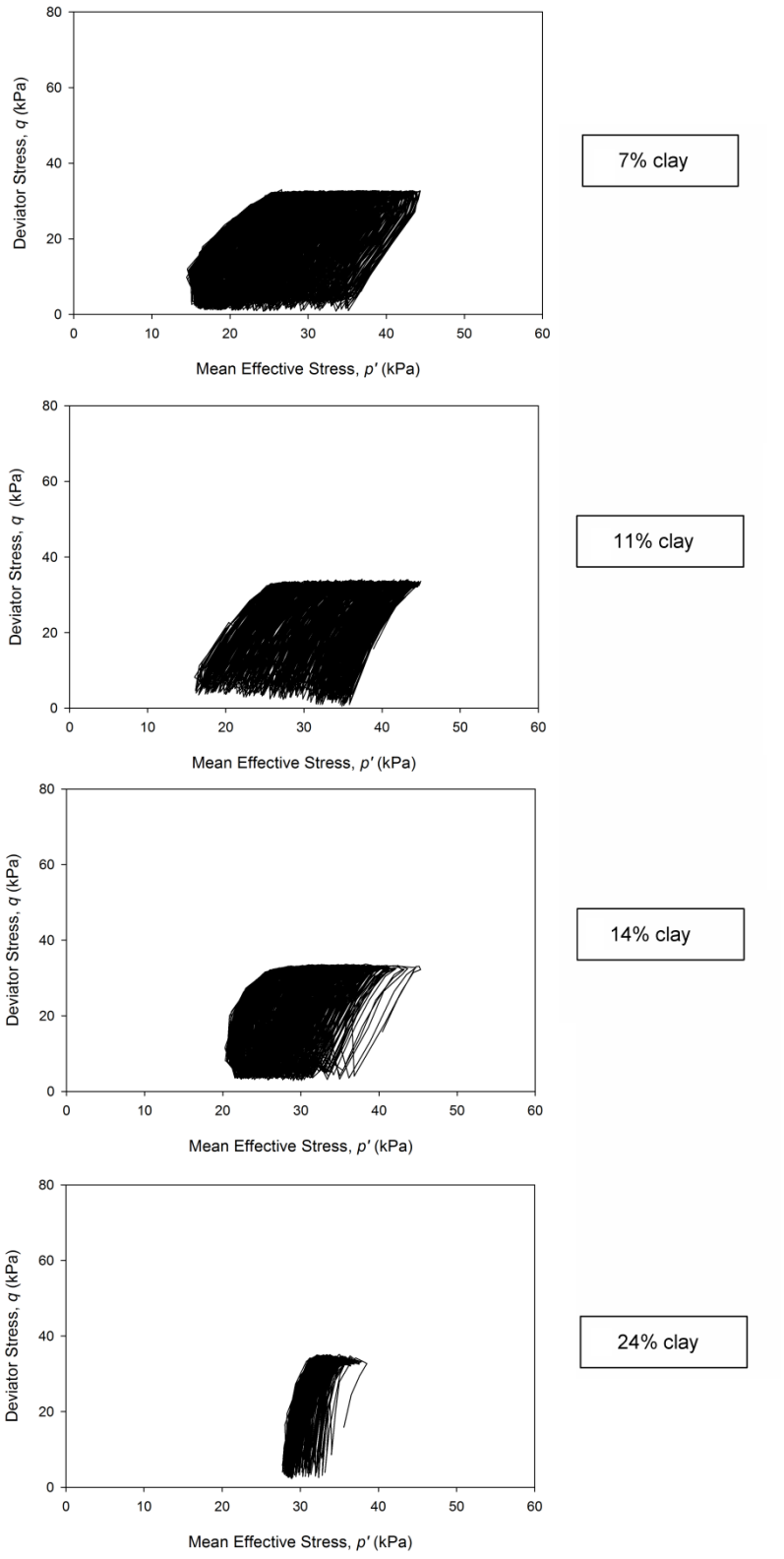

Figure 4.12: Stress paths of the 7%,11%,14% and 24% clay content mixes in the q-p' stress space during failure under undrained cyclic PSR.

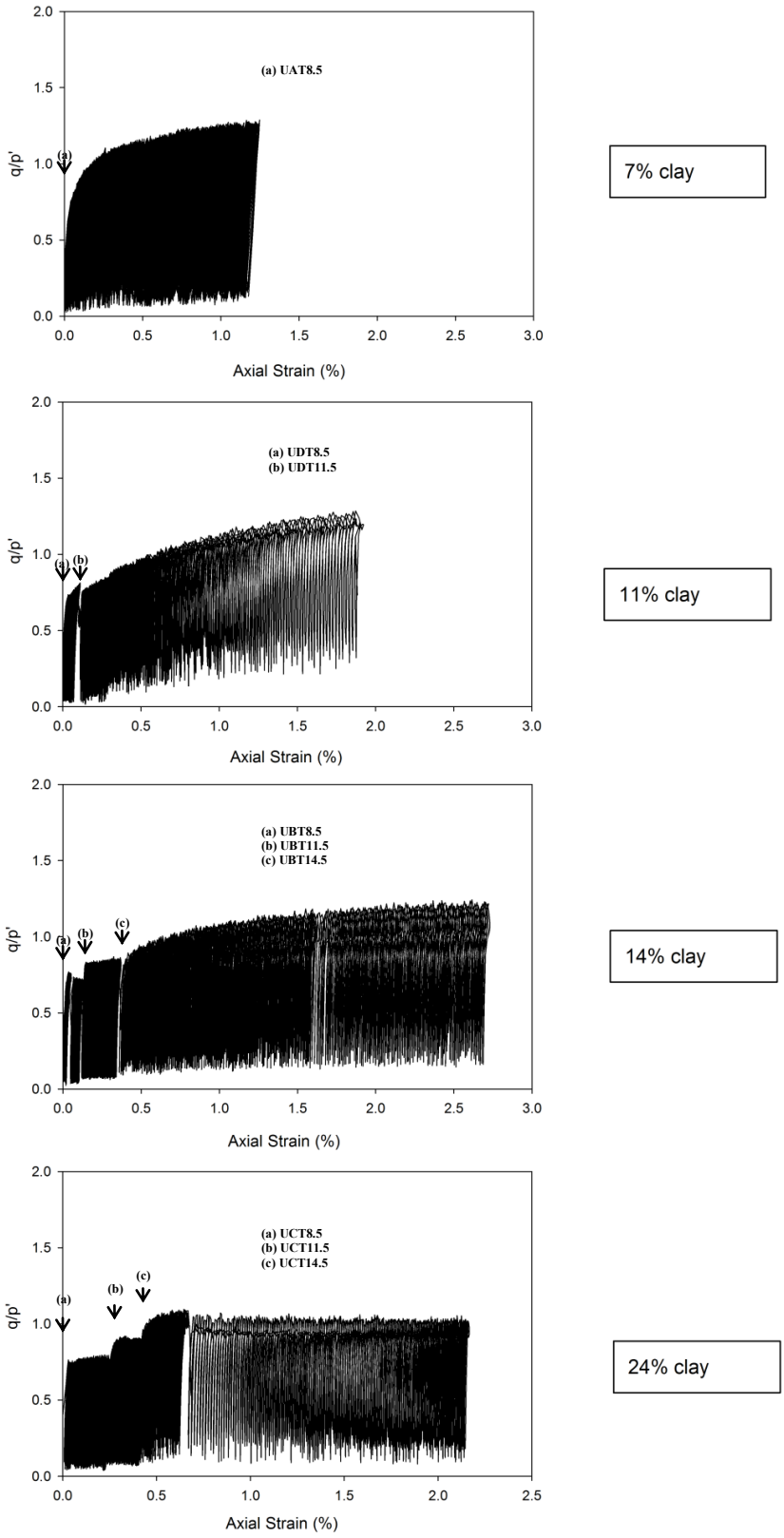

Figure 4.13: Mobilised q/p' ratio per axial strain of the 7%,11%,14% and 24% clay content mixes under undrained cyclic PSR.

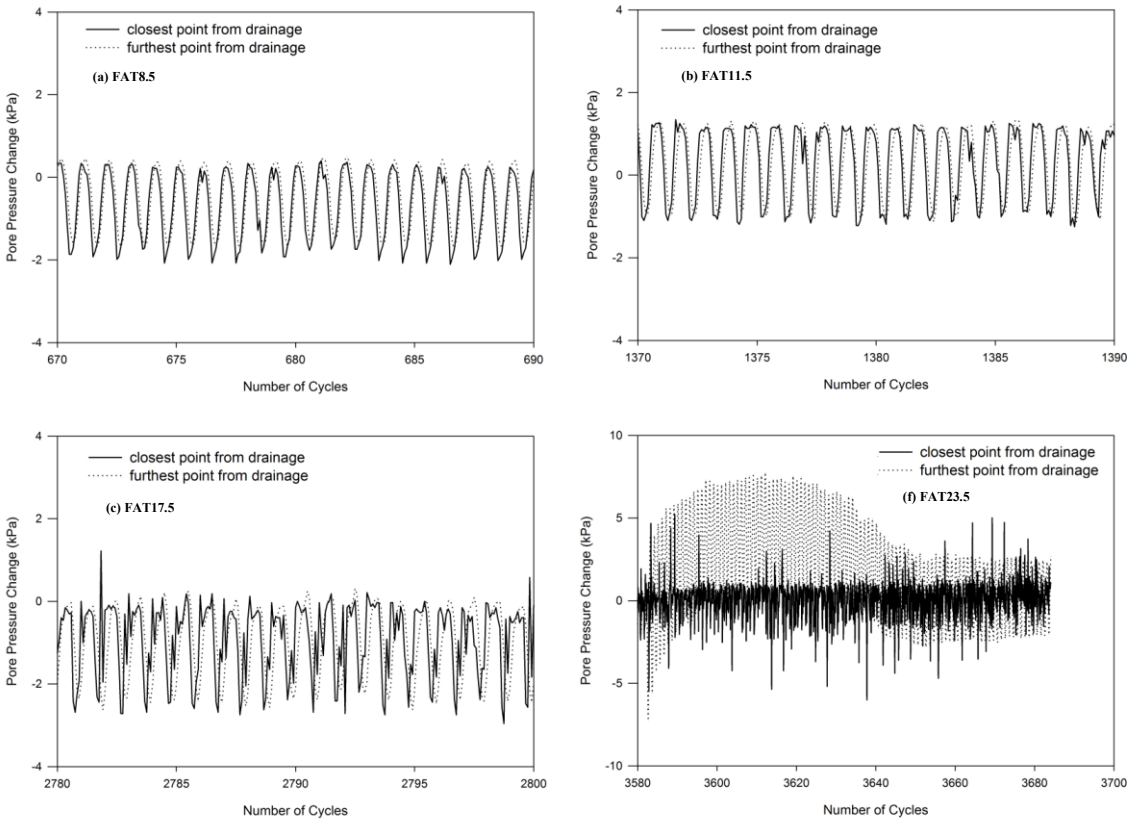

Figure 4.14: Pore pressure response at the furthest and closest point from drainage of the 7% clay content mix during cyclic increases in the magnitude of PSR.

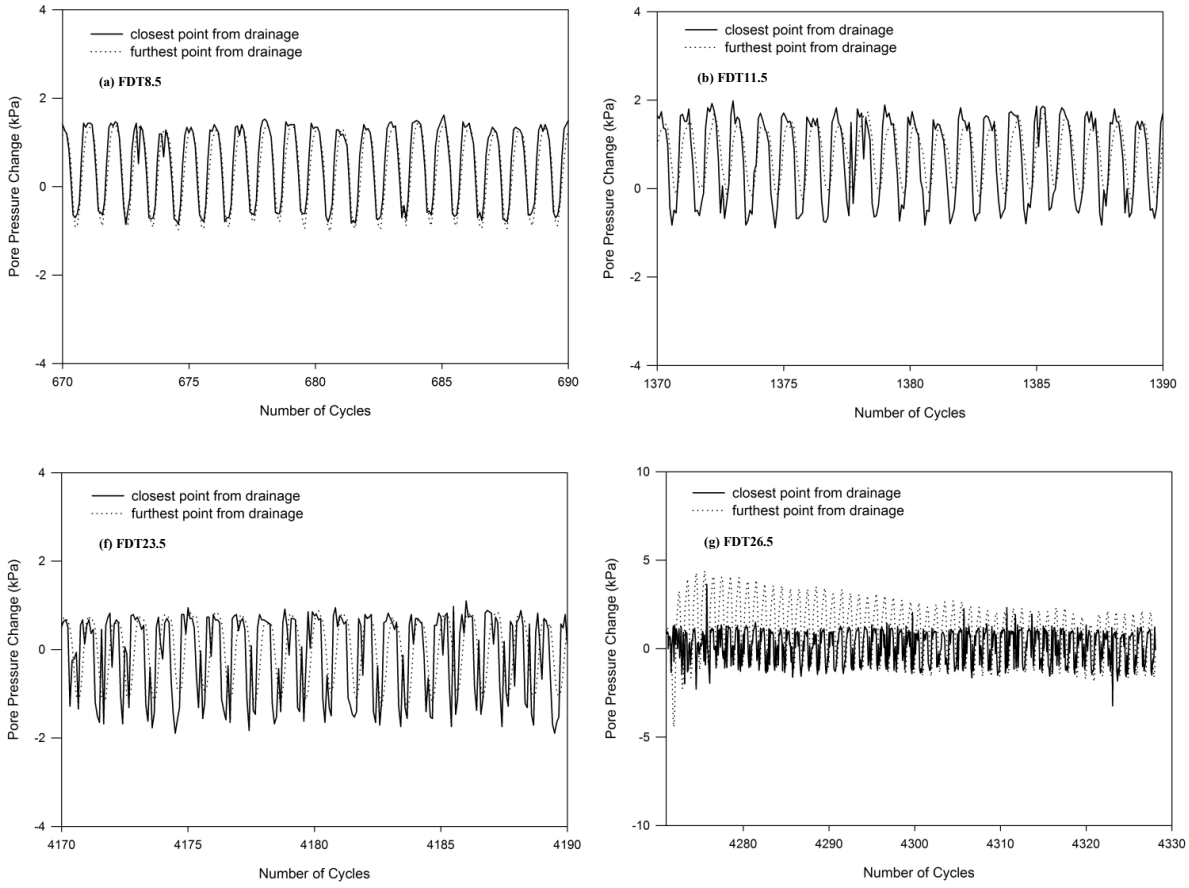

Figure 4.15: Pore pressure response at the furthest and closest point from drainage of the 11% clay content mix during cyclic increases in PSR up to failure.

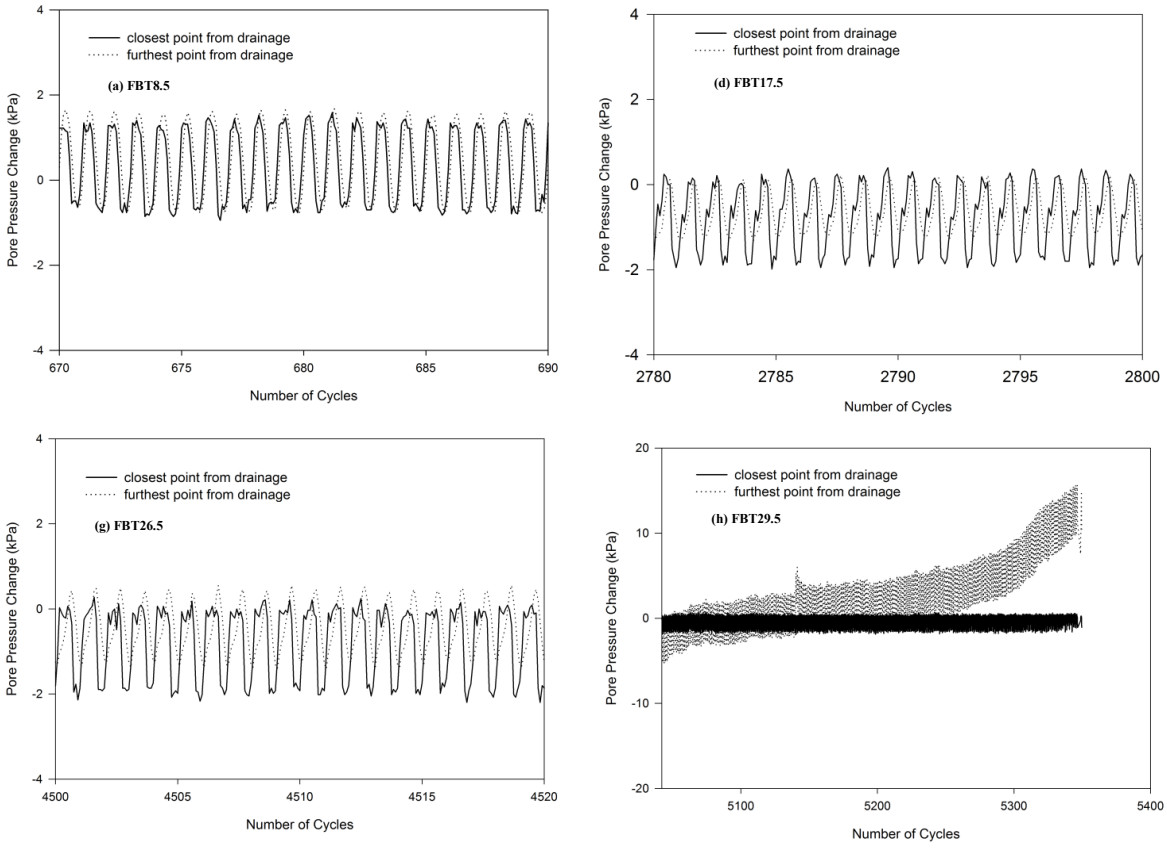

Figure 4.16: Pore pressure response at the furthest and closest point from drainage of the 14% clay content mix during cyclic increases in PSR up to failure.

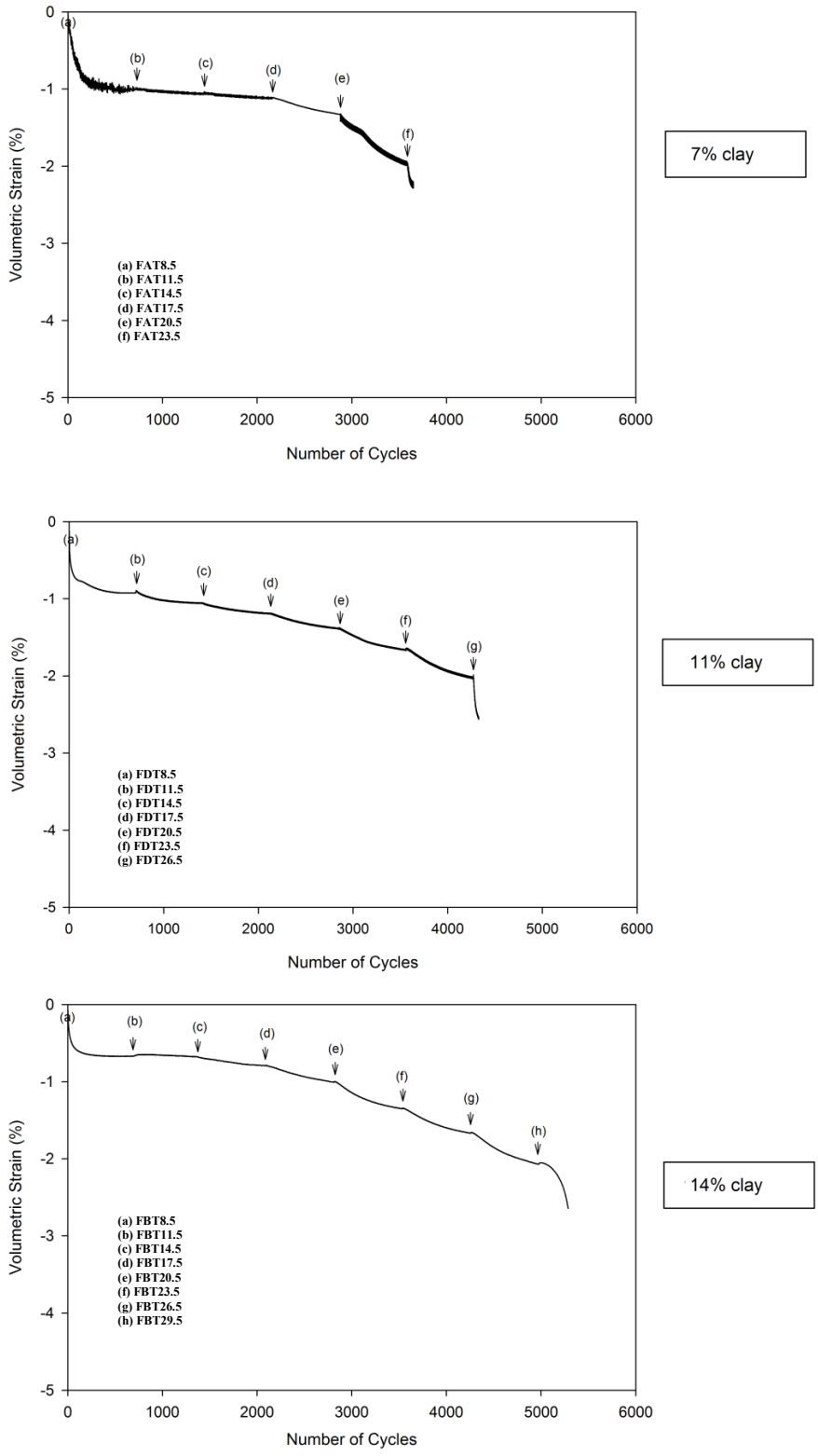

Figure 4.17: Volumetric strains of the 7%,11%,14% clay content mixes during cyclic increases in the magnitude of PSR up to failure.

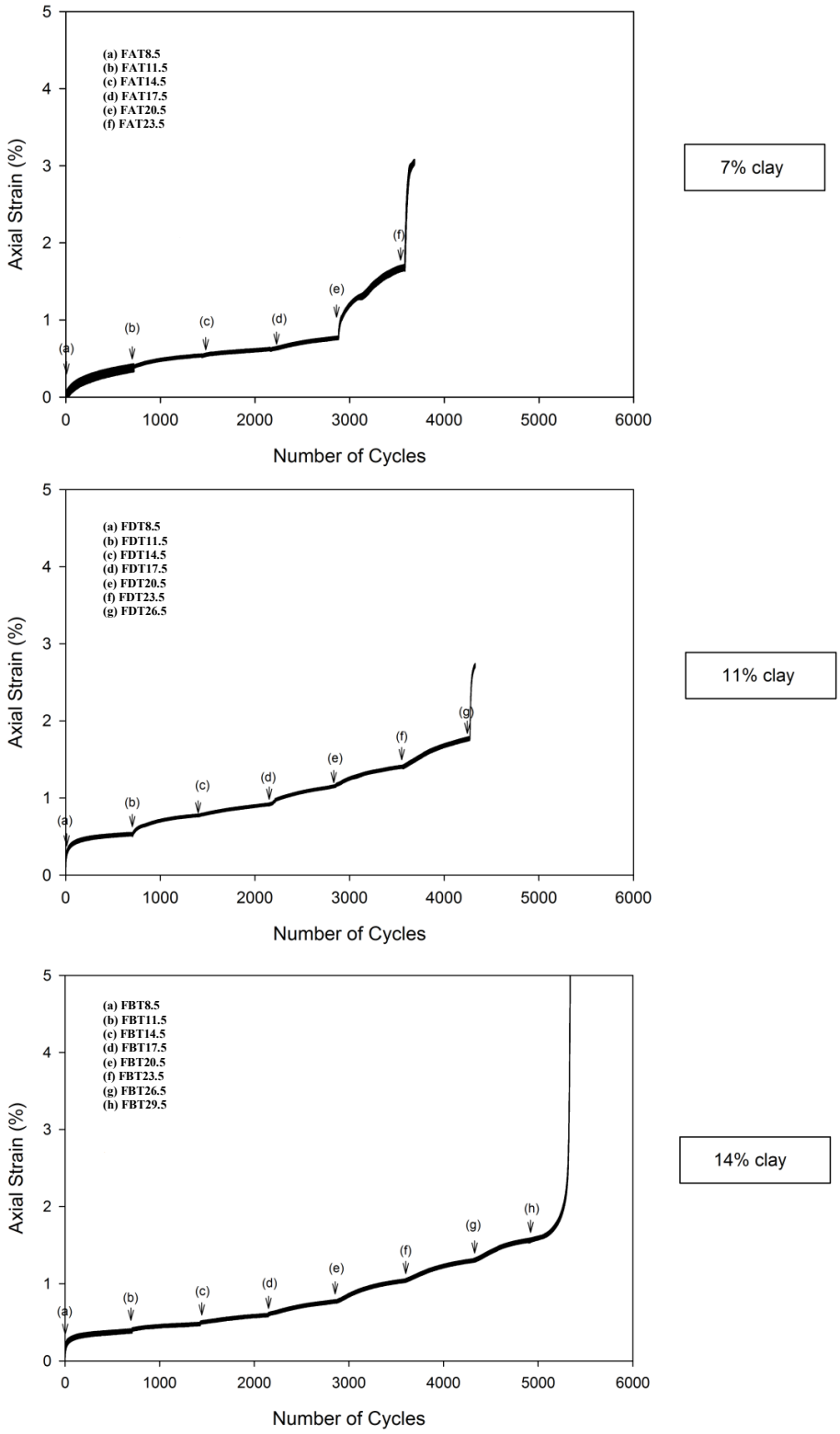

Figure 4.18: Axial strains of the 7%,11%,14% clay content mixes during free to drain cyclic increases in PSR up to failure.

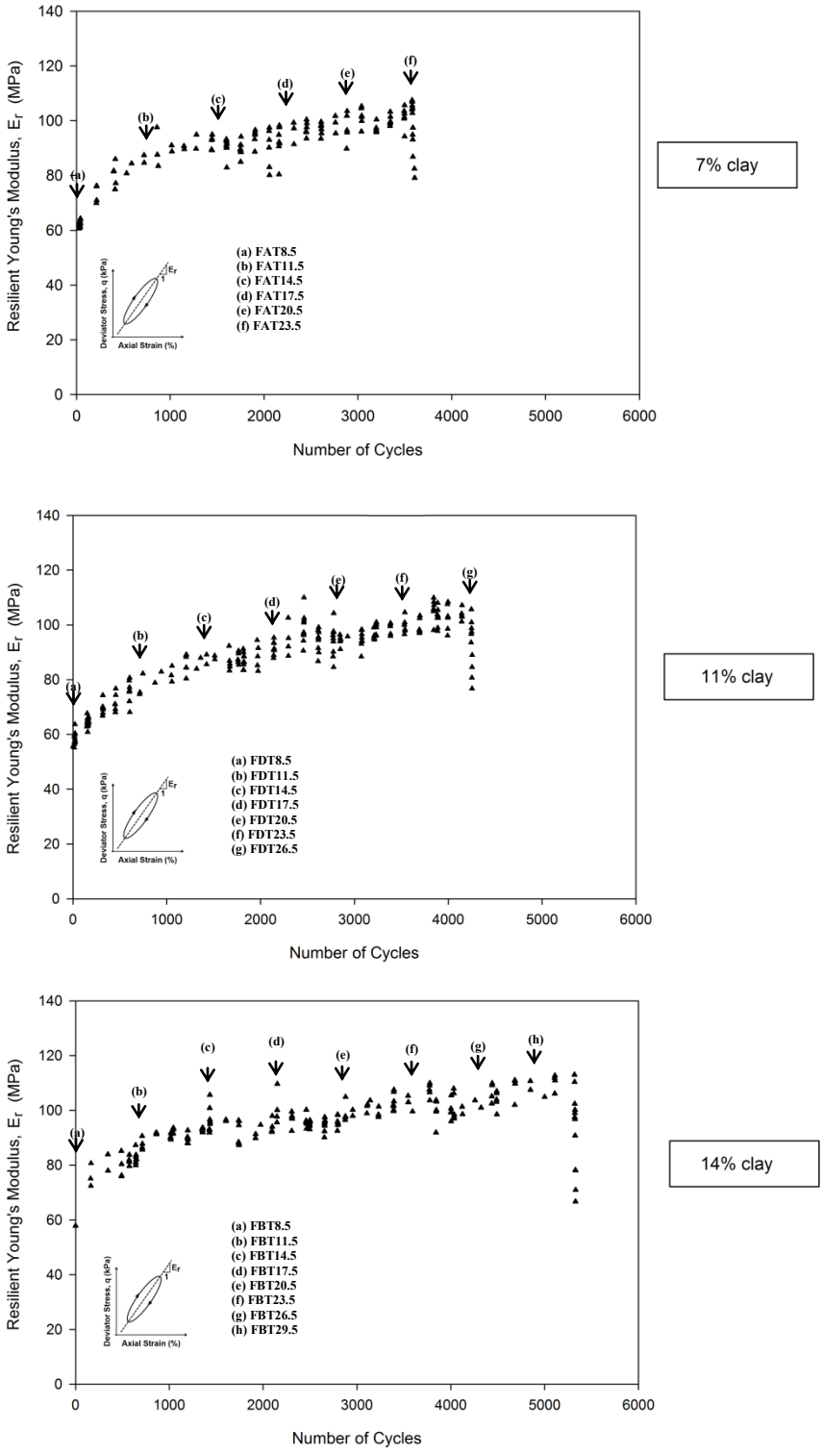

Figure 4.19 Resilient Young's modulus of the 7%,11%,14% clay content mixes during free to drain cyclic increases in PSR up to failure.

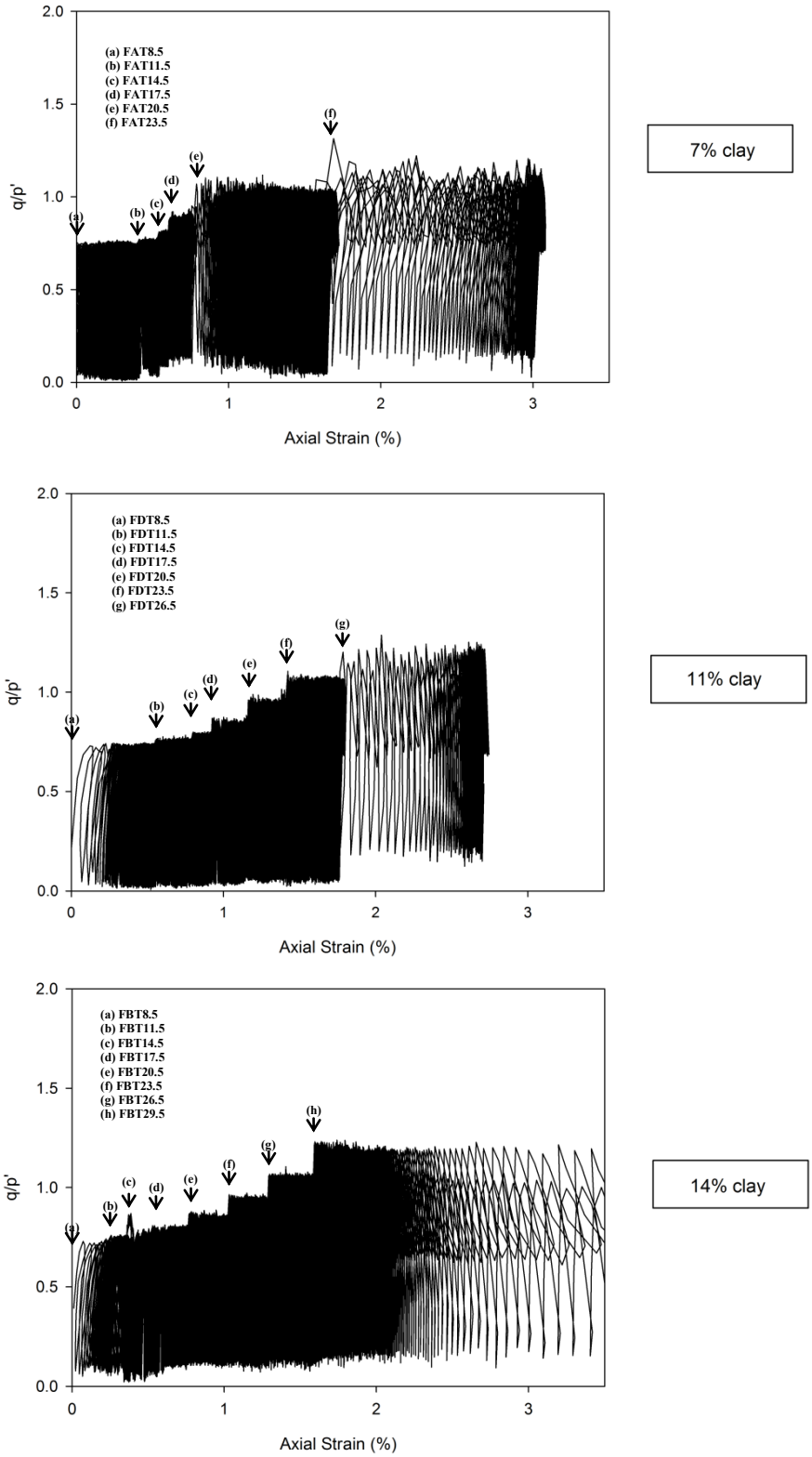

Figure 4.20: Mobilised q/p' ratio versus axial strain of the 7%,11%,14% clay content mixes during free to drain cyclic increases in PSR up to failure.

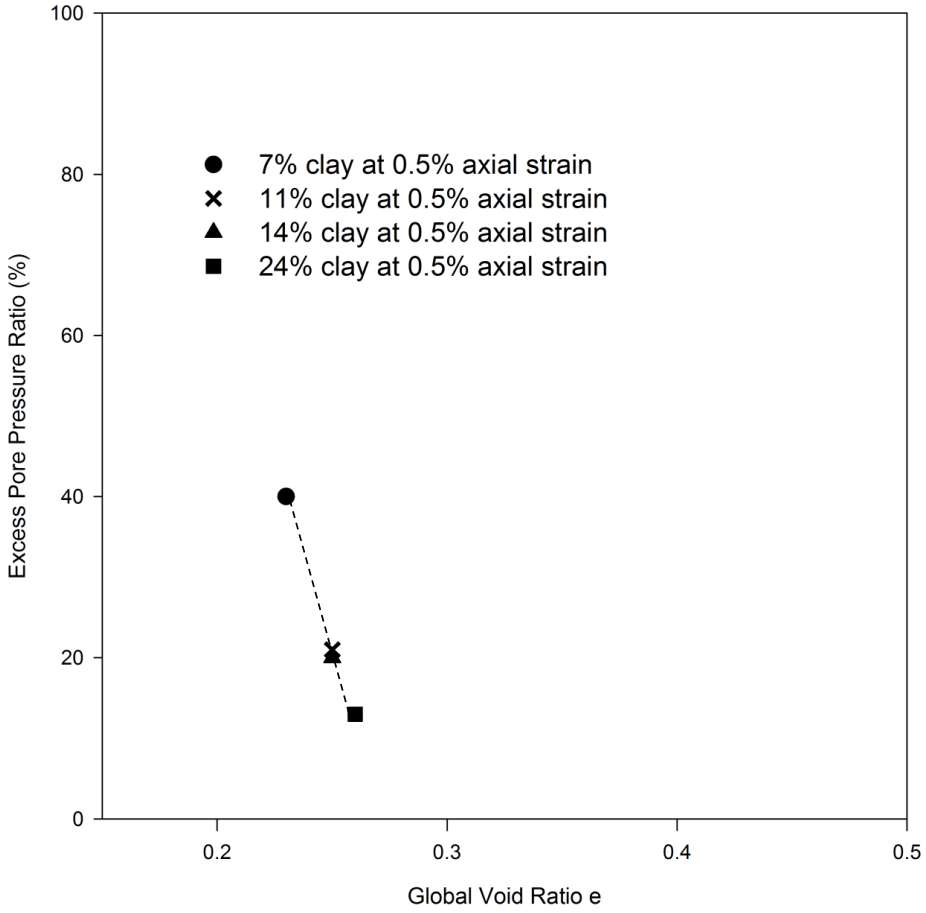

Figure 4.21: Excess pore pressure ratio versus global void ratio of the different sand-clay mixes at 0.5% axial strain.

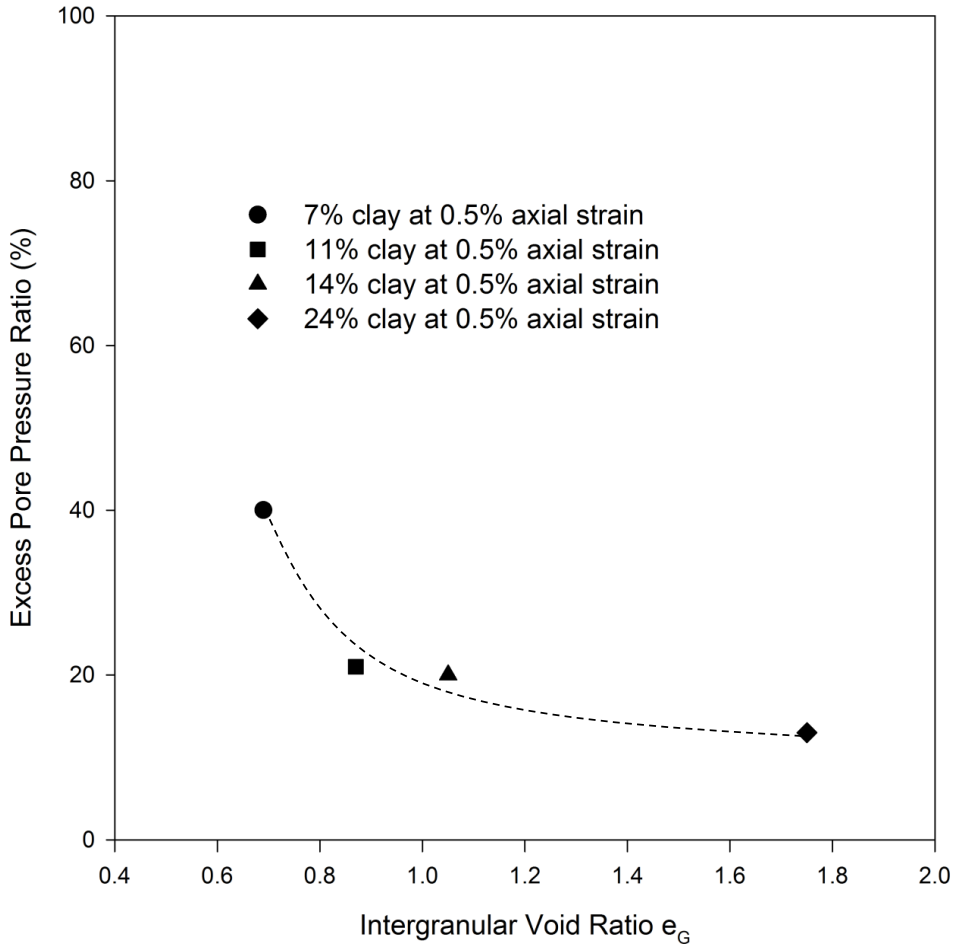

Figure 4.22: Excess pore pressure ratio versus inter-granular void ratio of the different sand-clay mixes at 0.5% axial strain.

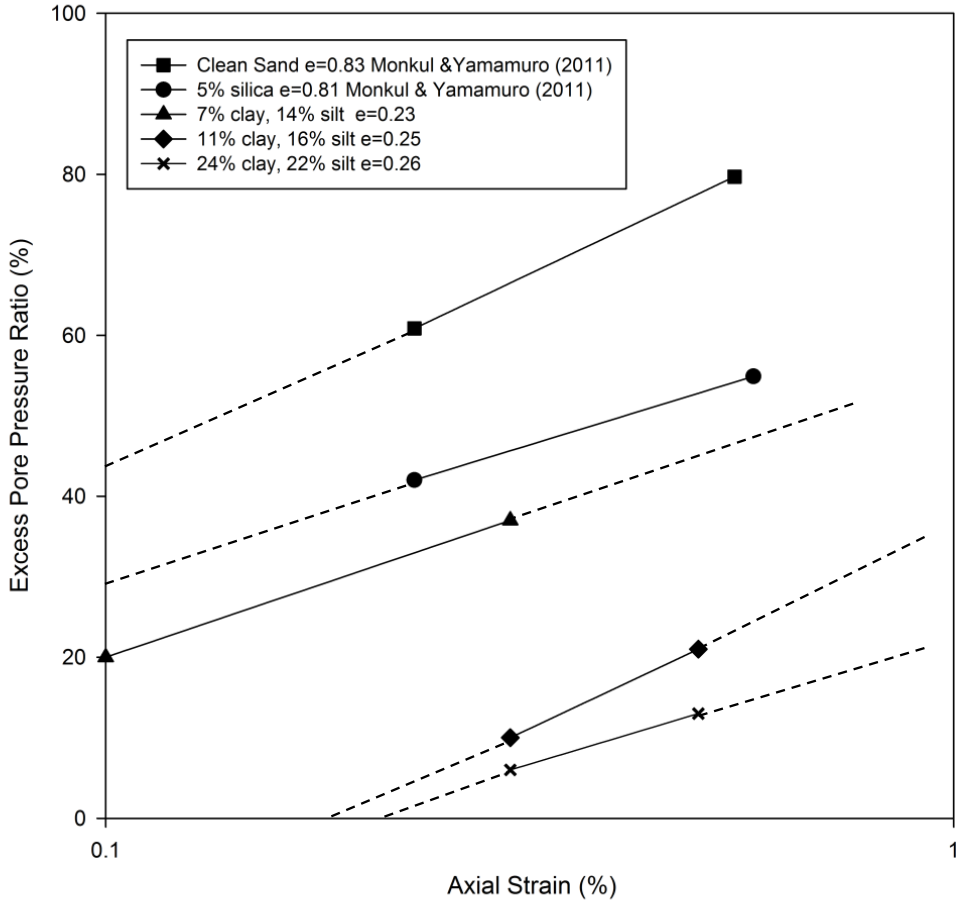

Figure 4.23: Excess pore pressure ratio versus the logarithm of axial strain for sands containing various amounts of fines.

Chapter 5

CONCLUSIONS AND SUGGESTIONS FOR FURTHER WORK

The quality of a railway track foundation lies at the core of an efficient railway infrastructure. Inadequate foundation design may give rise to irregularities in the overlying rail track geometry, which will affect the stability, safety and overall train ride quality. Maintenance of the track to the required standards is likely to be at considerable financial expense, if the quality of the railway track foundation is poor.

The reviewed literature revealed that premature failures associated with progressive shear and excessive plastic deformations may not simply be prevented by an increase in the thickness of the overlying ballast layer. Accelerated deterioration of railway track foundations may be associated with the neglect of the true stress path which involves principal stress rotation (PSR). Data relevant to the effects of PSR are relatively few and

therefore our understanding of how cyclic changes in the magnitude of PSR may affect different soils is still limited. To address this knowledge gap a set of hollow cylinder experiments was designed, which investigated the response of different sand-clay mixes representative of engineered railway track foundations soils, to a range of PSR changes typically expected within the depth of the foundation layer (Chapter 3). The results of these experiments were presented and discussed in the context of the practical implications for railway foundation design. The results were also analysed in the context of the divergence of views in the research community as to the role of increasing the fines content on the volume change behaviour of a sand (Chapter 4). This chapter draws together the main conclusions, before making some suggestions for potential areas of further research, which may help us better understand the performance of real railway track foundations.

5.1 Conclusions

A number of conclusions can be drawn from the reviewed literature in relation to PSR relevant to railway track foundations. There are few datasets relevant to the behaviour of a soil element under a stress path representative of that caused by a train passage. Powrie et al. (2007) presented an analytical FEM, which identified the stress changes likely to occur with depth within a railway track foundation, highlighting the relationship between vertical and shear stresses on a soil element. At shallow depths the influence of PSR was significant but it became negligible at higher depths as the magnitude of PSR was too small. The analysis also highlighted that during train acceleration and braking the magnitude of PSR can become even more pronounced, with a shear stress of up to 25% of the vertical wheel load being applied at the wheel rail interface. The results of this analysis were used to determine the range of stresses in conducting the laboratory investigation in this research.

It was also shown that little consideration is generally given to how the in situ drainage conditions may be simulated in the laboratory. In the field, drainage conditions will be controlled by the permeability and the volumetric compressibility of the soil comprising the railway track foundation. The volumetric compressibility will dictate the magnitude of change in pore pressure as a result of PSR. In addition the permeability will determine how quickly this change in pore pressure will be dissipated. In the case where drainage is inhibited by the railway track foundation itself or the neighbouring layers of soil, the susceptibility to PSR will be controlled by the potential of the material to accumulate excess pore pressures.

To extend our understanding of the effects of PSR to stress paths relevant to railway track foundations, a series of laboratory experiments was conducted, the main conclusions of which are detailed below:

Cyclic changes in PSR can have a significant effect on the rate of railway track deterioration as they not only influence the development of plastic strains but can also significantly affect the pore pressure, resilient stiffness and strength of soils. The addition of moderate amounts of clay in the volume of the sand reduced the susceptibility to cyclic changes in PSR.

- In undrained conditions this was indicated by a decrease in the rate of excess pore pressure generation with increasing clay content. Under free to drain conditions, moderate additions of clay were observed to reduce the generated volumetric contractions. However, further increases in clay content beyond 14% substantially reduced the permeability of the mixture resulting in insufficient excess pore pressure dissipation despite the reduced volumetric contractions. For moderate additions of clay, failure ultimately occurred as a result of the insufficient rate of excess pore pressure dissipation associated with the rate of generated volumetric contractions and was more pronounced for the granular mixes, verifying the results of the undrained dataset. In terms of railway track foundation design, this suggests that even under conditions where the rate of any

pore pressure dissipation is regulated by the permeability and the volumetric compressibility of the mixes, the susceptibility to PSR will be ultimately controlled by the propensity of the material to accumulate excess pore pressures. This suggests that in the field sand-clay mixes whose gradation is dominated by the granular particles are likely to be more susceptible to accelerated deterioration than sand-clay mixes with moderate quantities of clay.

- The rate of pore pressure increase with axial strain was similar for sands containing different amounts of clay. Increasing the fines content however caused a downward and almost parallel shift in the amount of generated excess pore pressures as a ratio of the effective stress of the mixes.

- Increasing the clay content increased the cyclic shear threshold the sand-clay mixes were able to sustain before rapid plastic strain accumulation occurred.

- Cyclic increases in PSR below the shear threshold increased the resilient stiffness of the sand-clay mixes but once this threshold was exceeded rapid stiffness degradation occurred. Under certain circumstances therefore, PSR may have a beneficial effect on the stability of railway track foundations by reducing the long term pavement deflection as a result of stiffness increases.

- Below the cyclic shear threshold, the response of the mixes was stable over a high number of loading cycles and no abrupt fatigue failures were observed.

- The sand-clay mixes were sensitive to even small changes in the magnitude of PSR near the cyclic shear threshold. Small increases in PSR could trigger the sudden collapse of a previously stable sand-clay mix. The current stability of a railway track foundation may therefore not necessarily be interpretable as an indicator of its suitability to accommodate heavier traffic volume.

- Under conditions where the rate of pore pressure dissipation was regulated by the permeability and the volumetric compressibility of the soil, the sand clay mixes

with moderate additions of fines were stable over a range of cyclic increases in PSR which correspond to the maximum expected changes in magnitude within the depth of a ballasted railway track foundation.

- The results reported in this research constitute one of the few attempts to explore the effect of increasing the fines content in the pore space of a host sand, under cyclic increases in the magnitude of PSR up to failure and therefore also contribute to the wider discussion about the effect of fines, which has been predominately investigated under monotonic and simple cyclic loading conditions

5.2 Recommendations for future work

This research investigated the effects of changes in PSR for gradual increases in clay content, under both drained and undrained conditions. However in dry periods, the soil may become unsaturated and suctions may influence soil behaviour. An understanding of how suction influences the effects of PSR is therefore important. To date, no data have been reported on unsaturated specimens involving cyclic changes in PSR and therefore such an endeavour would be worthwhile pursuing.

Another potential area of interest would be the testing of natural samples, retrieved from existing railway track foundations, which could be benchmarked against the observed response of reconstituted materials. For example, comparison of the mechanical response of natural and engineered materials, may improve our understanding of the influence of aging on principal stress rotation. The term aging is used in the context of soil's strength and stiffness improvement throughout time resulting from internal arching of stresses and thixotropic effects associated with the colloidal forces of attraction between clay particles that primarily occur at low effective stresses and may therefore be of interest for railway track foundations (Schmertmann, 1991).

Natural samples might also be used to investigate the effects of PSR at a micromechanical level. High resolution CT scanning equipment could be used to explore the morphology and fabric of particle contacts and reveal whether a specific pattern of particle alignment is favoured as a response to principal stress rotation.

APPENDIX

Models for the prediction of permanent deformations

The estimation of the total accumulated plastic deformations has attracted a strong interest among researchers. Analysing the permanent deformation growth patterns of a series of cyclic tests Barksdale (1972) proposed the following log-normal expression for the cumulative plastic strains

$$\varepsilon_p = a + b\log(N) \tag{A.1}$$

where N the number of repeated load applications, and α and b are parameters that depend on the soil type and stress state. Sweere (1990) however observed that the log-normal expression did not fit his cyclic test results well and revised the expression for the cumulative plastic strain on the basis of a log-log approach

$$\varepsilon_p = AN^b \tag{A.2}$$

where N the number of repeated load applications and A and b parameters that depend on soil type, soil properties, and stress state. Curve fitting of the log-log approach with a number of reported cyclic test results suggested that the coefficient A varied greatly from 0.0005-6.3 and depended on the deviator stress and the soil physical state (Li (1994) cited in Li & Selig (1996)). In contrast to coefficient A, exponent b was found to be

independent of the deviator stress as well as the soil physical state (soil-moisture content and dry density) (Li & Selig, 1996).

In a high number of repeated full-scale heavy vehicle simulator tests, Wolff &Visser (1994) observed that the log-log approach only gave a reasonable fit during the early loading cycles, but that it tended to diverge from the data after a very large number of load repetitions. Based on the laboratory data they suggested the following growth equation for the plastic strains

$$\varepsilon_p = (mN + a)\left(1 - e^{-bN}\right) \tag{A.3}$$

where N the number of load repetitions, m is the slope of the asymptote, α is the intercept of the asymptote and b is a constant controlling the curvature.

Khedr (1985) reported that the rate of permanent strain accumulation of a crushed limestone decreased logarithmically with increasing number of load repetitions according to the following expression

$$\frac{\varepsilon_p}{N} = AN^{-m} \tag{A.4}$$

where N the number of repeated load applications, m a material parameter and A a material and stress-strain parameter which was found to depend on the shear stress ratio. Paute et al. (1988) also observed that the permanent strain increased gradually towards an asymptotic value but proposed a different model for the accumulation of permanent axial strains

$$\varepsilon_{1,p} = \frac{A\sqrt{N}}{\sqrt{N} + D} \tag{A.5}$$

where $\varepsilon_{1,p}$ the additional permanent axial strain after the first 100 load cycles, and A and D regression parameters.

Based on cyclic triaxial tests on granular materials Paute et al. 1996 also observed that the permanent strain approached a limit value as the number of load repetitions increased toward infinity and reported that the accumulation of permanent strain after an initial period of 100 could be quantified by the following expression

$$\varepsilon_{1,p} = A\left(1-\left(\frac{N}{100}\right)^{-B}\right) \tag{A.6}$$

where A and B regression parameters. Given that $\left(1-\left(\frac{N}{100}\right)^{-B}\right)$ approaches a limit value with increasing load repetitions, parameter A is considered the limit value for total permanent axial strain.

Finally Bonaquist & Witczak (1997) proposed a constitutive model for the development of permanent strain under repeated loading utilising the flow theory of plasticity. According to the flow theory of plasticity the total strain increment consists of a reversible resilient strain increment and an irreversible plastic strain increment. The plastic strain increment was assumed to be a function of the current states of stress and strain and the incremental change in stress. The mathematical expression of this new model is presented below

$$\varepsilon_p = \sum \varepsilon_N = \sum \frac{1}{N^h}\varepsilon_\iota \tag{A.7}$$

where ε_l the stain increment, N the number of load repetitions and h a regression parameter.

Under repeated loading, the hardening behaviour of the material is modelled by expressing the permanent strain for any load cycle as a power function of permanent strain during the first load cycle. The accumulated permanent strain is then calculated as the sum of the permanent strain in each cycle.

Some researchers proposed models where the projected deformation is based on correlations between cyclic and static loading tests on the same materials (Duncan & Chang, 1970; Pappin, 1979; Lentz & Baladi, 1981). These models however have been met with some scepticism as it has been questioned whether cyclic and static loadings induce the same micro and macro mechanical response in soils (Lekarp et al., 2000). Some of these models are presented below. For example Barksdale (1972) performed cyclic triaxial tests on granular base course materials and used the results to relate the permanent axial strain to the ratio of repeated deviator stress and constant confining pressure as follows:

$$\varepsilon_p = \frac{q / K(\sigma_3)^n}{1 - \left[\frac{(R_f q) / 2(C\cos\phi + \sigma_3 \sin\phi)}{(1 - \sin\phi)} \right]} \tag{A.8}$$

where $K\ (\sigma_3)^n$ defines the initial tangent modulus as a function of the confining pressure σ_3, φ the angle of internal friction, C the apparent cohesion, R_F a constant relating compressive strength to an asymptotic stress difference, and K and n material constants.

Based on a series of data gathered from static and cyclic triaxial tests Lentz & Baladi (1981) suggested that the static test results could be used to predict the cumulative permanent strain of sand specimens subjected to repeated loading providing that the

specimen were repeatable and proposed the following expression for the permanent deformations

$$\varepsilon_p = \varepsilon_{0.95S}\, ln(1 - q/S)^{-0.15} + \left\{ \frac{n(q/S)}{[1 - m(q/S)]} \right\} ln(N) \qquad \text{(A.9)}$$

where $\varepsilon_{0.95S}$ ιe axial strain at 95% of the static strength, q the deviator stress, S the static strength, N the number of load repetitions and n, m regression parameters. However although Lentz & Baladi (1981) reported a good correlation between the above expression and tests on sands the validity of this model could not be verified by other researchers (Sweere, 1990).

In a recent study, Paute et al. (1996) expanded the expression they had proposed for the permanent axial strains by defining a limit value for parameter A in Equation (B.6) according to the hyperbolic expression given below

$$A = \frac{\left(\frac{q_{max}}{p_{max} + p^*} \right)}{b\left(m - \left(\frac{q_{max}}{p_{max} + p^*} \right) \right)} \qquad \text{(A.10)}$$

where q_{max} the maximum deviator stress, p_{max} the maximum mean normal stress, p^* a stress parameter defined by the intersection of the static failure line and the p axis in the p-q space, m the slope of the static failure line and b a regression parameter. This hyperbolic relationship suggests that A increases in line with the maximum shear stress ratio and that A becomes infinite as $\left(\frac{q_{max}}{p_{max} + p^*} \right)$ becomes equal to m.

The proposed expression for A implies that the static failure line, could be used to estimate the results of cyclic triaxial tests. On the other hand, if the failure parameters are known, a single triaxial test would be required to define the expression. Lekarp et al. (1996) reported that they could not verify the expression proposed by Paute et al. (1996).

Models for the prediction of the resilient Young's Modulus

Many different models have been proposed to predict the resilient modulus in relation with the stress state, the soil type and the soil physical state. For example Robnett & Thompson (1976) proposed a bilinear model for the resilient modulus E_r

$$E_r = K_1 + K_2\sigma_d \qquad \text{when} \qquad \sigma_d < \sigma_{di} \tag{A.11}$$

$$E_r = K_3 + K_4\sigma_d \qquad \text{when} \qquad \sigma_d > \sigma_{di} \tag{A.12}$$

where σ_d the deviator stress at which the slope of E_r versus σ_d changes, K_1, K_2, K_3, K_4 model parameters which depend on the soil type and its physical state.

Repeated load tests on fine grained materials subjected to a relatively low deviator stress of 6.895kPa revealed that a close correlation between their test data and the power model could be achieved (Moossazadeh & Witczak, 1981).

$$E_r = k\sigma_d{}^n \tag{A.13}$$

where σ_d the deviator stress and k and n parameters which depend on soil type and its physical state. Moossazadeh & Witczak (1981) reported that in their tests the soil dependent parameters attained values of k = 0-200 and n = 0-1.0. The validity of the power model was also verified by Pezo et al. (1991). Brown et al. (1975) however reported that in order to achieve a good fit between cyclic test data on saturated overconsolidated soils a small modification to the power model was required, which allowed the effective stress to be introduced into the expression as follows

$$E_r = k\left(\frac{\sigma_d}{\sigma'_3}\right)^n \tag{A.14}$$

Fredlund et al. (1977) however reported that the best fit to cyclic test data on moraine glacial till could be achieved using the semi-log approach

$$log(E_r) = k - n\sigma_d \tag{A.15}$$

where σ_d the deviator stress and k and n parameters which depend on soil type and its physical state. In the specific data set analysed Fredlund et al. (1977) reported that k varied between 3.6-4.3 and n between 0.005-0.09.

Based on the specific soil type and stress condition under consideration Drumm et al. (1990) proposed a hyperbolic model in their trend analysis of fine grained soil test data

$$E_r = \frac{k + n\sigma_d}{\sigma_d} \tag{A.16}$$

where σ_d the deviator stress and k and n parameters which depend on soil type and its physical state and observed that k varied between 2-70 and n between 2-12. Finally Shackel (1973) proposed an octahedral model for the resilient modulus

$$E_r = k\frac{\sigma^n{}_{oct}}{\tau^m{}_{oct}} \tag{A.17}$$

where σ_{oct}, τ_{oct} the octahedral normal and shear stresses. However due to the relative complicated expressions for the σ_{oct}, τ_{oct} the octahedral model was not extensively used.

REFERENCES

Adwan Chemicals. (2013). Silica Flour [Online], Available from: http://www.adwanchem.com/Silica_Flour.htm.

Airey, D. W., Fahey, M. (1991). Cyclic response of calcareous soil from the North West Shelf of Australia. *Géotechnique* **41,** No. 1, 101-121.

Alarcon, A., Chameau, J. L., Leonards, G. A. (1986). A new apparatus for investigating the stress-strain characteristics of sands. *Geotechnical Testing Journal* **9**, No. 4, 204-212.

Alvarado, G., Coop, M. R., Willson, S. (2012). On the role of bond breakage due to unloading in the behaviour of weak sandstones. *Géotechnique* **62**, No. 4, 303-316.

American Railway Engineering Association (1996). *Manual for railway engineering.* Vol. 1, Washington, D.C.

Amini, F., Qi, G. Z. (2000). Liquefaction testing of stratified silty sands. *Journal of Geotechnical and Geoenvironmental Engineering* **126**, No. 3, 208-217.

Ampadu, S. K., Tatsuoka, F. (1993). A hollow cylinder torsional simple shear apparatus capable of a wide range of shear strain measurement. *Geotechnical Testing Journal* **16**, No. 1, 3-17.

AREA (1996). Manual for Railway Engineering, *American Railway Engineering Association* **1**, Washington, D.C.

Arthur, J. R. F., Chua, K. S., Dunstan, T. (1977). Induced anisotropy in a sand. *Géotechnique* **27**, No. 1, 13-30.

Arthur, J. R. F., Chua, K. S., Dunstan, T. (1979). Dense sand weakened by continuous principal stress direction rotation. *Géotechnique* **29**, No. 1, 91-96.

Atkinson, J. H. (2000). Non-linear soil stiffness in routine design. *Géotechnique* **50**, No. 5, 487-508.

Bahadori, H., Ghalandarzadeh, A., Towhata, I. (2008). Effect of non plastic silt on the anisotropic behaviour of sand. *Soils and Foundations* **48**, No. 4, 531-545.

Barksdale, R. D. (1972). Laboratory evaluation of rutting in base course material. *Proceedings of the Third International Conference on Structural Design of Asphalt Pavements*, London, 161-174.

Bhandari, A. R. (2009). *The mechanics of an unbonded locked sand at low effective stresses*. PhD thesis, University of Southampton.

Black, D. K., Lee, K. L. (1973). Saturating laboratory samples by back pressure. *Journal of the Soil Mechanics and Foundations Division* **99**, No. 1, 75-93.

Bolton, M. D., Wilson, J. M. R. (1989). An experimental and theoretical comparison between static and dynamic torsional soil tests. *Géotechnique* **39***,* No. 4, 585-599.

Bonaquist, R. F., Witczak, M. W. (1997). A comprehensive constitutive model for granular materials in flexible pavement structures. *Proceedings of the 8th International Conference on Asphalt Pavements*, Vol. 1, 783–802.

Brown, S. F. (1996). Soil mechanics in pavement engineering. *Géotechnique* **46**, No. 3, 383-426.

Brown, S. F., Richardson, I. R. (2004). A hollow cylinder apparatus to study the cyclic loading behaviour of dry granular material. *Advances in Geotechnical Engineering* **1**, Thomas Telford, London, 369-380.

Brown, S. F., Lashine, A. K. F., Hyde, A. F. L. (1975). Repeated load triaxial testing of a silty clay. *Géotechnique* **25**, No. 1, 95-114.

BS1377:4 (1990). Compaction-related tests. *British Standards Methods of Test for Soils for Civil Engineering Purposes*, British Standards Institution, London.

Burrow, M. P. N., Bowness, D., Ghataora, G. S. (2007). A comparison of railway track foundation design methods. *Proceedings of the Institution of Mechanical Engineers, Part F: Journal of Rail and Rapid Transit* **221**, No. 1, 1-12.

Cai, Y., Yu, H. S., Wanatowski, D. (2012). Non coaxial behaviour of sand under various stress paths. *Journal of Geotechnical and Geoenvironmental Engineering*. ahead of print, doi:10.1061/(ASCE)GT.1943-5606.0000854.

Carraro, J. A. H., Prezzi, M., Salgado, R. (2009). Shear strength and stiffness of sands containing plastic or nonplastic fines. *Journal of Geotechnical and Geoenvironmental Engineering* **135**, No. 9, 1167-1178.

Casagrande, A. (1948). Classification and identification of soils, Trans. ASCE 113, 901-991.

Chameau, J. L., Sutterer, K. (1994). Influence of fines in liquefaction potential and steady state considerations. *Proceedings of the 13th International Conference on Soil Mechanics and Foundation Engineering,* New Delhi, India, 183-184.

Chan, F. W. K. (1990). *Permanent deformation resistance of granular layers in pavements*. PhD thesis, University of Nottingham.

Chan, F. W. K., Brown, S. F. (1994). Significance of principal stress rotation in pavements. *Proceedings of the 13th International Conference on Soil Mechanics and*

Foundation Engineering, New Delhi, India*,* 5-10 January 1994. Taylor & Francis, New York, 1823-1826.

Chang, C. S., Adegoke, C. W., Selig, E. T. (1980). The GEOTRACK model for railroad track performance. *Journal of the Geotechnical Engineering Division* **106**, No. 11, 1201-1218.

Chaudhary, S. K., Kuwano, J., Hayano, Y. (2004). Measurement of quasi-elastic stiffness parameters of dense toyoura sand in hollow cylinder apparatus and triaxial apparatus with bender elements. *Geotechnical Testing Journal* **27**, No.1, 23-35.

Chebli, H., Clouteau, D., Smitt, L. (2008). Dynamic response of high-speed ballasted railway tracks: 3D periodic model and in situ measurements. *Soil Dynamics and Earthquake Engineering* **28**, No. 2, 118–131.

Clayton, C. R. I. (2011). Stiffness at small strain: research and practice. *Géotechnique* **61**, No. 1, 5-37.

Clayton, C. R. I., Bica, A. V. D. (1993). The design of diaphragm-type boundary total stress cells. *Géotechnique* **43**, No. 4, 523–535.

Clayton, C. R. I., Heymann, G. (2001). Stiffness of geomaterials at very small strains. *Géotechnique* **51**, No. 3, 245-255.

Clayton, C. R. I., Khatrush, S. A. (1986). A new device for measuring local axial strains on triaxial specimens. *Géotechnique* **36**, No. 4, 593-597.

Clayton, C. R. I., Theron, M. & Vermeulen, N. J. (2004). The effect of particle shape on the behaviour of gold tailings. *Advances in geotechnical engineering: The Skempton conference, London,* 393-404.

Cresswell, A., Powrie, W. (2004). Triaxial tests on an unbounded locked sand. *Géotechnique* **54**, No. 2, 107–115.

Cuccovillo, T., Coop, M. R. (1997). The measurement of local axial strains in triaxial tests using LVDTs. *Géotechnique* **47**, No. 1, 167-171.

Dezfulian, H. (1982). Effects of silts content on dynamic properties of sandy soils. *Proceedings of the 8th World Conference on Earthquake Engineering,* 63-70.

Drumm, E. C., Boateng - Poku, Y., Pierce, T. J. (1990). Estimation of subgrade resilient modulus from standard tests. *Journal of Geotechnical Engineering* **116**, No. 5, 774–789.

Drumm, E. C., Reeves, J. S., Madgett, M. R., Trolinger, W. D. (1997). Subgrade resilient modulus correction for saturation effects. *Journal of Geotechnical and Geoenvironmental Engineering* **123**, No. 7, 663–670.

Duncan, J. M., Chang, C. Y. (1970). Nonlinear analysis of stress and strain in soils. *Journal of the Soil Mechanics and Foundations Division* **96**, No. 5, 1629–1653.

Duttine, A., Di Benedetto, H., Pham Van Bang, D., Ezaoui, A. (2007). Anisotropic small strain elastic properties of sands and mixture of sand-clay measured by dynamic and static methods. *Soils and Foundations* **47**, No. 3, 457-472.

Erten, D., Maher, M. H. (1995). Cyclic undrained behaviour of silty sand. *Soil Dynamics and Earthquake Engineering* **14**, No. 2, 115-123.

Fateen, S. (1972). *A finite element analysis of full depth asphalt railway track*. Master's Thesis, Department of Civil Engineering, University of Maryland.

Finn, L. W. D., Ledbetter, R. H., Guoxi, W. (1994). Liquefaction in silty soils: design and analysis. *ASCE Geotechnical Special Publication* **44**, 51-76.

Fredlund, D. G., Bergan, A. T., Wong, P. K. (1977). Relation between resilient modulus and stress conditions for cohesive subgrade soils. *Transportation Research Record* **642**, 73-81.

Frost, M. W., Fleming, P. R., Rogers, C. D. F. (2004). Cyclic triaxial tests on clay subgrades for analytical pavement design. *Journal of Transportation Engineering* **130**, No. 3, 378-386.

Frost, J. D., Park, J. Y. (2003). A critical assessment of the moist tamping technique. *Geotechnical Testing Journal* **26**, No. 1, 57-70.

Gasparre, A. (2005). *Advanced laboratory characterisation of London Clay*. PhD thesis, Imperial College London.

Gasparre, A., Nishimura, S., Minh, N. A., Coop, M. R., Jardine, R. J. (2007). The stiffness of natural London clay. *Géotechnique* **57**, No. 1, 33-47.

Georgiannou, V. N., Burland, J. B., Hight, D. W. (1990). The undrained behaviour of clayey sands in triaxial compression and extension. *Géotechnique* **41**, No. 3, 383–393.

Georgiannou, V. N., Tsomokos, A. (2008). Comparison of two fine sands under torsional loading. *Canadian Geotechnical Journal* **45**, No. 12, 1659-1672.

Georgiannou, V. N., Tsomokos, A., Stavrou, K. (2008). Monotonic and cyclic behaviour of sand under torsional loading. *Géotechnique* **58**, No. 2, 113-124.

Gräbe, P. J. (2002). *Resilient and permanent deformation of railway foundations under principal stress rotation.* PhD thesis, University of Southampton.

Gräbe, P. J., Clayton, C. R. I. (2009). Effects of principal stress rotation on permanent deformation in rail track foundations. *Journal of Geotechnical and Geoenvironmental Engineering* **135**, No. 4, 555-565.

Gräbe, P. J., Clayton, C. R. I., Shaw, F. J. (2005). Deformation measurement on a heavy haul track formation. *Proc. 8th Int. Heavy Haul Conf.,* Rio de Janeiro, Brazil: 287-295

Hazirbaba, K., Rathje, E. M. (2009). Pore pressure generation of silty sands due to induced cyclic shear strains. *Journal of Geotechnical and Geoenvironmental Engineering* **135**, No. 12, 1892-1905.

Heath, D. L., Shenton, M. J., Sparrow, R. W., Waters, J. M. (1972). Design of conventional rail track foundations. *Proceedings of the Institution of Civil Engineers* **51**, No. 2, 251-267.

Hight, D. W., Gens, A., Symes, M. J. (1983). The development of a new hollow cylinder apparatus for investigating the effects of principal stress rotation in soils. *Géotechnique* **33**, No. 4, 355-383.

Hsu, C. C., Vucetic, M. (2006). Threshold shear strain for cyclic pore water pressure in cohesive soils. *Journal of Geotechnical and Geoenvironmental Engineering* **132**, No. 10, 1325-1335.

Huang, Y. H., Lin, C., Deng, X. (1984). KENTRACK, a computer program for hot mix asphalt and conventional ballast railway trackbeds. *Res. Rep. No. RR-84-I,* The Asphalt Inst., College Park, Md.

Hyde, A. F. L. (1974). *Repeated load triaxial testing of soils*. PhD thesis, University of Nottingham.

Hyde, A. F. L., Ward, S. J. (1985). A pore pressure and stability model for a silty clay under repeated loading. *Géotechnique* **35**, No. 2, 113-125.

Hyodo, M., Aramaki, N., Itoh, M., Hyde, A. F. L. (1996). Cyclic strength and deformation of crushable carbonate sand. *Soil Dynamics and Earthquake Engineering* **15**, No. 5, 331-336.

Imerys performance minerals (2005). Hymod Prima Ball clay, Safety Data Sheet, Available from: http://www.docstoc.com/docs/54042200/SAFETY-DATA-SHEET-Hymod-Prima and http://www.imerys-perfmins.com/ball-clay/eu/ballclay.htm.

Indraratna, B., Attya, A., Rujikiatkamjorn, C. (2009). Experimental investigation on effectiveness of a vertical drain under cyclic loads. *Journal of Geotechnical and Geoenvironmental Engineering* **135**, No. 6, 835-839.

Indraratna, B., Nimbalkar, S., Christie, D., Rujikiatkamjorn, C., Vinod, J. (2010). Field Assessment of the Performance of a Ballasted Rail Track with and without Geosynthetics. *Journal of Geotechnical and Geoenvironmental Engineering* **136**, No. 7, 907–917.

Ip, M. C., Haque, A., Bouazza, A. (2012). Influence of cyclic stress pulse shapes on filtration behavior of railway subballast. *Journal of Geotechnical and Geoenvironmental Engineering* **138**, No. 2, 230-235.

Iwasaki, T., Tatsuoka, F., Takagi, Y. (1978). Shear moduli of sands under cyclic torsional shear loading. *Soils and Foundations* **18**, No. 1, 39-56.

Jardine, R. J., Symes, M. J., Burland, J. B. (1984). The measurement of soil stiffness in the triaxial apparatus. *Géotechnique* **34**, No. 3, 323-340.

Ju, S. H., Lin, H. T., Chen, T. K. (2007). Studying characteristics of train induced ground vibrations adjacent to an elevated railway by field experiments. *Journal of Geotechnical and Geoenvironmental Engineering* **133**, No. 10, 1302-1307.

Kaynia, A. M., Madshus, C., Zackrisson, P. (2000). Ground vibration from high speed trains: Prediction and countermeasure. *Journal of Geotechnical and Geoenvironmental Engineering* **126**, No. 6, 531–537.

Khedr, S. (1985). Deformation characteristics of granular base course in flexible pavement. *Transportation Research Record* **1043**, 131-138.

Koester, J. P. (1994). The influence of fine type and content on cyclic strength. *Ground failures under seismic conditions. Geotechnical Special Publication* No. 44, ASCE, 17-33.

Krylov, V. V. (1995). Generation of ground vibration by superfast trains. *Applied Acoustics* **44**, No. 2, 149–164.

Kuerbis, R., Negussey, D., Vaid, Y. P. (1988). Effect of gradation and fines content on the undrained response of sand. *Hydraulic fill structures*, ASCE, Fort Collins, Colo., 330–345.

Kumruzzaman, Md., Yin, J. H. (2010). Influences of principal stress direction and intermediate principal stress on the stress-strain-strength behaviour of completely decomposed granite. *Canadian Geotechnical Journal* **47**, No. 2, 164-179.

Kuwano, R., Jardine, R. J. (2002). On the applicability of cross-anisotropic elasticity to granular materials at very small strains. *Géotechnique* **52**, No. 10, 727-749.

Lacasse, S., Berre, T. (1988). Triaxial testing methods for soils. *ASTM STP* **977**, 264-289.

Lackenby, J., Indraratna, B., McDowell, G., Christie, D. (2007). Effect of confining pressure on ballast degradation and deformation under cyclic triaxial loading. *Géotechnique* **57**, No. 6, 527-536.

Lade, P. V. (1981). Laboratory shear strength of soil. *ASTM STP* **740**, 145-163.

Lade, P. V., Yamamuro, J. A. (1997). Effect of nonplastic fines on static liquefaction of sands. *Canadian Geotechnical Journal* **34**, No. 6, 918-928.

Ladd, R. S. (1978). Preparing test specimens using undercompaction. *Geotechnical Testing Journal* **1**, No. 1, 16-23.

Larew, H. G., Leonards, G. A. (1962). A repeated load strength criterion. *Proceedings of the Highway Research Board* **41**, 529-556.

Law, K. T., Ling, Y. H. (1992). Liquefaction of granular soils with noncohesive and cohesive fines. *Proceedings of the 10th World Conference on Earthquake Engineering, 1491-1496.*

Lee, D. H., Juang, C.H., Chen, J. W., Lin, H. M., Shieh, W. H. (1999). Stress paths and mechanical behaviour of a sandstone in hollow cylinder tests. *International Journal of Rock Mechanics and Mining Sciences* **36***, No. 7,* 857-870.

Lekarp, F., Isacsson, U., Dawson, A. (2000). State of the art.: permanent strain response of unbound aggregates. *Journal of Transportation Engineering* **126**, No. 1, 76-83.

Lekarp, F., Richardson, I. R., Dawson, A. (1996). Influences on permanent deformation behavior of unbound granular materials. *Transportation Research Record* **1547**, 68-75

Lentz, R. W., Baladi, G. Y. (1981). Constitutive equation for permanent strain of sand subjected to cyclic loading. *Transportation Research Record* **810**, 50–54.

Leshchinsky, D., Rawlings, D. L. (1988). Stress path and permanent deformations in sand subjected to repeated load. *Geotechnical Testing Journal* **11**, No. 1, 36-43.

Li, D. (1994). *Railway track granular layer thickness design based on subgrade performance under repeated loading*. PhD Thesis, University of Massachusetts.

Li, D., Selig, E. (1994). Resilient modulus for fine-grained subgrade soils. *Journal of Geotechnical Engineering* **120**, No. 6, 939–957.

Li, D., Selig, E. T. (1995). Evaluation of railway subgrade problems. *Transportation Research Record: Journal of the Transportation Research Board* **1489**, 17-25.

Li, D., Selig, E. T. (1996). Cumulative plastic deformation for fine grained subgrade soils. *Journal of Geotechnical and Geoenvironmental Engineering* **122**, No. 12, 1006–1013.

Li, D., Selig, E. T. (1998). Method for railroad track foundation design I: Development. *Journal of Geotechnical and Geoenvironmental Engineering* **124**, No. 4, 316-322.

Liu, J. K. (2006). *Subgrade engineering*. The Architecture and Building Industry Publishing House of China, Beijing.

Liu, J., Xiao, J. (2010). Experimental study on the stability of railroad silt subgrade with increasing train speed. *Journal of Geotechnical and Geoenvironmental Engineering* **136**, No. 6, 833–841.

Lo Presti, D. C. F., Jamiolkowski, M., Pallara, O., Cavallaro, A., Pedroni, S. (1997). Shear modulus and damping of soils. *Géotechnique* **47**, No. 3, 603–617.

Loh, R. B. H., Nikraz, H. R. (2012). Effective stress method on threshold stress of clay under high rate cyclic loading. Jotisankasa, Sawangsuriya, Soralump and Mairaing. In Loh, R. B. H., Nikraz, H. R. (2012). Compressibility and strength of clay subgrade of railroad foundation in highly saturated condition. *Journal of GeoEngineering* **7**, No. 2, 43-51.

Miller, G. A., Teh, S. Y., Li, D., Zaman, M. M. (2000). Cyclic shear strength of soft railroad subgrade. *Journal of Geotechnical and Geoenvironmental Engineering* **126**, No. 2, 139–147.

Mitchell, J. K. (1976). *Fundamentals of soil behavior*, Wiley, New York.

Modoni, G., Koseki, J., Anh Dan, L. Q. (2010). Cyclic stress–strain response of compacted gravel. *Géotechnique* **61**, No. 6, 473-485.

Momoya, Y., Sekine, E., Tatsuoka, F. (2005). Deformation characteristics of railway roadbed and subgrade under moving-wheel load. *Soils and Foundations* **45**, No. 4, 99-118.

Momoya, Y., Watanabe, K., Sekine, E., Tateyama, M., Shinoda, M., Tatsuoka, F. (2007). Effects *of continuous principal stress axis rotation on the deformation characteristics of sand under traffic loads. Proceedings of the International Workshop on Design and Construction of Pavements and Rail Tracks – Geotechnical Aspects and Processed Materials*, Osaka, Japan, Edited by Correia, A.G., Momoya, Y., and Tatsuoka. F., Taylor and Francis Group.

Monkul, M. M., Yamamuro, J. A. (2011). Influence of silt size and content on liquefaction behaviour of sands. *Canadian Geotechnical Journal* **48**, No. 6, 931-942.

Moossazadeh, J., Witczak, M. W. (1981). Prediction of subgrade moduli for soil that exhibit nonlinear behavior. *Transportation Research Record* **810**, 9-17.

Murthy, T. G., Loukidis, D., Carraro, J. A. H., Prezzi, M., Salgado, R. (2007). Undrained monotonic response of clean and silty sands. *Géotechnique* **57**, No. 3, 273–288

Naeini, S. A., Baziar, M. H. (2004). Effect of fines content on steady-state strength of mixed and layered samples of a sand. *Soil Dynamics and Earthquake Engineering* **24**, No. 3, 181-187.

Ni, Q., Tan, T. S., Dasari, G. R., Hight, D. W. (2004). Contribution of fines to the compressive strength of mixed soils. *Géotechnique* **54**, No. 9, 561–569.

Nishimura, S. (2006). *Laboratory study on anisotropy of natural London clay*. PhD thesis, Imperial College London.

Nishimura, S., Minh, N. A., Jardine, R. J. (2007). Shear strength anisotropy of natural London clay. *Géotechnique* **57**, No. 1, 49-62.

Noureddine, C., Ahmed, B., Mounir, H. (2006). Effect of confining pressure on lateral strain of cohesionless soil. *Journal of Engineering and Applied Sciences* **1**, No. 4, 360-369.

O'Kelly, B. C., Naughton, P. J. (2009). Study of the yielding of sand under generalised stress conditions using a versatile hollow cylinder torsional apparatus. *Mechanics of Materials* **41**, No. 3, 187-198.

O'Reilly, M. P., Brown, S. F., Overy, R. F. (1991). Cyclic loading of silty clay with drainage periods. *Journal of Geotechnical and Geoenvironmental Engineering* **117**, No. 2, 354-362.

Otter, L. (2011). *The influence of suction changes on the stiffness of railway formation.* PhD thesis, University of Southampton.

Papadopoulou, A., Tika, T. (2008).The effect of fines on critical state and liquefaction resistance characteristics of non-plastic silty sands. *Soils and Foundations* **48**, No. 5, 713-725.

Pappin, J. W. (1979). *Characteristics of granular material for pavement analysis*. PhD thesis, University of Nottingham.

Paute, J. L., Hornych, P., Benaben, J. P. (1996). Repeated load triaxial testing of granular materials in the French network of laboratories des Ponts et Chaussées. *Flexible Pavements*, editor Correia A. G., Lisbon, 53-64.

Paute, J. L., Jouve, P., Martinez, J., Ragneau, E. (1988). Modèle de calcul pour le dimensionnement des chaussées souples. *Bulletin de Liaison des Laboratoires des Ponts et Chaussées* **156**, 21-36.

Pezo, R. F., Kim, D. S., Stokoe, K. H., Hudson, W. R. (1991). Aspects of a reliable resilient modulus testing system. *Transportation Research Board Preprint, 70th Annual Meeting,* Washington, D.C.

Pitman, T. D., Robertson, P. K., Sego, D. C. (1994). Influence of fines on the collapse of loose sands. *Canadian Geotechnical Journal* **31**, No. 5, 728-739.

Polito, C. P., Martin, J. R. (2001). Effects of nonplastic fines on the liquefaction resistance of sands. *Journal of Geotechnical and Geoenvironmental Engineering* **127**, No. 5, 408-415.

Powrie, W. (2004). *Soil mechanics: concepts and applications*. Spon Press, 2nd edition.

Powrie, W., Priest, J. A., Clayton, C. R. I. (2008). Recent research on railway track sub-base behaviour. *Advances in Transportation Geotechnics: Proceedings of the 1st International Conference on Transportation Geotechnics*, Nottingham, UK, 25-27 August 2008. *Edited by* E. Ellis, H.S Yu, G. McDowell, A. R. Dawson, N. Thom.

Powrie, W., Yang, L. A., Clayton, C. R. I. (2007). Stress changes in the ground below ballasted railway track during train passage. *Proceedings of the Institution of Mechanical Engineers, Part F: Journal of Rail and Rapid Transit* **221**, No. 2, 247-261.

Priest, J. A., Powrie, W., Yang, L. A., Gräbe, P. J., Clayton, C. R. I. (2010). Measurements of transient ground movements below a ballasted railway line. *Géotechnique* **60**, No. 9, 667-677.

Qadimi, A., Coop, M. R. (2007). The undrained cyclic behaviour of a carbonate sand. *Géotechnique* **57**, No. 9, 739-750.

Raymond, G. P. (1985). Design for railroad ballast and subgrade support. *Journal of the Geotechnical Engineering Division* **104**, No. 1, 45-59.

Raymond, G. P., Gaskin, P. N., Addo-Abedi F. Y. (1979). Repeated compressive loading of Leda clay. *Canadian Geotechnical Journal* **16**. No. 1, 1-10.

Read, D., Li, D. (1995). Subballast considerations for heavy axle load trackage. TD 95-028, *Technology Digest, Association of American Railroads*, Research and Test Department.

Richards, D. J., Clark, J., Powrie, W., Heymann, G. (2007). Performance of push-in pressure cells in overconsolidated clay. *Proceedings of the Institution of Civil Engineers: Ground Engineering* **160**, No. GE1, 31–41.

Robnett, Q. L., Thompson, M. R. (1976). Effect of lime treatment on the resilient behaviour of fine grained soils. *Transportation Research Record* **560**, 11-20.

Rose, J. G., Agarwal, N. K., Brown, J. D., Ilavaia, N. (2010). KENTRACK, a performance based layered elastic railway trackbed structural design and analysis procedure: a tutorial. *American Society of Mechanical Engineers Conference Proceedings*: *Joint Rail Conference* **1**, 73-110.

Saada, A. S., Townsend, F. C. (1981). *Laboratory shear strength of soil*. *ASTM STP* **740**, 7-77.

Salgado, R., Bandini, P., Karim, A. (2000). Shear strength and stiffness of silty sand. *Journal of Geotechnical and Geoenvironmental Engineering* **126**, No. 5, 451-462.

Sayao, A., Vaid, Y. P. (1991). A critical assessment of stress nonuniformities in hollow cylinder test specimens. *Soils and Foundations* **31**, No. 1, 60-72.

Shackel, B. (1973). The derivation of complex stress-strain relations. *Proceedings of the 8th International Conference on Soil Mechanics and Foundation Engineering*, Moscow, 353-359.

Schmertmann, J. H. (1991). The mechanical aging of soils. *Journal of Geotechnical Engineering* **117**, No. 9, 1288-1330.

Seed, H., Idriss, I., Arango, I. (1983). Evaluation of liquefaction potential using field performance data. *Journal of Geotechnical Engineering* **109**, No. 3, 458–482.

Seed, H. B., Tokimatsu, K., Harder, L. F., Chung, R. M. (1985). Influence of SPT procedures in soil liquefaction resistance evaluations. *Journal of Geotechnical Engineering* **111**, No. 12, 1425–1445.

Selig, E. T., Waters, J. M. (1994). *Track Geotechnology and Substructure Management*, Thomas Telford, London.

Shahu, J. T. (1993). *Some analytical and experimental investigations to study the behaviour of soils under the railway tracks*. PhD thesis, Indian Institute of Technology.

Shahu, J. T., Yudhbir., Kameswara Rao, N. S. V. (1999). A simple test methodology for soils under transportation routes. *Géotechnique* **49**, No. 5, 639-649.

Shahu, J. T., Yudhbir, Kameswara Rao, N. S. V. (2000). A rational method for design of railroad track foundation. *Soils and Foundations* **40**, No. 6, 1-10.

Shaw, P., Brown, S. F. (1986). Cyclic simple shear testing of granular materials. *Geotechnical Testing Journal* **9**, No. 4, 213-220.

Shen, C. K., Vrymoed, J. L., Uyeno, C. K. (1977). The effect of fines on liquefaction of sands. *Proc., 9th Int. Conf. on Soil Mechanics and Foundation Engineering*, International Society of Soil Mechanics and Foundation Engineering, Tokyo, Japan, 381–385.

Shibuya, S., Hwang, S. C., Mitachi, T. (1997). Elastic shear modulus of soft clays from shear wave velocity measurement. *Géotechnique* **47**, No. 3, 593-601.

Shibuya, S., Mitachi, T., Fukuda, F., Degoshi, T. (1995). Strain rate effects on shear modulus and damping of normally consolidated clay. *Geotechnical Testing Journal* **18**, No. 3, 365-375.

Shibuya, S., Tatsuoka, F., Teachavorasinskun, S., Kong, X. J., Abe, F., Kim, Y. S., Park, C. S. (1992). Elastic deformation properties of geomaterials. *Soils and Foundations* **32**, No. 3, 26-46.

Simpson, B. (2010). Engineering in stiff sedimentary clays. *Géotechnique* **60**, No. 12, 903-911.

Sivathayalan, S., Vaid, Y.P. (2002). Influence of generalized initial state and principal stress rotation on the undrained response of sands. *Canadian Geotechnical Journal* **39**, No. 1, 63-76.

Smith, N. (2006). Stiffness and cyclic response of clayey fine sands. *Proceedings of the Institution of Civil Engineers: Geotechnical Engineering* **159**, Issue 4, 251 –268**.**

Sorensen, K. K., Baudet, B. A., Simpson, B. (2007). Influence of structure on the time-dependent behaviour of a stiff sedimentary clay. *Géotechnique* **57**, No 1, 113 –124.

Sorensen, K. K., Baudet, B. A., Simpson, B. (2010). Influence of strain rate and acceleration on the behaviour of reconstituted clays at small strains. *Géotechnique* **60**, No. 10, 751–763.

Suiker, A. S. J., Selig, E. T., Frenkel, R. (2005). Static and cyclic triaxial testing of ballast and subballast. *Journal of Geotechnical and Geoenvironmental Engineering* **131**, No. 6, 771-782.

Sweere, G. T. H. (1990). *Unbound granular bases for roads*. PhD thesis, University of Delft.

Symes, M. J. P. R., Gens, A., Hight, D. W. (1984). Undrained anisotropy and principal stress rotation in saturated sand. *Géotechnique* **34**, No. 1, 11-27.

Symes, M. J., Gens, A., Hight, D. W. (1988). Drained principal stress rotation in saturated sand. *Géotechnique* **38**, No. 1, 59-81.

Tatsuoka, F., Shibuya, S. (1992). Deformation characteristics of soils and rocks from field and laboratory tests. *Proceedings of the 9th Asian Conference on Soil Mechanics and Foundation Engineering*, 101–170.

Tatsuoka, F., Sonoda, S., Hara, K., Fukushima, S., Pradhan, T. B. S. (1986). Failure and deformation of sand in torsional shear. *Soils and Foundations* **26**, No. 4, 79-97.

Teachavorasinskun, S., Thongchim, P., Lukkunaprasit, P. (2002). Stress rate effect on the stiffness of a soft clay from cyclic, compression and extension triaxial tests. *Géotechnique* **52**, No. 1, 51-54.

Thevanayagam, S., Mohan, S. (2000). Intergranular state variables and stress-strain behaviour of silty sands. *Géotechnique* **50**, No. 1, 1-23.

Thevanayagam, S., Ravishankar, K., Mohan, S. (1996). Steady state strength, relative density and fines content relationship for sands. *Transportation Research Record: Journal of the Transportation Research Board* **1547**, 61-67.

Thevanayagam, S., Shenthan, T., Mohan, S., Liang, J. (2002). Undrained fragility of clean sands, silty sands, and sandy silts. *Journal of Geotechnical and Geoenvironmental Engineering* **128**, No. 10, 849–859.

Tokimatsu, K., Yoshimi, Y. (1983). Empirical correlation of soil liquefaction based on spt n-value and fines content. *Soils and Foundations* **23**, No. 4, 56–74.

Turner, J. P., Kulhawy, F. H. (1992). Strength changes in sand following cyclic shear. *Geotechnical Testing Journal* **15**, No. 3, 295-299.

Vaid, Y. P. (1994). Liquefaction of silty soils. *Ground failures under seismic conditions*. ASCE, Atlanda,1-16.

Whitlow, R. (1995). *Basic Soil Mechanics*, 3rd edition Longman Scientific & Technical, Harlow.

Wolff, H., Visser, A. T. (1994). Incorporating elasto-plasticity in granular layer pavement design. *Proceedings of the Institution of Civil Engineers: Transport* **105**, No. 4, 259–272.

Wong, R. K. S., Arthur, J. R. F. (1985). Induced and inherent anisotropy in sand. *Géotechnique* **35**, No. 4, 471-481.

Wong, R. K. S., Arthur, J. R. F. (1986). Sand sheared by stresses with cyclic variations in direction. *Géotechnique* **36**, No. 2, 215-226.

Wood, D. M. (1984). Technical note. On stress parameters. *Géotechnique* **34**, No. 2, 282-287.

Xenaki, V. C., Athanasopoulos, G. A. (2003). Liquefaction resistance of sand-silt mixtures: an experimental investigation of the effect of fines. *Soil Dynamics and Earthquake Engineering* **23**, No. 3, 183-194.

Xianzhang, L., Feng, Z., Zhanyuan, Z., Lin, D., Qingli, H. (2009). Field experiment of subgrade vibration induced by passing train in a seasonally frozen region of Daqing. *Earthquake Engineering and Engineering Vibration* **8**, No. 1, 149-157.

Yang, L. A., Powrie, W., Priest, J. A. (2009). Dynamic Stress Analysis of a Ballasted Railway Track Bed during Train Passage. *Journal of Geotechnical and Geoenvironmental Engineering* **135**, No. 5, 680-689.

Yang, J., Sze, H. Y. (2011). Cyclic behaviour and resistance of saturated sand under non-symmetrical loading conditions. *Géotechnique* **61**, No. 1, 59-73.

Yang, J., Wei, L. M. (2012). Collapse of loose sand with the addition of fines: the role of particle shape. *Géotechnique* **62**, No. 12, 1111–1125.

Yilmaz, M. T., Pekcan, O., Bakir, B. S. (2004). Undrained cyclic shear and deformation behaviour of silt-clay mixtures of Adapazari Turkey. *Soil Dynamics and Earthquake Engineering* **24**, No. 7, 497-507.

Zdravkovic, L., Jardine, R. J. (1997). Some anisotropic stiffness characteristics of a silt under general stress conditions. *Géotechnique* **47**, No. 3, 407-437.

Zdravkovic, L., Jardine, R. J. (2001). The effect on anisotropy of rotating the principal stress axes during consolidation. *Géotechnique* **51**, No. 1, 69-83.

Zlatovic, S., Ishihara, K. (1995). On the influence of nonplastic fines on residual strength. *First International Conference on Earthquake Geotechnical Engineering* **1**, Tokyo, Japan, 239-244.